SHIRSHOV INSTITUTE OF OCEANOLOGY

CRUISE REPORT No. 38

RV *AKADEMIK IOFFE* CRUISE 26 May - 29 June 2012

North Atlantic Repeat Hydrography of WOCE section along 59.5 N

Principal Scientists **S Gladyshev**[1]

2013

Shirshov Institute of Oceanology
36 Nakhimovskii prospect
Moscow 117997 RUSSIA
Tel: +7(495) 719 0255 Fax: +7(499) 124 6342 Email:

sgladyshev@ocean.ru

[1]**Shirshov Institute of Oceanology**

DOCUMENT DATA SHEET

AUTHOR	***PUBLICATION DATE***
GLADYSHEV, S	2013

TITLE

RV ***Akademik Ioffe*** Cruise 38 , 26 May - 29 June 2012.

REFERENCE

Shirshov Institute of Oceanology, Akademik Ioffe Cruise Report, No. 38, 87pp. tables & figs.

ABSTRACT

RV ***Akademik Ioffe*** Cruise 38 was a contribution to the RUSSIA CLIVAR Community Research Programme. The sections over North Atlantic sills between Greenland Iceland Faroe Islands and Shetlands were designed to estimate variability of the meridional fluxes and water mass exchange between the North Atlantic and the Arctic Ocean. The Denmark Strait section was not completed due to heavy ice field between Iceland and Greenland. The Iceland-Faroe section was repeated four times during twelve days and the Faroe-Shetland section three times during sixteen days to study short-term variability of the water mass properties circulation and meridional transport. The transatlantic 60 degree line also was not extended to the Greenland shelf because of the dense ice field there.

KEYWORDS

CRUISE 38 2012, *AKADEMIK IOFFE,* **CLIVAR, TRANSATLANTIC SECTION, DENMARK STRAIT, NORTH ATLANTIC SILLS, INTEROCEAN EXCHANGE, CTD OBSERVATIONS, VMADCP,LADCP**

ISSUING ORGANISATION

Shirshov Institute of Oceanology
36 Nakhimovskii prospect
Moscow 117997 RUSSIA

Director: Academician Robert Nigmatulin

Copies of this report are available from: **Department of Marine Operations,** Tel: +7(495)7190255 Fax: +7(499)124 6342

Email: sgladyshev**@ocean.ru**

Contents
Scientific Personnel

Scientific Personnel

GLADYSHEV, S.	Principal Scientist	Shirshov
SHCHUKA, S.	Chief of CTD group	Shirshov
ANDREEVA, C.	CTD, LADCP	Shirshov
GAVRIKOV, A.	CTD, Sampling	Shirshov
ZAPOTYL'KO, V.	CTD, LADCP	Shirshov
DOBROVOLSKII, M.	Sampling	Shirshov
PYATAKOV, V.	Winch	Shirshov Atlantic Branch
KULESHOV, A.	Winch	Shirshov Atlantic Branch
LUKASHIN, S.	Winch	Shirshov Atlantic Branch
NAGULEVICH, V.	Nutrients	Shirshov
KOLOKOLOVA, A.	Oxygen	Shirshov
BULYCHEV, V.	Sampling	Shirshov Atlantic Branch
BULYCHEVA E.	Nutrients	Shirshov Atlantic Branch
LUKYANOVA, O.	Oxygen	Shirshov
PANKRATOVA, N.	Oxygen	Shirshov Atlantic Branch
GLADYSHEVA, S.	Salinity	Shirshov
LYUBSHOV, K.	CTD, Sampling	Shirshov
SANTANA, M.	CO_2	University of Las Palmas
GONZÁLEZ, A.	CO_2	University of Las Palmas
ALVARADO, R.	CO_2	University of Las Palmas
BARRERA, A.	CO_2	University of Las Palmas

1. CRUISE NARRATIVE

1.1 Cruise Details

Expedition Designation: R/V ***Akademik Ioffe*** Cruise 38, RUSSIA CLIVAR

Principal Scientists: Dr Sergey V. Gladyshev (Shirshov).

Ship: RV ***Akademik Ioffe.***

Ports of Call: Bremerhaven (Germany) to St. John's (Canada).

Cruise Dates: 26th May to 29th June 2012.

1.2 Cruise Summary

1.2.1 Cruise Track and Stations

The cruise track with station positions is shown in **Fig. l**. Only small volume samples were taken, details are listed in **Table 1**.

1.2.2. Equipment

The principal instruments used during the cruise were a SBE 9P-743 CTD with dual temperature and conductivity sensors (SBE 3 SN 03P4399, SBE 4 SN 042827, SBE 3 SN 03P4401, SBE 4 SN 042925), oxygen sensor (SBE 43, SN 430699), turbidity sensor (SeaPoint Turbidity, SN 10218 STM), Benthos altimeter model PSA-900D, LADCP WHM-300 kHz down-looking (S/N 12312), LADCP WHM-300 kHz up-looking (S/N 12367). These were mounted together with a multisampler Carousel SBE 32 equipped with 22 5-litre Niskin bottles. Upon recovery each bottle was sampled in turn for dissolved oxygen, nutrients, salinity. All sampling was done on deck. Currents were measured using vessel mounted ADCP (VMADCP) TRDI OS38 kHz (S/N 1185) installed at the central point of the ship hall.

Navigation information was provided by a Trimble SPSx50/SPSx51 - Modular GPS receiver and every second was recorded on the PC. Additional measurements were made with an ELAC 12 kHz, Aanderaa meteorological package.

1.2.3 Sampling

Nominal depths sampled were: bottom, 3100, 3000, 2750, 2500, 2250, 2000, 1750, 1500, 1250, 1100, 1000, 900, 800, 700, 600, 500, 400, 300, 200, 150, 100, 50, 30, 20, 10 m. On deep casts fewer shallow and intermediate bottles were fired. The actual bottle depths are shown in **Fig. 2**.

1.2.4 Number of Stations Occupied

206 stations (210 casts) were occupied during the cruise that includes sections between Shetlands and Faroe (3 repeats) Faroe and Iceland (4 repeats) Denmark Strait (not competed because of ice, 2 repeats) as well as transatlantic section along 59.5 N (**Fig. l**).

1.3 Scientific Objectives

The cruise objectives were to:

1. To complete a CTD section from the Great Britain to Greenland.
2. To survey the North Atlantic sills with high-resolution CTD and LADCP/VMADCP data to determine the circulation and meridional fluxes.

1.4 Narrative

1.4.1 Introduction

The Meridional overturning circulation (MOC) in the North Atlantic is one of the main drivers of the widely known global oceanic "conveyor belt" – an important element of the Earth's climate system [e.g., van Aken, 2007]. Warm upper-ocean waters transported northward by the North Atlantic Current release heat to the atmosphere, gain density due to cooling and eventually sink in the subpolar North Atlantic and adjacent Arctic seas thereby generating the return southward flow of colder waters at depths (**Fig. 3**) [Dickson and Brown, 1994; Koltermann et al., 1999]. Temporal variability of the large-scale circulation and associated heat transport in the subpolar North Atlantic is one of the principal factors behind the high-latitude climate anomalies in the Northern Hemisphere.

Progress in understanding the causes of the ongoing climate change and forecasting climate variability in the Arctic and over European part of Russia for the next decades require

reliable observation-based estimates of the variability of the North Atlantic circulation and the Atlantic–Arctic heat and freshwater fluxes, as well as elucidation of the underlying mechanisms. In a number of recent studies, radical changes in the thermohaline regime and large-scale circulation in the Atlantic Ocean have been suggested to occur under global warming. For instance, the long-term freshening of the subpolar North Atlantic deep waters since the mid-1960s [Dickson et al., 2002] has been (cautiously) attributed to climate change-related factors [Curry et al., 2003; Hansen et al., 2004]. Hypothetically, under global warming, an increased evaporation in the tropics and increased precipitation at high latitudes, coupled with an intensified melting of Arctic ice, lead to the upper-ocean freshening in the regions of deep water formation and, hence, to the deep water freshening in the Atlantic Ocean. At the same time, milder winters along with the upper-ocean freshening lead to a decrease in the deep water production rates, which results in slowing of the Atlantic Meridional Overturning Circulation [e.g., Hansen et al., 2004; Bryden et al., 2005].

To better understand the past and present changes in the ocean-atmosphere dynamical system, as well as their causes and consequences, data on the full-depth oceanic variability are needed. An indispensable effective tool for assessing the large-scale circulation and thermohaline changes in the deep ocean and investigating mechanisms governing these changes are repeated full-depth transoceanic observations.

Since 1997, the P.P. Shirshov Institute of Oceanology has carried out the long-term monitoring of the North Atlantic circulation and water mass properties in the 59.5°N hydrographic section between Cape Farewell (Greenland) and Scotland (**Fig. 3**). Since 2002, the section has been repeated yearly on board the Russian research vessels, providing high precision data on temperature, salinity, oxygen and nutrients concentrations, and current velocities in the entire water column – "from shore to shore", from the sea surface to the bottom. In 2011, in addition to annual repeat measurements at 59.5°N, the P.P. Shirshov Institute of Oceanology started full-depth repeat observations of the oceanic exchange between the Atlantic and Arctic oceans through the straits between Greenland, Iceland, Faeroe and Shetland Islands (**Fig. 3**). The full-depth observations – of the same oceanic quantities as at 59.5°N – are performed in the straits from research vessels twice a year, in spring and fall. Based on the unique data set thus collected, a number of fundamental findings have already been achieved. Below, we briefly summarize the main subjects and results of our research.

The 59.5°N transatlantic section (**Fig. 3**) was designed for monitoring the large-scale circulation and thermohaline / chemical properties of oceanic waters at the northern periphery of the NA – the region where the warm upper-ocean waters are transformed by deep convection and mixing into the colder intermediate and deep waters – the Labrador Sea Water (LSW), Iceland Scotland Overflow Water (ISOW) and Denmark Strait Overflow Water (DSOW) (**Fig. 3**) – transported southward in the lower limb of the Atlantic MOC. Hydrographic data collected at 59.5°N along with those obtained within the framework of the kindred projects, primarily the French OVIDE (http://www.ifremer.fr/lpo/ovide), and historical data sets have been used for studying the dense water production [Falina et al., 2007; Falina et al., 2012], decadal temperature and salinity changes in the intermediate–deep water column [Sarafanov et al., 2007; Sarafanov et al., 2008; Sarafanov et al., 2010b], causes of these changes [Sarafanov, 2009; Sarafanov et al., 2010b], the mean state [Sarafanov et al, 2012] and long-term variability of the large-scale circulation in the region [Sarafanov et al., 2009; Sarafanov et al, 2010a; Våge et al., 2011].

1.4.2 Deep convection in the Irminger Sea

The oxygen data collected in 1997 in the northern North Atlantic in several sections ending nearby the southern tip of Greenland provided the observation-based support for the hypothesis [Pickart et al., 2003] that winter convection in the Irminger Sea may penetrate deep into the LSW layer (1000 – 2000 m) thus causing local renewal of this water mass. A separate lateral maximum of oxygen concentrations in the deep LSW layer was detected east of Cape Farewell (59.5°N, 36–40°W): the concentrations increased (by ~0.1 ml/l) from the Labrador Sea eastern edge toward the Irminger Sea (**Fig. 4**) rather than the reverse, as would be expected if LSW observed in the Irminger Sea interior in 1997 were solely of advective origin [Falina et al., 2007].

1.4.3. Reversal of the deep-water freshening

The LSW and Nordic Seas overflow-derived deep waters, ISOW and DSOW, freshened in the northern North Atlantic during the last three–four decades of the 20th century [Dickson et al., 2002]. Between the 1960s and 1990s, the water column in the region freshened on average by about 0.03 [Curry et al., 2003].

The long-term freshening reversed in the mid-1990s [Sarafanov et al., 2007; Sarafanov et al., 2008; Sarafanov et al., 2010b]. The salinification (and warming) of the intermediate and deep waters since the mid-1990s (**Fig. 5**) was much more intense than the preceding freshening. Over nearly a decade (1997–2006), temperature / salinity in the intermediate–deep water column ($\sigma_0 \geq 27.45$, depths > 500–1000 m) at 59.5°N increased by ~0.3°C / 0.03–0.04 [Sarafanov et al., 2008].

In the Irminger Sea, the long-term freshening in the deep water column (σ_0>27.80, depths > ~2000 m) reversed in the early 2000s [Sarafanov et al., 2010b]. The observed freshening reversal was a lagged consequence of the persistent ISOW salinification that occurred upstream, in the Iceland Basin, after 1996 due to salinification of the northeast Atlantic waters entrained into the overflow. It was demonstrated [Sarafanov et al., 2010b] that the entrainment salinity increase was associated with the North Atlantic Oscillation (NAO)-induced weakening and contraction of the Subpolar Gyre and corresponding northwestward advance of subtropical waters that followed the NAO decline in the mid-1990s and continued through the mid-2000s. Remarkably, the deep water freshening reversal was not related to changes in the overflow water salinity.

1.4.4. Deep-ocean salinity changes and the NAO

Close relationship between the thermohaline properties of the northern North Atlantic intermediate and deep waters and the winter NAO index on a decadal time scale ($r^2 \approx 0.65$, 1950s–2000s, **Fig. 6b** and **6c**) was revealed [Sarafanov, 2009] from the observation-based salinity time series for LSW in the Labrador Sea [Yashayaev, 2007] and ISOW in the Iceland basin [Boessenkool et al., 2007; Sarafanov et al., 2007]. Persistent NAO decline (amplification) leads to warming and salinification (cooling and freshening) in the intermediate–deep water column.

An explanation for the close link between the NAO and the coherent decadal changes in the intermediate and deep water properties in the region was proposed [Sarafanov, 2009]. The two factors dominate this link (**Fig. 6d**): (i) intensity of convection in the Labrador Sea controlling injection of relatively cold fresh waters into the intermediate layer and (ii) zonal extent of the Subpolar Gyre that regulates the relative contributions of cold fresh subpolar waters

and warm saline subtropical waters to the entrainment into the Norwegian Sea overflow south of the Iceland–Scotland Ridge and to the Atlantic inflow to the Nordic Seas. These factors act in phase leading to the observed coherent thermohaline changes in the intermediate–deep water column.

Due to weakening of the surface forcing associated with the NAO transition into neutral to low phase (1950s to mid-1960s, mid-1990s to mid-2000s), convection in the Labrador Sea weakens diminishing cold fresh water penetration into the intermediate layer. This results in warming and salinification at the intermediate depths in the Subpolar Gyre. Concurrently, the Subpolar Gyre contracts allowing northward advance of warm saline upper-ocean and intermediate subtropical waters in the northeastern North Atlantic. Northward progression of subtropical waters increases temperature and salinity at the upper intermediate levels and, correspondingly, increases temperature and salinity of the northeast Atlantic waters entrained into the Iceland–Scotland overflow along its pathway to the deep Iceland basin. As a result, temperature and salinity at the deep levels increase. The contrary changes – intensification of deep convection in the Labrador Sea and expansion of the Subpolar Gyre – caused by amplifying surface forcing (mid-1960s to mid-1990s) lead to cooling and freshening at the intermediate–deep levels. Additionally, under high-NAO conditions, deep convection may occur in the Irminger Sea potentially contributing to cooling and freshening at the intermediate (LSW) levels. The two regimes of convection and large-scale circulation corresponding to stronger (early 1990s) and weaker (mid-1960s, mid-2000s) NAO-related atmospheric forcing are schematically visualized in **Fig. 7**.

1.4.5 Deep-ocean salinity changes and climate change

There are increasing concerns that in the warmer climate, the MOC may substantially decline due to a decrease in the convective activity in the northern North Atlantic and Nordic Seas [e.g., Meehl et al., 2007]. The long-term freshening in the Nordic Seas and freshening of the northern North Atlantic deep waters in the 1960s–1990s have been considered as a likely indicator or precursor of the dramatic change in the MOC [e.g., Hansen et al., 2004]. The freshening has been attributed to a combination of factors potentially associated with the global warming: the increasing ice melt and net precipitation at high latitudes [e.g., Curry et al., 2003]. A probable causality between the climate change and the decreasing North Atlantic deep water

salinity has supported the concerns and unfavorable predictions, thus 'warming up' the reasonable scientific debate on climate change and overblown speculations in media.

Despite the long-term increase in freshwater input to the Arctic, freshening in the northern North Atlantic had reversed in the mid-1990s, as we demonstrated above. This reversal forces us to revise the hypotheses on the mechanisms behind the deep-water thermohaline anomalies. It seems doubtful that the persistent global temperature growth may lead to the opposite decadal trends (positive-then-negative-then-positive, **Fig. 6**) in the deep water salinity.

Our results [Sarafanov et al., 2008; Sarafanov, 2009; Sarafanov et al., 2010b] suggest that natural atmospheric variability over the North Atlantic plays the major role in the deep-water thermohaline variability on a decadal time scale. There are no reasons to associate the deep-water freshening in the 1960s–1990s with climate change, unless the 3-decade-long surface forcing amplification is evidently shown to be a consequence of the latter. Having said that, the net 1950s–2000s trends in the water mass salinities are negative implying that the global factors (e.g., probable intensification of hydrological cycle [Curry et al., 2003]) may act on longer time scales.

1.4.6 Decadal variability of the Deep Western Boundary Current at Cape Farewell

Recent decadal changes in the Deep Western Boundary Current (DWBC) transport southeast of Cape Farewell were assessed from hydrographic data (1991–2007, **Fig. 7a**), direct velocity measurements (2002–2006) and satellite altimetry (1992–2007). Following the approach used in earlier studies [e.g., Bacon, 1998], we first determined that the DWBC (σ_0>27.80) baroclinic transport (T_{BC}) referenced to 1000 m depth increased by ~2 Sv between the mid-1990s (1994–1997) and 2000s (2000–2007) (**Fig. 8b**) [Sarafanov et al., 2009]. In the next step, we quantified velocity changes at the reference level (1000 m) by combining estimates of the hydrography-derived velocity changes in the water column and the altimetry-derived velocity changes at the sea surface [see Sarafanov et al., 2010a]. The inferred increase in the southward velocity at 1000 m above the DWBC in 1994–2007 indicates that the increase in the DWBC absolute transport was larger but very close to the 2-Sv increase in the DWBC T_{BC}. This result along with the observed coherence of the DWBC absolute and baroclinic transport changes between individual observations [Sarafanov et al., 2010a] imply that the DWBC absolute

transport variability in the region is well represented by its baroclinic component on decadal and shorter time scales.

The historical record of the DWBC T_{BC} (1955–2007, **Fig. 8c**) updated after Bacon [1998] shows distinct decadal variability (±2–2.5 Sv) with the transport minima in the 1950s and mid-1990s, maximum in the early 1980s and moderate-to-high transport in the 2000s. The DWBC T_{BC} decadal variability is consistent with the general pattern of the recent decadal hydrographic and circulation changes in the northern North Atlantic. The DWBC T_{BC} anomalies negatively correlate (R = –0.80, 1955–2007) with thickness anomalies of the Labrador Sea Water (LSW) at its origin implying a close link between the DWBC transport southeast of Cape Farewell and the LSW production in the Labrador Sea (**Fig. 8d**). During the recent three decades (late 1970s – late 2000s), the DWBC T_{BC} changes were also in-phase with changes in the strength and zonal extent of the Subpolar Gyre [see Sarafanov et al., 2010a]. In particular, the Gyre weakening at shallow levels in the mid-1990s – mid-2000s was accompanied by the DWBC strengthening in the Irminger Sea [Sarafanov et al., 2009; Sarafanov et al., 2010a; Våge et al., 2011]. The results imply that the decadal changes in the (i) LSW production, (ii) SPG strength and (iii) DWBC transport in the Irminger Sea are linked, representing a complex coherent oceanic response to the decadal variability of the surface forcing.

1.4.7 Mean state of the full-depth circulation in the 2000s

A mean state of the full-depth summer circulation in the Atlantic Ocean in the region in between Cape Farewell (Greenland), Scotland and the Greenland-Scotland Ridge (see **Fig. 3**) was assessed by combining 2002–2008 yearly hydrographic measurements at 59.5°N, mean dynamic topography, satellite altimetry data and available estimates of the Atlantic–Nordic Seas exchange [see Sarafanov et al., 2012]. The mean absolute transports by the upper-ocean, mid-depth and deep currents and the MOC (MOCσ=16.5±2.2 Sv, at σ_0=27.55) at 59.5°N were quantified in the density space. Inter-basin and diapycnal volume fluxes in between the 59.5°N section and the Greenland-Scotland Ridge were then estimated from a box model.

The estimated meridional and diapycnal volume fluxes contributing to the MOC are schematically visualized in **Fig. 9**. The dominant components of the meridional exchange across 59.5°N are the North Atlantic Current (NAC, 15.5±0.8 Sv, σ_0<27.55) east of the Reykjanes Ridge, the northward Irminger Current (IC, 12.0±3.0 Sv) and southward Western Boundary

Current (WBC, 32.1±5.9 Sv) in the Irminger Sea and the deep water export from the northern Iceland Basin (3.7±0.8 Sv, σ_0>27.80). About 60% (12.7±1.4 Sv) of waters carried in the MOCσ upper limb (σ_0<27.55) by the NAC/IC across 59.5°N (21.1±1.0 Sv) recirculates westwards south of the Greenland-Scotland Ridge and feeds the WBC. 80% (10.2±1.7 Sv) of the recirculating NAC/IC-derived upper-ocean waters gains density of σ_0>27.55 and contributes to the MOCσ lower limb. Accordingly, the contribution of light-to-dense water conversion south of the Greenland-Scotland Ridge (~10 Sv) to the MOCσ lower limb at 59.5°N is one and a half times larger than the contribution of dense water production in the Nordic Seas (~6 Sv).

1.4.8 Cascading of dense shelf waters in the Irminger Sea

Based on the hydrographic data collected at 59.5°N, 64.3°N and 65–66°N in the western Irminger Sea in the 1990s – 2000s, an observational evidence for the deep-reaching cascading of dense shelf waters south of the Denmark Strait was found [Falina et al., 2012]. The data collected in the northwestern Irminger Sea (65–66°N) indicate that the East Greenland Current ~200 km south of the Denmark Strait occasionally carries shelf waters as dense as the overflow-derived deep waters transported by the DWBC (σ_0 > 27.80). Hydrographic traces of cascading of dense shelf waters down the East Greenland slope were found from repeat measurements at 64.3ºN, where the densest fresh plumes were observed within the DWBC (σ_0 > 27.80) (**Fig. 10**). Using the data collected at 59.5°N, we showed that the fresh 'signals' originating from the shelf can be traced in the DWBC as far downstream as the latitude of Cape Farewell, where the anomalously fresh oxygenated plumes are repeatedly observed in the ISOW and DSOW density classes.

The results of our analysis along with the results from earlier studies [e.g., Rudels et al., 1999; Rudels et al., 2002] indicate that shelf water cascading in the northern Irminger Sea is an intermittent process occurring in all seasons of the year. This implies that, despite the apparent short duration of a particular cascading event, the cumulative contribution of such events to the thermohaline variability and southward export of the deep waters in the WBC can be considerable. Our tentative estimate based on data from two synoptic surveys at ~59.5°N suggests that the transient contribution of a cascading event in the northern Irminger Sea to the DWBC transport at Cape Farewell can be as large as ~25%.

References

1. Bacon, S. (1998), Decadal variability in the outflow from the Nordic seas to the deep Atlantic Ocean, *Nature*, *394*, 871–874.
2. Dickson, R. R., and J. Brown (1994), The production of North Atlantic Deep Water: Sources, rates and pathways, *J. Geophys. Res.*, *99*, C6, 12319–12341.
3. Dickson, R., Yashayaev, I., Meincke, J., Turrell, B., Dye, S., and J. Holfort (2002), Rapid freshening of the deep North Atlantic Ocean over the past four decades, *Nature*, *416*, 832–837.
4. Boessenkool, K. P., Hall, I. R., Elderfield, H., and I. Yashayaev (2007), North Atlantic climate and deep-ocean flow speed changes during the last 230 years, *Geophys. Res. Lett.*, *34*, L13614, doi:10.1029/2007GL030285.
5. Curry, R., Dickson, R., and I. Yashayaev (2003), A change in the freshwater balance of the Atlantic Ocean over the past four decades, *Nature*, *426*, 826–829.
6. Falina, A., A. Sarafanov, and A. Sokov (2007), Variability and renewal of Labrador Sea Water in the Irminger Basin in 1991–2004, *J. Geophys. Res.*, *112*, C01006, doi: 10.1029/2005JC003348.
7. Falina A., A. Sarafanov, H. Mercier, P. Lherminier, A. Sokov, and N. Daniault (2012), On the cascading of dense shelf waters in the Irminger Sea, *J. Phys. Oceanogr.*, doi:http://dx.doi.org/10.1175/JPO-D-12-012.1 (in press)
8. Hansen, B., Osterhus S., Quadfasel D., and W. Turrell (2004), Already the day after tomorrow?, *Science*, *305*, 953–954.
9. Hurrell, J. W. (1995), Decadal trends in the North Atlantic Oscillation: regional temperatures and precipitation, *Science*, *269*, 676–679.
10. Koltermann, K. P., A. Sokov, V. Tereschenkov, S. Dobroliubov, K. Lorbacher, and A. Sy (1999), Decadal changes in the thermohaline circulation of the North Atlantic, *Deep Sea Res.*, *Part II*, *46*, 109–138, doi:10.1016/S0967-0645(98)00115-5.
11. Lherminier, P., H. Mercier, T. Huck, C. Gourcuff, F. F. Perez, P. Morin, A. Sarafanov, and A. Falina (2010), The Atlantic Meridional Overturning Circulation and the subpolar gyre observed at the A25–Ovide section in June 2002 and 2004, *Deep-Sea Res.*, *Part I*, *57*, 1374–1391, doi:10.1016/ j.dsr.2010.07.009.

12. Meehl, G. A., (2007), Global climate projections. Climate Change 2007: The Physical Science Basis, S. Solomon et al., Eds., Cambridge University Press, 747–847.
13. Pickart, R. S., Spall, M., Ribergaard, M. H., Moore, G. W. K. and R. Milliff (2003), Deep convection in the Irminger Sea forced by the Greenland tip jet, *Nature*, *424*, 152–156.
14. Rudels B., Eriksson P., Grönvall H., Hietala R. and Launiainen J. (1999), Hydrographic Observations in Denmark Strait in Fall 1997, and their Implications for the Entrainment into the Overflow Plume, *Geophys. Res. Lett.*, *26*, 1325–1328.
15. Rudels, B., E. Fahrbach, J. Meincke, G. Budeus, and P. Eriksson (2002), The East Greeenland Current and its contribution to the Denmark Strait overflow, *ICES J. Marine Science*, *59*, 1133–1154.
16. Sarafanov, A., A. Sokov, A. Demidov, and A. Falina (2007), Warming and salinification of intermediate and deep waters in the Irminger Sea and Iceland Basin in 1997–2006, *Geophys. Res. Lett.*, *34*, L23609, doi:10.1029/2007GL031074.
17. Sarafanov, A., A. Falina, A. Sokov, and A. Demidov (2008), Intense warming and salinification of intermediate waters of southern origin in the eastern subpolar North Atlantic in the 1990s to mid-2000s, *J. Geophys. Res.*, *113*, C12022, doi:10.1029/2008JC004975.
18. Sarafanov, A. (2009), On the effect of the North Atlantic Oscillation on temperature and salinity of the subpolar North Atlantic intermediate and deep waters, *ICES J. Marine Science*, *66 (7),* 1448–1454, doi:10.1093/icesjms/fsp094.
19. Sarafanov, A., A. Falina, H. Mercier, P. Lherminier, and A. Sokov (2009), Recent changes in the Greenland–Scotland overflow-derived water transport inferred from hydrographic observations in the southern Irminger Sea, *Geophys. Res. Lett.*, *36*, L13606, doi:10.1029/2009GL038385.
20. Sarafanov A., A. Falina, P. Lherminier, H. Mercier, A. Sokov, and C. Gourcuff (2010a), Assessing decadal changes in the Deep Western Boundary Current absolute transport southeast of Cape Farewell (Greenland) from hydrography and altimetry, *J. Geophys. Res.*, *115*, C11003, doi:10.1029/2009JC005811.
21. Sarafanov A., H. Mercier, A. Falina, A. Sokov, and P. Lherminier (2010b), Cessation and partial reversal of deep water freshening in the northern North Atlantic: observation-

based estimates and attribution, *Tellus*, *62A*, 80–90, doi:10.1111/j.1600-0870.2009.00418.x.

22. Sarafanov A., A. Falina, H. Mercier, A. Sokov, P. Lherminier, C. Gourcuff, S. Gladyshev, F. Gaillard, and N. Daniault (2012) Mean full-depth summer circulation and transports at the northern periphery of the Atlantic Ocean in the 2000s, *J. Geophys. Res., 117,* C01014, doi:10.1029/2011JC007572.
23. Schmitz, W. J., Jr., and M. S. McCartney (1993), On the North Atlantic Circulation, *Rev. Geophys.*, *31*, 29–49.
24. Schott, F. A., and P. Brandt (2007), Circulation and deep water export of the subpolar North Atlantic during the 1990s, *in Ocean Circulation: Mechanisms and Impacts*, *Geophys. Monograph Series*, *173*, Eds. A. Schmittner, J. Chiang, and S. Hemmings, 91–118, doi:10.1029/173GM08.
25. Sutherland, D. A., and R. S. Pickart (2008), The East Greenland Coastal Current: structure, variability, and forcing, *Prog. Oceanogr.*, *78*, 58–77, doi:10.1016/j.pocean.2007.09.006.
26. Våge K., R. Pickart, A. Sarafanov, Ø. Knutsen, H. Mercier, P. Lherminier, H. van Aken, J. Meincke, D. Quadfasel, and S. Bacon (2011a), The Irminger Gyre: circulation, convection, and interannual variability, *Deep-Sea Res. Part I*, *58*, 590–614, doi:10.1016/j.dsr.2011.03.001.
27. van Aken, H. M. (2007), The oceanic thermohaline circulation: An introduction, New York, Springer, 326 p., ISBN 978-0-387-36637-1.
28. Yashayaev, I. (2007), Hydrographic changes in the Labrador Sea, 1960–2005, *Prog. Oceanogr.*, *73*, 242–276.

.

1.5 Preliminary Results

The upper-ocean, mid-depth and deep water circulation patterns, merging the results of the present analysis with those from the earlier studies [e.g., *Macrander et al.*, 2005; *Østerhus et al.*, 2005, 2008; *Schott and Brandt*, 2007; *Sutherland and Pickart*, 2008; *Lherminier et al.*, 2010; *Våge et al.*, 2011], are schematically visualized Figures 12–14. A schematic diagram of the meridional overturning circulation in the Atlantic Ocean north of 59.5°N is displayed in Fig. 9.

The results provide the following conceptual view of the gyre / overturning circulation at the northern periphery of the Atlantic Ocean in the 2000s.

The NAC and IC collectively carry 21.1 ± 1.0 Sv of warm upper-ocean waters across 59.5°N northwards within the MOCσ upper limb ($\sigma_0 < 27.55$). About 40% of this flow forms the Atlantic Inflow to the Nordic Seas, and 60% (12.7 ± 1.4 Sv) recirculates westwards in the subpolar gyre northern limb south of Iceland to feed the WBC in the Irminger Sea. Only 20% (2.4 ± 1.2 Sv) of the recirculating NAC/IC-derived waters exits the Irminger Sea in the WBC at shallow levels ($\sigma_0 < 27.55$), while 80% (10.2 ± 1.7 Sv, a half of the NAC/IC northward flow across 59.5°N) gains density of $\sigma_0 > 27.55$ and enters the MOCσ lower limb. The resulting net southward transport in the MOCσ lower limb at the latitude of Cape Farewell is 16.5 ± 2.2 Sv, of which ~60% (~10.2 Sv) is due to light-to-dense water transformation south of the GSR.

As no dense-to-light water re-conversion is expected to occur in the subpolar gyre, the NAC/IC-derived waters, once entering the MOCσ lower limb in the Irminger Sea, will eventually contribute to the MOCz lower limb (~11 Sv at 59.5°N) at the southern margin of the subpolar region. There, at ~48°N, the MOCσ and MOCz are of nearly the same magnitude, 16 ± 2 Sv, as estimated from data collected in the 1990s [see *Schott and Brandt*, 2007; *Lumpkin et al.*, 2008]. This is very close to our estimate of the mean MOCσ at 59.5°N. The comparison is tentative, though, because it does take into account the decadal variability of the MOC [*Koltermann et al.*, 1999; *Willis*, 2010]. With this caveat in mind, our results imply a minor contribution to the MOCσ by the net dense water formation in the subpolar gyre between ~48°N and 59.5°N. This inference concurs with the results by *Pickart and Spall* [2007] suggesting a

minor contribution to the Atlantic MOC by the net water mass transformation in the Labrador Sea.

To conclude, the results of the present study, verified with independent estimates where possible, provide the first observation-based quantitative view of a mean state of the gyre / overturning circulation at the northern periphery of the Atlantic Ocean. The most interesting features of the obtain circulation pattern are as follows:

• Nearly half of volume of the upper-ocean waters transported northward across 59.5°N in the eastern limb of the subpolar gyre (NAC and IC, $\sigma_0 < 27.55$) overturns in the density plane south of the GSR and feeds the lower limb of the Atlantic MOCσ.

• The contribution to the MOCσ lower limb at 59.5°N by overturning (light-to-dense transformation) of the NAC / IC-derived upper-ocean waters south of the GSR is one and a half times as large as the contribution of the Nordic Seas overflows.

• The net southward flow in MOCσ lower limb at 59.5°N is associated primarily with the deep water ($\sigma_0 > 27.80$) export. Nearly half of the net southward flow of deep waters across 59.5°N is due to entrainment of the Atlantic waters in the Irminger Sea.

• The DWBC at 59.5°N is fed primarily by the Denmark Strait Overflow and by the diapycnal flux / entrainment from the mid-depth layer, while the contribution to the DWBC transport from the ISOW flow is minor. A major part of the ISOW transported into the Irminger Sea from the Charlie-Gibbs Fracture Zone recirculates southward in the eastern Irminger Sea and exits the basin via an interior pathway rather than along the western boundary. The results can be used for validation of numerical models. From this perspective, multi-year mean transports have an obvious advantage over individual section-based synoptic estimates, which bear the impress of vigorous variability occurring on a variety of spatial and temporal scales. The methodological outcome is that the combined use of repeat hydrography, the MDT by *Rio and Hernandez* [2004] and satellite altimetry data can provide a useful estimate of the mean full-depth circulation across a transatlantic section without imposing *a priori* constraints.

1.6 Major Problems and Goals Not Achieved

SBE 9P-0767 was replaced after two first stations because of power problem by SBE 9P-0743. The CTD secondary pump was replaced after sta. 2778 due to its bad performance (noisy data of the secondary sensors). Seasave did not work properly at sta. 2805 and 2824. This caused PC rebooting and forced us to repeat casts. There was large cable angle up to 15-20° during sta. 2691, 2702, 2736, 2770, 2771 and 2818 that influenced on LADCP data quality. The LADCP batteries were replaced after sta. 2663 and 2781. The Master did not collect data on sta. 2665 and stopped the data collection during up-cast at sta. 2662.

2. CONTINUOUS MEASUREMENTS (on station and underway)

2.1 Navigation

Navigation data from Trimble SPSx50/SPSx51 GPS was recorded every 1 second and was stored on the PC in binary format.

2.2 Meteorological Measurements

The standard mean meteorological measurements were stored in the separate files on the same PC with navigation data. Recording were running immediately after departure from Bremerhaven (Germany) on 26th May, and worked reliably until completion of the cruise in St. John's (Canada) on 29th June.

2.3 Thermosalinograph

SBE 21 S/N 3254 data were collected along the section line starting on May 28.

2.4 Echosounding

The bathymetric equipment aboard during RV Akademik Ioffe Cruise 38 consists of an ELAC 12 kHz hydrographic echosounder. Data were collected for most of the cruise. The Hull mounted transducer is located 5.8 metres below the sea surface and this value was entered to estimate the depth.

Depth was indicated on the echosounder display and stored on the PC together with the navigation.

Two files with extension NAV and MET with maximum size 256032 b were created. File name corresponded to GMT time when the file was opened for records.

2.5 Vessel Mounted Acoustic Doppler Current Profiler (VMADCP) OS 38 kHz

The Ocean Surveyor 38 kHz is designed for vessel-mount current profile measurement in the upper ocean water from depths greater than 40-50 meters. The system consists of a transducer and electronics chassis connected to PC. Data are transmitted in binary format through the I/O cable. GPS data in NMEA format are transmitted separately to another PC COM – port. The VMADCP can operate in two regimes (Narrow Bandwith and Broad Bandwith Profiling). Its main specifications are shown below.

To collect OS 38 kHz data we used *VmDas* software (version 1.46). The NMEA messages *VmDas* reads are standard GGA, HDG, HDT, VTG messages.

	Bin size	Maximum range	Accuracy $(cm/s)^2$
NarrowBand (long-range mode)	16 m	800 - 1000 m	30
	24 m	900 - 1200 m	23
BroadBand (high-precision mode)	16 m	520 - 730 m	12
	24 m	730 – 780 m	9

We used a following configuration to collect the data.

NP00001 – Narrow Bandwidth profiling
NN060 – number of bins 60
NS1600 – cell size 16 m
NF1600 – blanking size 16 m
BP00 – no bottom track (BP),

VmDas saves data in a few files with extension ENX, ENS, ENR (raw data with and without navigation), NR – NMEA messages, STA and LTA averaged data. Misalignment angle was introduced in configuration file and was used by VmDas for data correction.

Data processing performed STA files with 40-profile averaging. Taking into account that single ping takes about 3 seconds, one 40-profile ensemble lasts near 120 seconds in Narrow Bandwidth regime.

Data processing consists of data conversion in NetCDF format with extension NC and further cleaning, filtering, tide removing (using barotropic tidal model TPXO 7.2) and averaging. The standard averaging was 3 km. IFREMER software was used to process OS 38 kHz data.

3. ON-STATION MEASUREMENTS

3.1 CTD

3.1.1 Equipment

The deep profiler system used during the cruise included the following components: SBE 32 painted aluminum 24 bottle multisampler frame, SBE 9P-0743 CTD (SBE 9P-0767 during first two stations), Up and Down looking RD Instruments WHM – 300 kHz Acoustic Doppler Current Profiler (LADCP), Separate Battery pack pressure case ext. 6000 m connected to LADCPs with star cable, 24 x 5 litre Test Oceanic Niskin bottles, Benthos altimeter PSA-900D.

Lab equipment for data acquisition and archiving of CTD/LADCP data consisted of the following items mounted on the deck.

Pentium IV – Intel 2.2 GHz, PC Intel Core 2 Duo 2.4GHz Personal Computers. APC Back-UPS 550VA/330W, SBE 11p Deck Unit.

Cruise Preparation

Equipment and sensors were assembled when the ship crossed the North Sea (26-27th May). Water bottles were checked for integrity of seals, taps, stoppers and lanyards before being fitted and roped to the multisampler frame.

Deployment

At the beginning of the cruise the main CTD failed due to power problem. The spare CTD performed well during the cruise with little evident instrument drift and good accuracy.

The CTD was deployed with a lowering rate of 60 metres/min (30-40 metres/min in the upper 200 metres or deeper if the conditions are rough). It is recovered at a rate of 60 metres/min.

The LADCPs fitted within the frame with a separate battery pressure case performed well. These units contain a compass and tilt sensors which could possibly provide useful information on the attitude and rotation of the whole profiler package throughout deployments.

Bottle firing using the deck unit and pylon was very reliable during the cruise.

Operationally this has been a successful cruise with virtually no time being lost due to mechanical or equipment failure.

3.1.2 Data processing and calibration

CTD data were logged at 24 scans per second and passed from the CTD deck unit to the PC.

The CTD data was recorded onto disk by the PC using SEABIRD SEASOFT-Win 32: Seasave 7, Software Release 7.21d. A screen display of temperature, oxygen, salinity and density profiles vs pressure are used to decide the depths at which bottles are to be tripped on the up cast. The bottles are tripped using the enable and fire buttons on the PC screen. During post-processing, the SEASAVE software stores 35 scans at each bottle trip within a separate file. At the end of the station, all the data and header files associated with the station are transferred immediately via ethernet to the second PC. The SBE data processing software is used to create 1 dbar processed data files.

The data processing takes the following steps:

DATCNV Converts the raw data to physical parameters.

WILDEDIT For every block of 100 scans, flags all scans whose pressure, temperature, conductivity and oxygen values differ from the mean by more than 2 standard deviations. Recomputes mean from unflagged data then marks as bad all scans exceeding 20 standard deviations from these new values.

FILTER Low pass filter pressure channel with time constant used for pressure 0.150 seconds.

ALIGNCTD Aligns the oxygen values relative to the pressure values accounting for the time delays in the system. Time offsets of 4.000 secs for oxygen are used.

CELLTM A recursive filter used to remove the thermal mass effects from the conductivity data. Thermal anomaly amplitude and time constants of 0.0300 and 7.0000 were used.

LOOPEDIT Marks as bad, all cycles on the down trace for which the vertical velocity of the CTD unit is less than 0.25 metres/sec.

WINDOW FILTER cosine filter temperature and conductivity, window size 23 scans.

DERIVE Computes salinity, potential temperature, sigma-t, sigma theta and oxygen values.

BINAVG Averages the down cast into 1 dbar pressure bins.

SPLIT Splits the data into DOWN and UP cast.

Calibration data

The CTD calibrations used during this cruise were supplied by Sea Bird Electronics and are as follows:

Pre-cruise calibration:

CALIBRATION DATE: 21-Mar-2012 (all stations)

Conductivity Sensor 042827
Conductivity = (g + hf2 + if3 + jf4) /10(1 + dt + ep) Siemens/meter
t = temperature [°C)]; p = pressure[decibars]; d = CTcor; e= CPcor;
g = -1.0038502 9 e +001
h = 1.3712968 2 e +000
i = 3.6505478 5 e -005
j = 6.3168796 7 e -005
CPcor = -9.5700e-008
CTcor = 3.2500e-006

Post-cruise calibration:
CALIBRATION DATE: 27-Jul 2012 (all stations)
Conductivity Sensor S/N 042827
g = -1.0034748 3 e +001
h = 1.3698533 5 e +000
i = 4.6731011 0 e -004
j = 2.9400787 5 e -005
CPcor = -9.5700e-008
CTcor = 3.2500e-006
Average drift between *pre* and *post-cruise* calibrations: +0.0000 ms/m

Pre-cruise calibration:
CALIBRATION DATE: 22-Mar-12 (all stations)
Temperature Sensor S/N 034399
Temperature ITS-90 = 1/{g + h[*ln*(f0/f)] + i[*ln*2(f0/f)] + j[*ln*3(f0/f)]} - 273.15 (°C)
Following the recommendation of JPOTS: T68 is assumed to be 1.00024 * T90 (-2 to 35°C)
f is the frequency
g = 4.3633681 4 e -003
h = 6.3878530 3 e -004
i = 2.2117150 1 e -005
j = 1.9951788 6 e -006
f0 = 1000.0

Post-cruise calibration:
CALIBRATION DATE: 27-Jul-12 (all stations)
Temperature Sensor 034424
g = 4.3634177 2 e -003
h = 6.3886772 4 e -004
i = 2.2159173 8 e -005
j = 2.0006601 6 e -006
f0 = 1000.0
Average drift between *pre* and *post-cruise* calibrations: +0.00023 Degrees Celsius

Pressure Sensor S/N 89105 (all stations) no drift
CALIBRATION DATE: 27-June-11
C1 = -4.9053 7 1 e+004
C2 = -1.2105 9 4 e+000
C3 = 1.4283 5 0 e-002
D1 = 3.9016 0 0 e-002
D2 = 0.0000 0 0 e+000

T1 = 3.0010 1 7 e+001
T2 = -5.7583 8 4 e-004
T3 = 4.2101 2 0 e-006
T4 = 2.2654 0 0 e-009
T5 = 0.0000 0 0 e+000)
AD590M = 1.28912e-002
AD590B = -8.43097e+000
Slope = 0.99995
Offset = 1.4284 (dbars)

Oxygen Sensor 430699
CALIBRATION DATE: 18-Apr-2013 (All Stations)
$Oxygen(\ ml/l) = \{Soc * (V + Voffset)\} * Oxsat\ (T,S) * e^{(Tcorr*T)} * e^{(Pcor*P)}$

Where:
V = SBE 43 output voltage signal (volts)
T = CTD temperature (°C)
S = CTD salinity (psu)
P = CTD pressure (dbars)
Oxsat(T,S) = oxygen saturation (ml/l)
Soc, Voffset, tcor, and *pcor* are calibration coefficients

Let:
$\varphi = Oxsat\ (T,S) * e^{(Tcorr*T)} * e^{(Pcor*P)}$
$Oxygen(\ ml/l) = Soc * (V + Voffset) * \varphi$
$Oxygen(\ ml/l)/\ \varphi = Soc * (V + Voffset) = M * V + B$
Where:
Soc = M
Voffset = B / M

In our case for northern sections (sills)
Soc = 4.0404e-001
Tau = 0.0
Boc = 0.0000
Voffset = -0.3712
tcor = 0.001700
pcor = 1.35e-004

and for the section along 59.5 N

Soc = 4.1315e-001
Tau = 0.0
Boc = 0.0000
Voffset = -0.4255
tcor = 0.001700
pcor = 1.35e-004

3.1.3 Final Post-Cruise CTD Calibrations

Temperature Calibration Temperature Sensor 034399

Because of the small sensor drift between *pre*- and *post*-cruise calibrations (+0.00023°C) we used *pre-calibration coefficients* for all stations of the cruise, introducing correction equaled -+0.00020°C.

Pressure Calibration Pressure Sensor S/N 89105

Final CTD pressure correction: Since no drift for pressure sensor was defined by SeaBird Electronics pressure was corrected for atmospheric pressure only. With offset in *.con* or *.xmlcon* file set to -0.0026 db, pressure measured by CTD should equal barometric pressure

• Calculate offset (db) = barometer reading – CTD reading

– Conversion of psia to decibars: decibars = (psia - 14.7) * 0.6894759

• Enter calculated offset in *.con* or *.xmlcon* file

• Example:

– CTD reads -2.5 dbars

– Barometer reads 14.65 psia.

Converting to decibars, barometer reads (14.65 - 14.7) * 0.6894759 = -0.034 dbars

– offset (db) = barometer reading – CTD reading = -0.034 - (-2.5) = 2.466

Salinity Calibration Conductivity Sensor 042827

We used *pre-cruise calibration coefficients* for all stations of the cruise corrected by -0.0019 PSU (sensor slope correction 1.0000484). This drift was defined by taking 860 salinity samples from depth deeper than 300 m between 29 May and 23 June 2012. These samples were measured with Autosal 8400 B laboratory salinometer (S/N 67465) between 30th May and 24th June. The results of these measurements are shown in **Fig. 11**.

Description of Equipment and Technique

Salinity samples are analyzed on Guildline Autosal model 8400 B salinometer. Samples are drawn in 150 ml dark glass medicine bottles. All bottles were equipped with plastic liners and caps. The salinometer cell is filled and rinsed three times with sample water before readings are recorded. Minimum three salinometer readings were recorded for every sample and standardization. If the values are fluctuating, more readings are taken.

Sampling Procedure and Data Processing Technique

Salinity samples are drawn into 150 ml medicine bottles after three rinses. The bottles are filled up to the shoulders and then capped with caps with plastic liners. Files for each separate run are prepared. These files consist of various metadata (date, cruise, lab temperature, geographic location, operator, etc.) and sample specific data such as the bath temperature, sample ID number, and average conductivity ratio. A PC based program computes the salinity using average conductivity ratio of the runs and the standard IAPSO formula. Any changes in the salinometer readings between successive standardizations are assumed to have occurred as a linear drift of the instrument. Thus, the program applies a correction to the ratios, which varies linearly with the samples analyzed. The salinity data is then placed in the water sample database.

Laboratory and Sample Temperatures

Full cases of samples are taken from the winch room to the salinometer lab where they are left for a period of at least 24 hours to equilibrate to laboratory temperature before being analyzed.
The bath in the salinometer was kept at 21°C.

Standards Used

The salinometer was standardized using IAPSO standard water, Batch P152, dated May, 2013. Standardization with a new bottle was carried out at the beginning and end of the run as well as after 50 bottle samples.

3.1.4 SBE 43 Dissolved Oxygen Sensor Calibration using Winkler Titrations

We use a method for statistically estimating calibration coefficients for calculating dissolved oxygen in milliliters per liter from SBE 43 output voltage. The technique requires dissolved oxygen concentration in ml/l (determined from Winkler titration of water samples) and SBE 43 oxygen voltage outputs at the times the water samples were collected. Sea-Bird's data processing software, SBE Data Processing, is used to produce a data table suitable for the analysis.

Background

The equation used in Sea-Bird's software for calculating dissolved oxygen in ml/l from SBE 43 output voltage is a form of that given in Owens-Millard (1985):

$$Oxygen(\ ml/l) = \{Soc * (V + Voffset + tau * \partial V/\partial t) + Boc * e^{(-0.03*T)}\} * Oxsat\ (T,S) * e^{(Tcorr*T)} * e^{(Pcor*P)} \qquad eqn\ 1$$

Where:
V = SBE 43 output voltage signal (volts)
$\partial V/\partial t$ = time derivative of SBE 43 output signal (volts/second)
T = CTD temperature (°C)
S = CTD salinity (psu)
P = CTD pressure (dbars)
$Oxsat(T,S)$ = oxygen saturation (ml/l)
Soc, Boc, Voffset, tau, tcor, and *pcor* are calibration coefficients

Characterization of the SBE 43 in the laboratory and ocean suggest that the most accurate results are obtained by setting *Boc* and *tau* to zero. Equation 1 then reduces to:

$$Oxygen(\ ml/l) = \{Soc * (V + Voffset)\} * Oxsat\ (T,S) * e^{(Tcorr*T)} * e^{(Pcor*P)} \qquad eqn\ 2$$

The SBE 43 is expected to provide an output voltage that is linear with respect to oxygen concentration. Normal calibration drift manifests itself as a loss of sensitivity and is evident as a change of slope and offset in the linear relationship between oxygen concentration and voltage output. The coefficients *tcor* and *pcor* correct for small secondary responses to temperature and pressure. Because these coefficients change very slowly over time, the values given on the SBE 43 calibration certificate are used in this analysis.

Setting *Boc* and *tau* to zero, we will rearrange equation 2 into a linear form and perform a linear regression to obtain a new *Soc* and *Voffset*.

Let:
$\varphi = Oxsat\ (T,S) * e^{(Tcorr*T)} * e^{(Pcor*P)}$

The oxygen equation then reduces to:
$Oxygen(\ ml/l) = Soc * (V + Voffset) * \varphi$

This may be expressed in a linear form as shown in equation 3 below. A linear regression is calculated using Winkler oxygen concentration divided by φ as the dependent variable and SBE 43 output voltage as the independent variable.

$$Oxygen(\ ml/l)/\varphi = Soc * (V + Voffset) = M * V + B \qquad eqn\ 3$$

Where:

Soc = M
Voffset = B / M

Winkler oxygen divided by φ versus SBE 43 output voltage for this cruise is shown in **Fig. 12** and includes a linear regression line calculated from the data.

The *Soc* value is 4.0404e-001.
The *Voffset* value is -0.3712 for the sill sections
and
The *Soc* = 4.1315e-001
The *Voffset* = -0.4255 for the transatlantic section along 59.5 N

2509 oxygen samples were used to build this linear fits (1342 samples for the sill sections and 1167 samples for the 59.5 N line, correspondingly).

Procedure

As a first step, extract pressure, temperature, salinity, oxygen saturation, and SBE 43 voltage from the parts of your CTD data collected when the water sampler closures occurred.

We run SBE Data Processing, and select Data Conversion in the Run menu. Select the appropriate configuration (*.con*) and data (*.dat*) files on the *File Setup* tab. In the *Data Setup* tab we set *Convert data from* to *Upcast and downcast* and *Create file types* to *Create bottle (.ros) file only*.

To extract CTD data concurrent to the water sampler closures, Data Conversion must know when the closures occurred. Select an appropriate *Source of scan range data*, depending on your instrument type and how the sampler was commanded to close bottles:

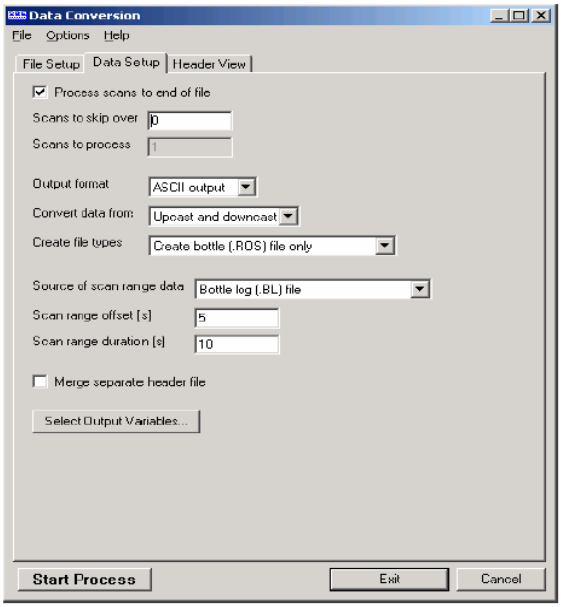

• SBE 9*plus* with SBE 11*plus* - The data stream is marked with a *bottle confirm* bit each time a closure occurred.
• Using SEASAVE to operate the water sampler - A *.bl* file, with scan ranges corresponding to closures, is created during the cast.

Like all sensors, the SBE 43 has a finite response time to a change in dissolved oxygen concentration. This response time is usually on the order of 6 seconds. For this reason, good sampling procedure dictates that the instrument package should be stopped in the water column long enough for the SBE 43 and all other sensors to completely equilibrate before closing the water sampler. An equilibration time of 5 to 6 response times, or 30 to 36 seconds, is adequate. We used to wait 30 seconds.

Data Conversion is extracting data 5 seconds before each water sampler closure and will extract 10 seconds of data. Note that 10 seconds is longer than the SBE 43 response time. Because we are extracting data for 5 seconds after the water sampler closure, the instrument package must remain stopped for at least this long.

To estimate *Soc* and *Voffset*, we need pressure, temperature, salinity, oxygen saturation (ml/l), and SBE 43 Oxygen Voltage to go with each Winkler titration data value. We use *Select Output Variables* and add each of the required parameters; the dialog box is shown below.

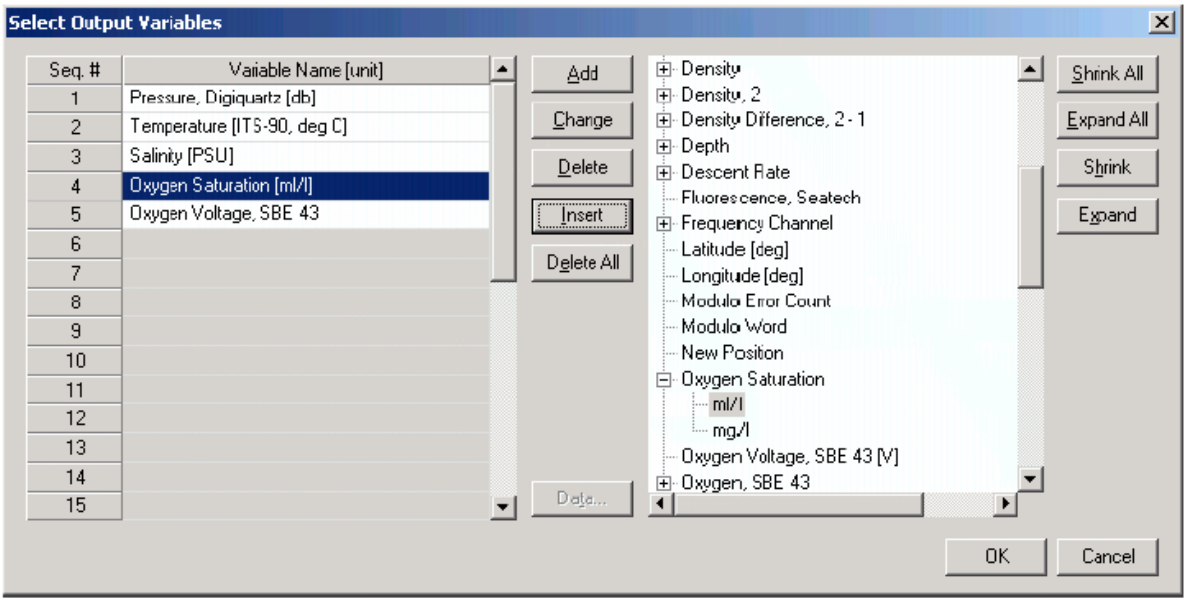

After selecting all the variables, click *OK* to return to the Data Conversion Data Setup tab. Then click *Start Process* to create the *.ros* file.

In our case, the *.ros* file contains 10 seconds of data centered on the moment the bottle closure occurred for every bottle closure. To make a useful table, we select Rosette Summary from SBE Data Processing's Run menu. Rosette Summary calculates averages and standard deviations for the variables selected in Data Conversion. Select the appropriate *.con* and *.ros* files on the *File Setup* tab. To average the data in the *Data Setup* tab we click the *Select Averaged Variables* button; after selecting all the variables, click *OK* to return to the Rosette Summary Data Setup tab. Then click *Start Process* to create a data table file with the *.btl* extension.

Further, we run a program READBTLDATA to create a file with average pressure, temperature, salinity, oxygen saturation, and SBE 43 output voltage for each water sampler closure depth, by importing the *.btl* file and the Winkler titration dissolved oxygen values from our titration log, matching water sampler closures to number of station, bottle number and pressures. The program also calculates φ, using *tcor* and *pcor* from the SBE 43 calibration sheet.

Then, calculate *Winkler* O_2 / φ.

Using the table we perform a linear regression, with:

- *Winkler* O_2 / φ (shown as Winkler/phi in the table) as the *Y* data
- SBE 43 output voltages as the *X* data

Reference

Owens, W. B., and R. C. Millard Jr., 1985: A new algorithm for CTD oxygen calibration. J. Physical Oceanography, 15, 621-631.
(NOTE: calibration expressed as ml/l)

3.2 Oxygen Bottle Samples

Oxygen samples were drawn first from every bottle. Duplicate samples were taken on each cast, usually from the first two bottles. Samples were drawn into clear, wide necked calibrated glass bottles and fixed on deck with reagents dispensed using Aquastep bottle top dispensers. A test station used to check on the oxygen bottle calibrations and as an opportunity to train a number of people to take the samples. The samples were shaken on deck and again in the laboratory 1/2 hour after collection, when the bottles were checked for the tightness of the stoppers and presence of bubbles. The samples were then stored under water until analysis.

Bottle temperatures were taken, following sampling for oxygen, using a hand held electronic thermometer probe. The temperatures were used to calculate any temperature-dependent changes in the sample bottle volumes.

Samples were analyzed in the constant temperature laboratory, starting three hours after sample collection, following the Winkler whole bottle titration with an amperometric method of endpoint detection, as described by Culberson (1991). The equipment used was supplied by Metrohm and included the Titrino unit and control pad, exchange unit with 10 ml burette to dispense the thiosulphate in increments of 2 μl , with an electrode for amperometric end point detection.

The difference for the duplicate pairs sampled on each station was in a range 0.00-0.03 ml/l (Table 2).

The thiosulphate normality was checked on each run and recalculated every time the reservoir was topped up against potassium iodate. The exact weight of this standard, the calibrated 5 ml exchange unit driven by a Metrohm Dosimat and the 1L glass volumetric flask used to dispense and prepare the standard.

The introduction of oxygen with the reagents and impurities in the manganese chloride were corrected for by blank measurements made on each run, as described in the WOCE Manual of Operations and Methods (Culberson, 1991).

Collected data shows that dissolved oxygen concentrations varied from 4.78 to 9.34 ml/l. In order to control the accuracy of the oxygen measurements at each cast were taken parallel samples from the 1-2 bottles or duplicate samples.

Reproducibility of measurements

7664 samples were taken during the cruise; in addition, 1022 duplicates were analyzed. Statistics on the duplicates are given in Table 2. These include both duplicates taken from the same bottle (replicates) and those taken from different bottles fired at the same depth. The data gave a standard deviation of 0.005 ml/l, or 0.074%.

3.3 Nutrient Bottle Samples

Samples for nutrient measurements were collected following oxygen samples from each Niskin bottle. Water was collected in clean plastic containers that had been rinsed three times by seawater through the latex tube.

Concentrations of silicate and phosphate were determined by photometric methods with spectrophotometer Cary 100 Seam Varian. All samples were analyzed immediately after sampling.

Silicate determined by Korolev's method based on colorimeter of blue silicomolybdic complex (methodology described in Modern methods..., 1992). The ascorbic acid used as a restorative. The absorbance was read at 810 nm. Relative error of this method on concentration of dissolved silicate at 4.5 μM is ±4%, on concentration at 45 μM - ± 2,5%. Measured concentrations were in a range from 0.03 to 17.16 μM.

Phosphates determined according to the method Murphy and Raily (Modern methods..., 1992). Phosphate, dissolved in sea water, react with ammonium molibdate in a presence of sulfuric acid and tartrate potassium-antimony. The generated complex aggregate of phosphomolybdic heteropolyacid and trivalent antimony restorative by the ascorbic acid, and then determined the absorbance at 885 nm (we use the cavity 10cm). Relative error of this method ± 1%.

In order to ensure accuracy and increase precision of determination 3-8 duplicate samples were analyzed at each run. The mean difference for the duplicate pairs sampled on each station was in a error limits of the methods (Table 2).

References:

Culberson, C.H. 1991.15 pp in the WOCE Operations Manual (WHP Operations and Methods) WHPO 91/1, Woods Hole.

Modern methods of hydrochemical research of the ocean, 1992. IO RAS, Moscow (in Russian).

(O. Lukyanova)

3.4 Lowered Acoustic Doppler Current Profiler (LADCP)

The TRDI WHS 300 kHz ADCPs consists of a pressure case rated to 6000 metres with 4 transducers at one end in a convex arrangement and the beams diverging at 20 degrees from the vertical. At the opposite end to the transducers is a connector that enables downloading of data and connects it to other pressure cases containing another ADCP and the power supply pack. This arrangement allowed the ADCPs and the battery pack to be mounted vertically as up and down-looking on the CTD frame. Connection amongst all units was established using star cable with three male and two female terminations. Two male cable ends were always attached to the frame, this enabled comms leads to be readily connected pre and post deployment.

Communications: The 20-m communication leads (which also allow external power to be supplied to the ADCP) were sufficiently long to route it through to the port side of the deck lab where it was connected to a dedicated PC and external power supply. The latter was set at 48+ volts and was left on whilst the ADCP was on deck. 5 minutes prior to deployment the external power supply was shut off, the instrument checked and the configuration file sent to the ADCP as described in the manual instructions. The free end of the fly leads was greased and the end cap refitted, this was then taped to the frame for security.

Post deployment: When the CTD/LADCP was brought inboard, the fly-lead connectors were dried and the comms leads were connected to them. This stopped undue bending of the cables and kept them clear of the water bottles, aiding sampling. External power was applied again and the cast data downloaded as per the manual with a baud rate of 57600. The processing is accomplished using software developed by Visbeck after transferring the data to the PC.

Battery power was supplied to the ADCP in the form of 42 volts from 28 x 1.5 volt alkaline cells. Four of these packs were available for the cruise, as the ADCP will function at a minimum of 32 volts this was deemed an adequate stock for the duration.

Data quality: The data quality from the ADCP was good throughout. Due to the bad weather instrument titles sometimes exceeded 12° and this data was rejected during processing.

The LADCPs seem to function well and generates useful information on currents. The battery supply has its limitations though and thought should be given to alternatives to the present set-up.

3.4.1 LADCP Processing for Current Profiles

A brief account of the LADCP current data processing, file nomenclature and directory structure is provided in the following lines. Little emphasis is put into a detailed description of the main programming tools used, since these are part of a standard software package developed by by Gerd Krahmann (version 10.13).

Outline of LADCP current calculation method

The Broad Band LADCP used during AI38 cruise was designed to measure the instantaneous relative velocities of scatterers in the water column by taking advantage of the Doppler frequency shift, phase changes and correlation between coded pulses transmitted and received by the LADCP's four transducers. Conversion of this raw data stream to a profile of absolute currents involved an elaborate calculation method.

Firstly, Doppler shifts needed to be scaled to velocity units by taking into account the depth-dependent sound velocity (estimated from CTD T and S measurements). Directions could be inferred from trigonometric calculations based on the geometry of the transducer set, the orientation of the package (measured with a flux gate compass) and the local magnetic declination. The depth of the instrument was calculated from the integration of the measured vertical velocity and later adjusted to match the depth given by the CTD's pressure sensor.

The velocities corresponding to each single ensemble (or, in effect, to each transducer ping) were gridded in bins of depth set 10 meters. Statistical rejection of spiky measurements within each of these bins followed.

In order to reject the unwanted motion of the instrument (but also the barotropic component of the current), shear profiles were calculated for each ensemble. A complicated editing scheme preceded this shear calculation. A final shear profile (baroclinic current) was derived by real- depth gridding of the shear profiles calculated for individual ensembles. It was hoped that any relative velocities introduced by the high-frequency motion of the CTD package would be smoothed out by this repeated averaging.

The barotropic component of the flow was finally calculated from bottom-tracking measurements (bottom-track mode) or, in most occasions, in an integral sense from differential GPS positions of the ship (water-track mode).

The definitive velocity profile was hence obtained as the sum of the baroclinic and barotropic components.

During AI38 cruise, no specific error calculation was performed. Profiles of shear standard deviation were included in the cast log sheet folder. Internal wave signals were obvious throughout the cruise.

Relevant PC files

The raw data were downloaded from the LADCP into a devoted PC after each cast and stored as a binary file called vNNNNm_01.000 for Master and vNNNNs_01.000 for Slave the c:\ladcp\AI38\dNNN

directory, where NNNN stands for the CTD cast number, e.g. raw data from cast 2721 were stored in the files d:\AI38\data\ladcp\v2721m_01.000 and v2721s_01..000.

The configuration files (named Mconf.txt and Sconf.txt) containing the operating instructions (setting of track mode, bin depth, etc.) given to the LADCP previously to deployment was stored in the same directory.

Text files of the form NNNNm.log and NNNNs.log are the log of the 'bbtalk' session (testing the state and functioning of the instrument) previous to deployment. The details of the sessions for every single cast in the cruise are to be found in the cast log sheets.

A whole variety of files were created and manipulated during the different processing stages, and no mention will be made of the majority of them for reasons of clarity. The processing procedure may be summarised in two steps:

1- create CTD pressure, temperature and salinity data file as well as navigation collected every second in order to obtain the best possible estimates of depth and sound velocity. This is done using 'SBE Data Processing software and ConvLADCP Fortran program.
2- use the Gerd Krahmann's standard matlab package (v.10.13) with P. Lherminier's improvements (IFREMER) to process LADCP and CTD data

References

M. Visbeck 1994: Deep Velocity Profiling using Lowered Acoustic Doppler Current Profiler: Bottom Track and Inverse Solutions J. Atmos. Oceanic Technol. 10, 764-773.

3.5 Carbonate System Measurements

The QUIMA-ULPGC group has been invited by Drs. Sokov and Gladyshev from Shirshov Institute of Oceanology (SIO), Russian Academy of Science to collaborate in the project "Interannual monitoring of thermohaline and current structure along 59.5º N for evaluation of climate change in the North Atlantic" inside the hydrographic section CLIVAR A5930N (A1E), as responsible of the carbon parameters measurements. This is the fourth time that the group has been invited to participate in the project. This year the QUIMA-ULPGC group has also participated in the sections between Shetlands-Feroes-Island-Greenland. Four member of the group participated in the cruise, Dr. J. Magdalena Santana-Casiano, two postgraduate students and one technician. The data treatment and discussions of the results are responsibility of Dr. J. M. Santana-Casiano and Dr. Melchor González-Dávila

From 26-5-2012 to 1-7-2012 the Oceanography Cruise AI38 took place on board R/V Akademik Ioffe departing from the Bremerhaven Harbor. Two sections were done. The first (section 1) - Shetlands-Faroes-Island-Greenland-Faroes-Shetlands, and the second (section 2), the section 59.5ºN, (CLIVAR A1E) from Europe to Greenland.

3.5.1. Measured parameters

In both sections three parameters of the carbon dioxide system were measured along the water column in order to achieve the highest level of data quality and resolution: the pH, the total alkalinity and the total dissolved inorganic carbon.

- The pH was measured in total scale, $pH_{T,15ºC}$, by a potentiometry technique using the TRIS buffer to calibrate the electrodes (González-Dávila et al., 2003). In the section 2, the pH was also measured by the UV-Vis spectrophotometric technique using the m-cresol purple as a dye (Clayton and Byrne, 1993). An intercalibration exercise between these two techniques was done during the section 2.

- The total alkalinity, AT in μmol kg^{-1} was measured by potentiometry (Mintrop et al., 2000). CRM reference material was used to check the method.

- The total disolved inorganic carbon, CT in μmol kg^{-1}, was measured using a VINDTA 3C system by coulombimetry (Mintrop et al., 2000). CRM were also used for the quality control.

3.5.2 Sampling procedure

500 ml glass bottles were used for the determination of AT. 100 ml glass bottles were used to analyse both CT and pH. The bottles were rinsed twice with seawater and over-filled with seawater. Samples were preserved from the light and analysed between stations. In shallow stations and in case the samples are not possible to be analysed for CT in less than 5 hours after sampling, they were poisoned with $HgCl_2$ (60 μl, saturated solution).

3.5.3 Stations and parameters sampled

Table 1 and 2 show the number of station done for each section and the amount of sampled measured for the pH, AT and CT. A total of 206 stations have been done considering the two sections, with 2750 Niskin bottles closed and 2646 Niskin sampled (the non-repetitive one) for the carbon dioxide parameters. 2644 samples were analyzed for potentiometric pH, 983 for UV-Vis spectrophotometric pH, 2603 for AT and 2179 for CT

References

- Mintrop, L., Pérez, F.F., González-Dávila, M., Santana-Casiano, J.M., Körtzinger, A., 2000. Alkalinity determination by potentiometry: Intercalibration using three different methods, Ciencias Marinas 26, 23-37.
- González-Dávila, M., Santana-Casiano, J. M., Rueda, M. J., Llinás, O., González-Dávila, E., 2003. Seasonal and interanual variability of sea-surface carbon dioxide species at the European station for Time Series in the Ocean at the Canary Islands (ESTOC) between 1996 and 2000. Global. Biochem. Cycles 17(3), 1076, doi:10.1029/2002GB001993.
- Clayton, T. D. Byrne, R.H., 1993. Spectrophotometric seawater pH measurements: total hydrogen ion concentration scale calibration of m-cresol purple and at-sea results, Deep Sea Res. I 40, 2115-2129.

(Dr. J. M. Santana-Casiano)

4. CRUISE LOGISTICS

Mobilization

Mobilization for the cruise took place on the way from Bremerhaven (Germany) to the first station of the cruise. It took three days. The scientific team arrived at the ship on May 23th.

ACKNOWLEDGEMENTS

The principal scientists would like to thank the Master, officers, crew and scientists of the RV Akademik Ioffe for making this such an enjoyable, as well as successful cruise.

TABLES

FIGURES

Fig. l Station location and ship track (in red). The shelf area with depth less than 200 m is shaded

Fig.2 Vertical distribution of samples (a) along the sill sections, (b) along the 59.5 section.

Fig. 3. Schematic diagram of the large-scale circulation in the northern North Atlantic compiled from [Schmitz and McCartney, 1993; Schott and Brandt, 2007; Sutherland and Pickart, 2008; Lherminier et al., 2010]. Abbreviations for the main topographic features, currents and water masses are explained in the legend. The nominal locations of the 59.5°N hydrographic section (1997 – present) and sections across the straits between Greenland, Iceland, Faeroe and Shetland Islands (2011 – present) are shown with the solid green lines.

Fig. 4. Oxygen concentrations (ml/l) in the water column (lower panel) as observed in March–October 1997 in four hydrographic sections (upper panel) ending nearby the southern tip of Greenland. A separate oxygen maximum in the LSW layer (1000–2000 m) in the Irminger Sea at 59.5°N strongly implies local convective renewal of LSW before 1997. Adapted from [Falina et al., 2007].

Fig. 5. Warming and salinification in the northern North Atlantic between the mid-1990s and mid-2000s, as observed at 59.5°N. The figure shows the 2006–1997 temperature (°C, left) and salinity (right) differences on isobaric surfaces in the Irminger Sea and Iceland Basin. Adapted from [Sarafanov et al., 2007].

Fig. 6. Coherence of the decadal salinity changes (1950s – 2000s) of the intermediate (LSW) and deep (ISOW) waters in the northern North Atlantic and their link to the North Atlantic Oscillation (NAO) index. **(a)** Schematic representation of the LSW and ISOW pathways and locations of the Icelandic Low (L) and Azores High (H) centers constituting the NAO dipole pattern. The red dotted line indicates the 59.5°N transatlantic section. **(b)** Salinity time series for LSW in the Labrador Sea [Yashayaev, 2007] and ISOW in the Iceland basin [Boessenkool et al., 2007; Sarafanov et al., 2007] overlaid by the third order polynomial fits. **(c)** Time series of the winter NAO index, after [Hurrell, 1995], overlaid by 7-year running mean and third order polynomial fit. **(d)** Mechanism of the NAO effect on the decadal changes in temperature (T) and salinity (S) of the northern North Atlantic intermediate and deep waters. Positive / negative links shown with the dark / light grey arrows mean that changes in ‘causative’ and ‘consequential’ characteristics have the same / opposite sign(s). The overall effect of the NAO on T and S of the in the water column is negative: persistent NAO decline leads to warming and salinification of the water masses and vice versa, as shown in (b) and (c). Adapted from [Sarafanov, 2009].

Fig. 7. Schematic representation of the upper-ocean circulation and convection intensity in the northern North Atlantic under high (left) and low (right) NAO conditions. Blue (magenta) solid arrows indicate the upper-ocean flows with higher fraction of colder fresher subpolar (warmer saltier subtropical) waters. The main pathways of the Nordic overflow-derived deep waters are shown with the dotted curves. "C" and "E" symbols are used to denote, respectively, the deep convection sites and the domain, where the Atlantic waters are entrained into ISOW. Larger (smaller) circles indicate stronger (weaker) convection. SPG and STG – the subpolar and subtropical gyres, respectively. Adapted from [Sarafanov, 2009].

Fig. 8. The Deep Western Boundary Current (DWBC) transport variability and its link to the convection intensity in the Labrador Sea. **(a)** Locations of the hydrographic sections (1991–2007) and schematic of the deep water circulation in the Irminger Sea. **(b)** The DWBC transport anomalies at Cape Farewell in 1991–2007, 1 Sv = 10^6 m^3 s^{-1}. The 1994–1997 and 2000–2007 mean anomalies and the 1994–2007 linear trend are shown. **(c)** Anomalies of the DWBC transport at Cape Farewell and the Labrador Sea Water (LSW) thickness in the Labrador Sea in the 1950s–2000s. **(d)** Correlation coefficient (R^2) for the two times series shown in **(c)** at the 0–5-year lag, the LSW thickness leads. The correlation maximum is achieved at the 1–3-year lag. The DWBC transport anomalies in the southern Irminger Sea are foregone by the convection intensity anomalies in the Labrador Sea. Adapted from [Sarafanov et al., 2009].

Fig. 9. Schematic diagram of the Meridional Overturning Circulation (MOC) at the northern periphery of the Atlantic Ocean, northeast of Cape Farewell. The dotted lines refer to the σ_0 isopycnals 27.55 and 27.80. The arrows denote the integral meridional and diapycnal volume fluxes. Where the signs are specified, the positive (negative) transports are northward (southward). The NAC and EGIC transports in the upper layer ($\sigma_0 < 27.55$) at 59.5°N are the throughputs accounting for the recirculations. EGIC – the East Greenland / Irminger Current – refers to the upper part of the Western Boundary Current. Other abbreviations are explained in the legend to **Fig. 3**. Adapted from [Sarafanov et al., 2012].

Fig. 10. Salinity observed in the northwestern Irminger Sea at 64.3°N in February 1998. The σ_0 isopycnals 27.55, 27.70, 27.80 and 27.88 are plotted as the thick black lines; the station locations are marked with the ticks on the top axis. The plot shows fresh dense waters descending (cascading) down the continental slope of Greenland down to the LSW layer ($27.70 < \sigma_0 < 27.80$) and the layer of the Nordic Seas overflow-derived deep waters ($\sigma_0 > 27.80$). Adapted from [Falina et al., 2012].

.

R/V Ak. Ioffe CRUISE 38 **Table 1**

SHIP/CRS	CLIVAR		UTC			POSITION						
STNNBR	CASTNO	TYPE	DATE	TIME	CODE	LATITUDE	LONGITUDE	NAV	DEPTH	BOTTOM	BOTTLES	COMMENTS
2621	1	ROS	052812	1944	BE	60 24.9 N	001 54.7 W	GPS	0113.79	6	6	CTD,LADCP,O2,SiO3,PO4,CO2
2621	1	ROS	052812	1957	BO	60 25.0 N	001 55.0 W	GPS	0113.79	6	6	CTD,LADCP,O2,SiO3,PO4,CO2
2621	1	ROS	052812	2006	EN	60 25.0 N	001 55.1 W	GPS	0113.79	6	6	CTD,LADCP,O2,SiO3,PO4,CO2
2622	1	ROS	052812	2133	BE	60 31.0 N	002 15.2 W	GPS	0144.49	5	8	CTD,LADCP,O2,SiO3,PO4,CO2
2622	1	ROS	052812	2147	BO	60 31.2 N	002 15.4 W	GPS	0144.49	5	8	CTD,LADCP,O2,SiO3,PO4,CO2
2622	1	ROS	052812	2156	EN	60 31.1 N	002 15.5 W	GPS	0144.49	5	8	CTD,LADCP,O2,SiO3,PO4,CO2
2623	1	ROS	052812	2323	BE	60 37.6 N	002 35.3 W	GPS	0122.83	20	0	CTD,LADCP,O2,SiO3,PO4,CO2
2623	1	ROS	052812	2336	BO	60 38.0 N	002 35.7 W	GPS	0122.83	20	0	CTD,LADCP,O2,SiO3,PO4,CO2
2623	1	ROS	052812	2337	EN	60 38.0 N	002 35.8 W	GPS	0122.83	20	0	CTD,LADCP,O2,SiO3,PO4,CO2
2623	2	ROS	052812	2340	BE	60 38.0 N	002 35.8 W	GPS	0134.44	3	7	CTD,LADCP,O2,SiO3,PO4,CO2
2623	2	ROS	052812	2344	BO	60 38.0 N	002 36.0 W	GPS	0134.44	3	7	CTD,LADCP,O2,SiO3,PO4,CO2
2623	2	ROS	052812	2354	EN	60 37.9 N	002 36.0 W	GPS	0134.44	3	7	CTD,LADCP,O2,SiO3,PO4,CO2
2624	1	ROS	052912	0122	BE	60 44.8 N	002 54.5 W	GPS	0358.13	5	10	CTD,LADCP,O2,SiO3,PO4,CO2
2624	1	ROS	052912	0137	BO	60 45.0 N	002 54.9 W	GPS	0358.13	5	10	CTD,LADCP,O2,SiO3,PO4,CO2
2624	1	ROS	052912	0153	EN	60 45.0 N	002 55.1 W	GPS	0358.13	5	10	CTD,LADCP,O2,SiO3,PO4,CO2
2624	2	ROS	052912	0239	BE	60 45.2 N	002 54.9 W	GPS	0359.10	4	9	CTD,LADCP,O2,SiO3,PO4,CO2
2624	2	ROS	052912	0252	BO	60 45.1 N	002 54.7 W	GPS	0359.10	4	9	CTD,LADCP,O2,SiO3,PO4,CO2
2624	2	ROS	052912	0305	EN	60 45.2 N	002 54.9 W	GPS	0359.10	4	9	CTD,LADCP,O2,SiO3,PO4,CO2
2625	1	ROS	052912	0439	BE	60 51.9 N	003 17.5 W	GPS	0692.25	4	14	CTD,LADCP,O2,SiO3,PO4,CO2
2625	1	ROS	052912	0500	BO	60 52.0 N	003 18.0 W	GPS	0692.25	4	14	CTD,LADCP,O2,SiO3,PO4,CO2
2625	1	ROS	052912	0523	EN	60 52.0 N	003 18.1 W	GPS	0692.25	4	14	CTD,LADCP,O2,SiO3,PO4,CO2
2626	1	ROS	052912	0647	BE	60 59.0 N	003 38.0 W	GPS	1115.08	6	18	CTD,LADCP,O2,SiO3,PO4,CO2
2626	1	ROS	052912	0711	BO	60 59.1 N	003 38.5 W	GPS	1115.08	6	18	CTD,LADCP,O2,SiO3,PO4,CO2
2626	1	ROS	052912	0747	EN	60 59.1 N	003 39.1 W	GPS	1115.08	6	18	CTD,LADCP,O2,SiO3,PO4,CO2
2627	1	ROS	052912	0856	BE	61 04.1 N	003 51.9 W	GPS	1161.47	4	15	CTD,LADCP,O2,SiO3,PO4,CO2
2627	1	ROS	052912	0921	BO	61 04.1 N	003 52.2 W	GPS	1161.47	4	15	CTD,LADCP,O2,SiO3,PO4,CO2
2627	1	ROS	052912	0954	EN	61 04.0 N	003 52.8 W	GPS	1161.47	4	15	CTD,LADCP,O2,SiO3,PO4,CO2
2628	1	ROS	052912	1052	BE	61 07.9 N	004 03.6 W	GPS	1135.47	4	16	CTD,LADCP,O2,SiO3,PO4,CO2
2628	1	ROS	052912	1115	BO	61 07.9 N	004 03.7 W	GPS	1135.47	4	16	CTD,LADCP,O2,SiO3,PO4,CO2

2628	1	ROS	052912	1147	EN	61 08.0 N	004 04.1 W	GPS	1135.47	4	16	CTD,LADCP,O2,SiO3,PO4,CO2
2629	1	ROS	052912	1254	BE	61 12.0 N	004 17.7 W	GPS	1090.86	6	15	CTD,LADCP,O2,SiO3,PO4,CO2
2629	1	ROS	052912	1315	BO	61 12.0 N	004 17.9 W	GPS	1090.86	6	15	CTD,LADCP,O2,SiO3,PO4,CO2
2629	1	ROS	052912	1346	EN	61 11.9 N	004 18.1 W	GPS	1090.86	6	15	CTD,LADCP,O2,SiO3,PO4,CO2
2630	1	ROS	052912	1451	BE	61 15.9 N	004 27.8 W	GPS	1066.23	6	16	CTD,LADCP,O2,SiO3,PO4,CO2
2630	1	ROS	052912	1518	BO	61 16.3 N	004 27.8 W	GPS	1066.23	6	16	CTD,LADCP,O2,SiO3,PO4,CO2
2630	1	ROS	052912	1549	EN	61 16.5 N	004 27.5 W	GPS	1066.23	6	16	CTD,LADCP,O2,SiO3,PO4,CO2
2631	1	ROS	052912	1655	BE	61 19.9 N	004 43.0 W	GPS	0735.59	7	12	CTD,LADCP,O2,SiO3,PO4,CO2
2631	1	ROS	052912	1711	BO	61 20.0 N	004 43.2 W	GPS	0735.59	7	12	CTD,LADCP,O2,SiO3,PO4,CO2
2631	1	ROS	052912	1731	EN	61 20.0 N	004 43.3 W	GPS	0735.59	7	12	CTD,LADCP,O2,SiO3,PO4,CO2
2632	1	ROS	052912	1840	BE	61 24.9 N	005 00.9 W	GPS	0226.69	5	7	CTD,LADCP,O2,SiO3,PO4,CO2
2632	1	ROS	052912	1851	BO	61 24.8 N	005 01.0 W	GPS	0226.69	5	7	CTD,LADCP,O2,SiO3,PO4,CO2
2632	1	ROS	052912	1901	EN	61 24.7 N	005 01.2 W	GPS	0226.69	5	7	CTD,LADCP,O2,SiO3,PO4,CO2
2633	1	ROS	052912	2014	BE	61 30.8 N	005 18.5 W	GPS	0289.86	6	9	CTD,LADCP,O2,SiO3,PO4,CO2
2633	1	ROS	052912	2027	BO	61 30.9 N	005 19.0 W	GPS	0289.86	6	9	CTD,LADCP,O2,SiO3,PO4,CO2
2633	1	ROS	052912	2039	EN	61 30.9 N	005 19.4 W	GPS	0289.86	6	9	CTD,LADCP,O2,SiO3,PO4,CO2
2634	1	ROS	052912	2155	BE	61 37.0 N	005 35.7 W	GPS	0322.33	7	10	CTD,LADCP,O2,SiO3,PO4,CO2
2634	1	ROS	052912	2206	BO	61 36.9 N	005 36.2 W	GPS	0322.33	7	10	CTD,LADCP,O2,SiO3,PO4,CO2
2634	1	ROS	052912	2218	EN	61 36.7 N	005 36.3 W	GPS	0322.33	7	10	CTD,LADCP,O2,SiO3,PO4,CO2
2635	1	ROS	052912	2340	BE	61 42.4 N	005 57.2 W	GPS	0300.44	3	9	CTD,LADCP,O2,SiO3,PO4,CO2
2635	1	ROS	052912	2352	BO	61 42.5 N	005 57.4 W	GPS	0300.44	3	9	CTD,LADCP,O2,SiO3,PO4,CO2
2635	1	ROS	053012	0005	EN	61 42.4 N	005 57.8 W	GPS	0300.44	3	9	CTD,LADCP,O2,SiO3,PO4,CO2
2636	1	ROS	053012	0147	BE	61 50.0 N	006 21.5 W	GPS	78.93	6	4	CTD,LADCP,O2,SiO3,PO4,CO2
2636	1	ROS	053012	0158	BO	61 50.2 N	006 22.1 W	GPS	78.93	6	4	CTD,LADCP,O2,SiO3,PO4,CO2
2636	1	ROS	053012	0202	EN	61 50.2 N	006 22.1 W	GPS	78.93	6	4	CTD,LADCP,O2,SiO3,PO4,CO2
2637	1	ROS	053012	0947	BE	62 19.9 N	007 15.2 W	GPS	92.35	5	4	CTD,LADCP,O2,SiO3,PO4,CO2
2637	1	ROS	053012	0953	BO	62 19.9 N	007 15.5 W	GPS	92.35	5	4	CTD,LADCP,O2,SiO3,PO4,CO2
2637	1	ROS	053012	0959	EN	62 19.9 N	007 15.7 W	GPS	92.35	5	4	CTD,LADCP,O2,SiO3,PO4,CO2
2638	1	ROS	053012	1133	BE	62 25.9 N	007 39.2 W	GPS	105.76	5	5	CTD,LADCP,O2,SiO3,PO4,CO2
2638	1	ROS	053012	1141	BO	62 25.9 N	007 39.8 W	GPS	105.76	5	5	CTD,LADCP,O2,SiO3,PO4,CO2
2638	1	ROS	053012	1148	EN	62 25.8 N	007 40.0 W	GPS	105.76	5	5	CTD,LADCP,O2,SiO3,PO4,CO2
2639	1	ROS	053012	1334	BE	62 35.0 N	008 01.7 W	GPS	414.35	5	10	CTD,LADCP,O2,SiO3,PO4,CO2
2639	1	ROS	053012	1344	BO	62 35.1 N	008 01.8 W	GPS	414.35	5	10	CTD,LADCP,O2,SiO3,PO4,CO2

2639	1	ROS	053012	1403	EN	62 35.1 N	008 02.2 W	GPS	414.35	5	10	CTD,LADCP,O2,SiO3,PO4,CO2
2640	1	ROS	053012	1556	BE	62 43.9 N	008 26.9 W	GPS	488.25	4	14	CTD,LADCP,O2,SiO3,PO4,CO2
2640	1	ROS	053012	1613	BO	62 43.9 N	008 26.8 W	GPS	488.25	4	14	CTD,LADCP,O2,SiO3,PO4,CO2
2640	1	ROS	053012	1631	EN	62 43.9 N	008 26.8 W	GPS	488.25	4	14	CTD,LADCP,O2,SiO3,PO4,CO2
2641	1	ROS	053012	1802	BE	62 50.8 N	008 50.0 W	GPS	466.49	5	11	CTD,LADCP,O2,SiO3,PO4,CO2
2641	1	ROS	053012	1816	BO	62 51.0 N	008 49.9 W	GPS	466.49	5	11	CTD,LADCP,O2,SiO3,PO4,CO2
2641	1	ROS	053012	1835	EN	62 51.0 N	008 49.8 W	GPS	466.49	5	11	CTD,LADCP,O2,SiO3,PO4,CO2
2642	1	ROS	053012	1949	BE	62 57.8 N	009 09.0 W	GPS	449.03	4	12	CTD,LADCP,O2,SiO3,PO4,CO2
2642	1	ROS	053012	2003	BO	62 57.9 N	009 09.2 W	GPS	449.03	4	12	CTD,LADCP,O2,SiO3,PO4,CO2
2642	1	ROS	053012	2022	EN	62 57.8 N	009 09.6 W	GPS	449.03	4	12	CTD,LADCP,O2,SiO3,PO4,CO2
2643	1	ROS	053012	2208	BE	63 05.8 N	009 37.5 W	GPS	496.91	5	13	CTD,LADCP,O2,SiO3,PO4,CO2
2643	1	ROS	053012	2224	BO	63 05.9 N	009 37.6 W	GPS	496.91	5	13	CTD,LADCP,O2,SiO3,PO4,CO2
2643	1	ROS	053012	2243	EN	63 05.9 N	009 37.5 W	GPS	496.91	5	13	CTD,LADCP,O2,SiO3,PO4,CO2
2644	1	ROS	053112	0014	BE	63 13.7 N	009 57.4 W	GPS	487.64	6	12	CTD,LADCP,O2,SiO3,PO4,CO2
2644	1	ROS	053112	0033	BO	63 14.0 N	009 58.0 W	GPS	487.64	6	12	CTD,LADCP,O2,SiO3,PO4,CO2
2644	1	ROS	053112	0051	EN	63 13.9 N	009 58.3 W	GPS	487.64	6	12	CTD,LADCP,O2,SiO3,PO4,CO2
2645	1	ROS	053112	0242	BE	63 19.9 N	010 24.7 W	GPS	331.62	5	9	CTD,LADCP,O2,SiO3,PO4,CO2
2645	1	ROS	053112	0301	BO	63 20.0 N	010 24.9 W	GPS	331.62	5	9	CTD,LADCP,O2,SiO3,PO4,CO2
2645	1	ROS	053112	0314	EN	63 20.0 N	010 24.8 W	GPS	331.62	5	9	CTD,LADCP,O2,SiO3,PO4,CO2
2646	1	ROS	053112	0502	BE	63 28.9 N	010 49.0 W	GPS	446.69	8	11	CTD,LADCP,O2,SiO3,PO4,CO2
2646	1	ROS	053112	0514	BO	63 28.9 N	010 48.9 W	GPS	446.69	8	11	CTD,LADCP,O2,SiO3,PO4,CO2
2646	1	ROS	053112	0530	EN	63 29.0 N	010 48.8 W	GPS	446.69	8	11	CTD,LADCP,O2,SiO3,PO4,CO2
2647	1	ROS	053112	0709	BE	63 35.9 N	011 14.9 W	GPS	305.81	4	11	CTD,LADCP,O2,SiO3,PO4,CO2
2647	1	ROS	053112	0718	BO	63 35.8 N	011 14.9 W	GPS	305.81	4	11	CTD,LADCP,O2,SiO3,PO4,CO2
2647	1	ROS	053112	0733	EN	63 35.8 N	011 14.7 W	GPS	305.81	4	11	CTD,LADCP,O2,SiO3,PO4,CO2
2648	1	ROS	053112	0917	BE	63 43.9 N	011 39.9 W	GPS	349.13	5	10	CTD,LADCP,O2,SiO3,PO4,CO2
2648	1	ROS	053112	0928	BO	63 43.8 N	011 40.4 W	GPS	349.13	5	10	CTD,LADCP,O2,SiO3,PO4,CO2
2648	1	ROS	053112	0942	EN	63 43.6 N	011 40.9 W	GPS	349.13	5	10	CTD,LADCP,O2,SiO3,PO4,CO2
2649	1	ROS	053112	1111	BE	63 50.0 N	011 59.7 W	GPS	391.22	5	14	CTD,LADCP,O2,SiO3,PO4,CO2
2649	1	ROS	053112	1123	BO	63 49.9 N	012 00.1 W	GPS	391.22	5	14	CTD,LADCP,O2,SiO3,PO4,CO2
2649	1	ROS	053112	1141	EN	63 49.9 N	012 00.4 W	GPS	391.22	5	14	CTD,LADCP,O2,SiO3,PO4,CO2
2650	1	ROS	053112	1312	BE	63 56.8 N	012 19.5 W	GPS	467.15	6	15	CTD,LADCP,O2,SiO3,PO4,CO2
2650	1	ROS	053112	1333	BO	63 57.0 N	012 21.2 W	GPS	467.15	6	15	CTD,LADCP,O2,SiO3,PO4,CO2

2650	1	ROS	053112	1353	EN	63 57.1 N	012 21.8 W	GPS	467.15	6	15	CTD,LADCP,O2,SiO3,PO4,CO2
2651	1	ROS	053112	1508	BE	64 00.9 N	012 37.7 W	GPS	583.32	5	14	CTD,LADCP,O2,SiO3,PO4,CO2
2651	1	ROS	053112	1525	BO	64 00.9 N	012 37.7 W	GPS	583.32	5	14	CTD,LADCP,O2,SiO3,PO4,CO2
2651	1	ROS	053112	1557	EN	64 00.3 N	012 37.9 W	GPS	583.32	5	14	CTD,LADCP,O2,SiO3,PO4,CO2
2652	1	ROS	053112	1658	BE	64 05.1 N	012 51.9 W	GPS	574.52	7	14	CTD,LADCP,O2,SiO3,PO4,CO2
2652	1	ROS	053112	1713	BO	64 05.4 N	012 51.7 W	GPS	574.52	7	14	CTD,LADCP,O2,SiO3,PO4,CO2
2652	1	ROS	053112	1737	EN	64 05.9 N	012 51.0 W	GPS	574.52	7	14	CTD,LADCP,O2,SiO3,PO4,CO2
2653	1	ROS	053112	1821	BE	64 07.7 N	013 02.6 W	GPS	166.86	6	6	CTD,LADCP,O2,SiO3,PO4,CO2
2653	1	ROS	053112	1832	BO	64 07.9 N	013 02.7 W	GPS	166.86	6	6	CTD,LADCP,O2,SiO3,PO4,CO2
2653	1	ROS	053112	1839	EN	64 07.9 N	013 02.7 W	GPS	166.86	6	6	CTD,LADCP,O2,SiO3,PO4,CO2
2654	1	ROS	053112	1954	BE	64 14.0 N	013 20.8 W	GPS	174.74	7	6	CTD,LADCP,O2,SiO3,PO4,CO2
2654	1	ROS	053112	2002	BO	64 14.1 N	013 20.7 W	GPS	174.74	7	6	CTD,LADCP,O2,SiO3,PO4,CO2
2654	1	ROS	053112	2010	EN	64 14.1 N	013 20.7 W	GPS	174.74	7	6	CTD,LADCP,O2,SiO3,PO4,CO2
2655	1	ROS	053112	2111	BE	64 16.8 N	013 35.5 W	GPS	159.04	7	6	CTD,LADCP,O2,SiO3,PO4,CO2
2655	1	ROS	053112	2121	BO	64 16.9 N	013 35.5 W	GPS	159.04	7	6	CTD,LADCP,O2,SiO3,PO4,CO2
2655	1	ROS	053112	2128	EN	64 16.8 N	013 35.5 W	GPS	159.04	7	6	CTD,LADCP,O2,SiO3,PO4,CO2
2656	1	ROS	053112	2321	BE	64 24.5 N	014 02.8 W	GPS	107.23	6	5	CTD,LADCP,O2,SiO3,PO4,CO2
2656	1	ROS	053112	2330	BO	64 24.4 N	014 03.0 W	GPS	107.23	6	5	CTD,LADCP,O2,SiO3,PO4,CO2
2656	1	ROS	053112	2337	EN	64 24.3 N	014 03.2 W	GPS	107.23	6	5	CTD,LADCP,O2,SiO3,PO4,CO2
2657	1	ROS	060212	1818	BE	65 34.7 N	024 54.5 W	GPS	66.54	5	5	CTD,LADCP,O2,SiO3,PO4,CO2
2657	1	ROS	060212	1829	BO	65 35.0 N	024 54.7 W	GPS	66.54	5	5	CTD,LADCP,O2,SiO3,PO4,CO2
2657	1	ROS	060212	1834	EN	65 35.2 N	024 54.7 W	GPS	66.54	5	5	CTD,LADCP,O2,SiO3,PO4,CO2
2658	1	ROS	060212	1940	BE	65 39.9 N	025 15.7 W	GPS	91.86	6	5	CTD,LADCP,O2,SiO3,PO4,CO2
2658	1	ROS	060212	1948	BO	65 40.1 N	025 16.1 W	GPS	91.86	6	5	CTD,LADCP,O2,SiO3,PO4,CO2
2658	1	ROS	060212	1953	EN	65 40.1 N	025 16.1 W	GPS	91.86	6	5	CTD,LADCP,O2,SiO3,PO4,CO2
2659	1	ROS	060212	2110	BE	65 44.8 N	025 38.2 W	GPS	271.47	4	9	CTD,LADCP,O2,SiO3,PO4,CO2
2659	1	ROS	060212	2121	BO	65 44.8 N	025 38.4 W	GPS	271.47	4	9	CTD,LADCP,O2,SiO3,PO4,CO2
2659	1	ROS	060212	2131	EN	65 44.8 N	025 38.5 W	GPS	271.47	4	9	CTD,LADCP,O2,SiO3,PO4,CO2
2660	1	ROS	060212	2246	BE	65 49.7 N	025 59.7 W	GPS	223.35	5	8	CTD,LADCP,O2,SiO3,PO4,CO2
2660	1	ROS	060212	2256	BO	65 49.7 N	025 59.9 W	GPS	223.35	5	8	CTD,LADCP,O2,SiO3,PO4,CO2
2660	1	ROS	060212	2306	EN	65 49.6 N	026 00.0 W	GPS	223.35	5	8	CTD,LADCP,O2,SiO3,PO4,CO2
2661	1	ROS	060312	0044	BE	65 55.8 N	026 28.5 W	GPS	284.64	6	9	CTD,LADCP,O2,SiO3,PO4,CO2
2661	1	ROS	060312	0057	BO	65 55.7 N	026 29.0 W	GPS	284.64	6	9	CTD,LADCP,O2,SiO3,PO4,CO2

2661	1	ROS	060312	0107	EN	65 55.5 N	026 29.2 W	GPS	284.64	6	9	CTD,LADCP,O2,SiO3,PO4,CO2
2662	1	ROS	060312	0224	BE	66 00.9 N	026 47.5 W	GPS	446.2	6	12	CTD,LADCP,O2,SiO3,PO4,CO2
2662	1	ROS	060312	0238	BO	66 00.8 N	026 47.8 W	GPS	446.2	6	12	CTD,LADCP,O2,SiO3,PO4,CO2
2662	1	ROS	060312	0253	EN	66 00.6 N	026 48.0 W	GPS	446.2	6	12	CTD,LADCP,O2,SiO3,PO4,CO2
2663	1	ROS	060312	0413	BE	66 04.9 N	027 03.0 W	GPS	658.13	5	15	CTD,LADCP,O2,SiO3,PO4,CO2
2663	1	ROS	060312	0444	BO	66 05.0 N	027 04.7 W	GPS	658.13	5	15	CTD,LADCP,O2,SiO3,PO4,CO2
2663	1	ROS	060312	0505	EN	66 05.1 N	027 05.2 W	GPS	658.13	5	15	CTD,LADCP,O2,SiO3,PO4,CO2
2664	1	ROS	060312	0621	BE	66 09.0 N	027 14.9 W	GPS	521.27	5	15	CTD,LADCP,O2,SiO3,PO4,CO2
2664	1	ROS	060312	0633	BO	66 09.1 N	027 15.0 W	GPS	521.27	5	15	CTD,LADCP,O2,SiO3,PO4,CO2
2664	1	ROS	060312	0656	EN	66 09.3 N	027 14.8 W	GPS	521.27	5	15	CTD,LADCP,O2,SiO3,PO4,CO2
2665	1	ROS	060312	0910	BE	66 06.3 N	027 16.7 W	GPS	593.62	5	17	CTD,LADCP,O2,SiO3,PO4,CO2
2665	1	ROS	060312	0925	BO	66 06.4 N	027 16.6 W	GPS	593.62	5	17	CTD,LADCP,O2,SiO3,PO4,CO2
2665	1	ROS	060312	0948	EN	66 06.5 N	027 16.5 W	GPS	593.62	5	17	CTD,LADCP,O2,SiO3,PO4,CO2
2666	1	ROS	060312	1055	BE	66 08.5 N	027 14.0 W	GPS	556.57	6	14	CTD,LADCP,O2,SiO3,PO4,CO2
2666	1	ROS	060312	1107	BO	66 08.5 N	027 14.0 W	GPS	556.57	6	14	CTD,LADCP,O2,SiO3,PO4,CO2
2666	1	ROS	060312	1127	EN	66 08.4 N	027 13.9 W	GPS	556.57	6	14	CTD,LADCP,O2,SiO3,PO4,CO2
2667	1	ROS	060312	1318	BE	66 05.0 N	027 02.9 W	GPS	661.49	5	16	CTD,LADCP,O2,SiO3,PO4,CO2
2667	1	ROS	060312	1332	BO	66 04.9 N	027 03.1 W	GPS	661.49	5	16	CTD,LADCP,O2,SiO3,PO4,CO2
2667	1	ROS	060312	1356	EN	66 04.7 N	027 03.5 W	GPS	661.49	5	16	CTD,LADCP,O2,SiO3,PO4,CO2
2668	1	ROS	060312	1506	BE	66 00.9 N	026 48.2 W	GPS	448.93	3	12	CTD,LADCP,O2,SiO3,PO4,CO2
2668	1	ROS	060312	1517	BO	66 00.8 N	026 48.1 W	GPS	448.93	3	12	CTD,LADCP,O2,SiO3,PO4,CO2
2668	1	ROS	060312	1532	EN	66 00.6 N	026 48.1 W	GPS	448.93	3	12	CTD,LADCP,O2,SiO3,PO4,CO2
2669	1	ROS	060312	1654	BE	65 56.0 N	026 29.1 W	GPS	289.86	6	9	CTD,LADCP,O2,SiO3,PO4,CO2
2669	1	ROS	060312	1702	BO	65 56.0 N	026 29.1 W	GPS	289.86	6	9	CTD,LADCP,O2,SiO3,PO4,CO2
2669	1	ROS	060312	1713	EN	65 56.0 N	026 29.2 W	GPS	289.86	6	9	CTD,LADCP,O2,SiO3,PO4,CO2
2670	1	ROS	060312	1855	BE	65 49.8 N	025 59.9 W	GPS	224.01	6	8	CTD,LADCP,O2,SiO3,PO4,CO2
2670	1	ROS	060312	1904	BO	65 49.9 N	025 59.9 W	GPS	224.01	6	8	CTD,LADCP,O2,SiO3,PO4,CO2
2670	1	ROS	060312	1913	EN	65 50.0 N	025 59.8 W	GPS	224.01	6	8	CTD,LADCP,O2,SiO3,PO4,CO2
2671	1	ROS	060312	2029	BE	65 45.1 N	025 38.3 W	GPS	274.67	7	8	CTD,LADCP,O2,SiO3,PO4,CO2
2671	1	ROS	060312	2049	BO	65 45.0 N	025 38.5 W	GPS	274.67	7	8	CTD,LADCP,O2,SiO3,PO4,CO2
2671	1	ROS	060312	2059	EN	65 45.0 N	025 38.6 W	GPS	274.67	7	8	CTD,LADCP,O2,SiO3,PO4,CO2
2672	1	ROS	060312	2226	BE	65 40.1 N	025 15.6 W	GPS	94.69	5	5	CTD,LADCP,O2,SiO3,PO4,CO2
2672	1	ROS	060312	2238	BO	65 40.1 N	025 15.6 W	GPS	94.69	5	5	CTD,LADCP,O2,SiO3,PO4,CO2

2672	1	ROS	060312	2243	EN	65 40.1 N	025 15.7 W	GPS	94.69	5	5	CTD,LADCP,O2,SiO3,PO4,CO2
2673	1	ROS	060312	2356	BE	65 34.9 N	024 54.9 W	GPS	65.79	6	4	CTD,LADCP,O2,SiO3,PO4,CO2
2673	1	ROS	060412	0008	BO	65 34.5 N	024 54.6 W	GPS	65.79	6	4	CTD,LADCP,O2,SiO3,PO4,CO2
2673	1	ROS	060412	0013	EN	65 34.4 N	024 54.7 W	GPS	65.79	6	4	CTD,LADCP,O2,SiO3,PO4,CO2
2674	1	ROS	060512	2053	BE	64 24.7 N	014 02.7 W	GPS	107.2	7	5	CTD,LADCP,O2,SiO3,PO4,CO2
2674	1	ROS	060512	2109	BO	64 24.9 N	014 02.6 W	GPS	107.2	7	5	CTD,LADCP,O2,SiO3,PO4,CO2
2674	1	ROS	060512	2114	EN	64 24.9 N	014 02.6 W	GPS	107.2	7	5	CTD,LADCP,O2,SiO3,PO4,CO2
2675	1	ROS	060512	2306	BE	64 16.8 N	013 36.5 W	GPS	161.08	6	6	CTD,LADCP,O2,SiO3,PO4,CO2
2675	1	ROS	060512	2316	BO	64 16.9 N	013 36.3 W	GPS	161.08	6	6	CTD,LADCP,O2,SiO3,PO4,CO2
2675	1	ROS	060512	2324	EN	64 16.9 N	013 36.3 W	GPS	161.08	6	6	CTD,LADCP,O2,SiO3,PO4,CO2
2676	1	ROS	060612	0041	BE	64 13.7 N	013 20.9 W	GPS	176.49	2	6	CTD,LADCP,O2,SiO3,PO4,CO2
2676	1	ROS	060612	0052	BO	64 13.7 N	013 21.2 W	GPS	176.49	2	6	CTD,LADCP,O2,SiO3,PO4,CO2
2676	1	ROS	060612	0100	EN	64 13.6 N	013 21.4 W	GPS	176.49	2	6	CTD,LADCP,O2,SiO3,PO4,CO2
2677	1	ROS	060612	0244	BE	64 07.5 N	013 02.5 W	GPS	188.08	9	6	CTD,LADCP,O2,SiO3,PO4,CO2
2677	1	ROS	060612	0313	BO	64 06.7 N	013 02.9 W	GPS	188.08	9	6	CTD,LADCP,O2,SiO3,PO4,CO2
2677	1	ROS	060612	0321	EN	64 06.3 N	013 03.5 W	GPS	188.08	9	6	CTD,LADCP,O2,SiO3,PO4,CO2
2678	1	ROS	060612	0445	BE	64 05.0 N	012 52.2 W	GPS	585.69	8	13	CTD,LADCP,O2,SiO3,PO4,CO2
2678	1	ROS	060612	0503	BO	64 04.8 N	012 52.5 W	GPS	585.69	8	13	CTD,LADCP,O2,SiO3,PO4,CO2
2678	1	ROS	060612	0521	EN	64 04.6 N	012 53.4 W	GPS	585.69	8	13	CTD,LADCP,O2,SiO3,PO4,CO2
2679	1	ROS	060612	0639	BE	64 01.0 N	012 38.0 W	GPS	572.08	6	14	CTD,LADCP,O2,SiO3,PO4,CO2
2679	1	ROS	060612	0655	BO	64 00.9 N	012 38.3 W	GPS	572.08	6	14	CTD,LADCP,O2,SiO3,PO4,CO2
2679	1	ROS	060612	0716	EN	64 01.0 N	012 38.5 W	GPS	572.08	6	14	CTD,LADCP,O2,SiO3,PO4,CO2
2680	1	ROS	060612	0836	BE	63 56.8 N	012 20.3 W	GPS	464.13	5	15	CTD,LADCP,O2,SiO3,PO4,CO2
2680	1	ROS	060612	0855	BO	63 57.0 N	012 20.4 W	GPS	464.13	5	15	CTD,LADCP,O2,SiO3,PO4,CO2
2680	1	ROS	060612	0913	EN	63 56.9 N	012 20.9 W	GPS	464.13	5	15	CTD,LADCP,O2,SiO3,PO4,CO2
2681	1	ROS	060612	1045	BE	63 49.9 N	011 59.9 W	GPS	389.52	7	11	CTD,LADCP,O2,SiO3,PO4,CO2
2681	1	ROS	060612	1057	BO	63 49.8 N	011 59.6 W	GPS	389.52	7	11	CTD,LADCP,O2,SiO3,PO4,CO2
2681	1	ROS	060612	1111	EN	63 49.7 N	011 59.2 W	GPS	389.52	7	11	CTD,LADCP,O2,SiO3,PO4,CO2
2682	1	ROS	060612	1232	BE	63 44.0 N	011 40.0 W	GPS	349.35	5	12	CTD,LADCP,O2,SiO3,PO4,CO2
2682	1	ROS	060612	1242	BO	63 43.9 N	011 39.9 W	GPS	349.35	5	12	CTD,LADCP,O2,SiO3,PO4,CO2
2682	1	ROS	060612	1256	EN	63 43.7 N	011 39.7 W	GPS	349.35	5	12	CTD,LADCP,O2,SiO3,PO4,CO2
2683	1	ROS	060612	1441	BE	63 35.9 N	011 15.0 W	GPS	305.4	5	9	CTD,LADCP,O2,SiO3,PO4,CO2
2683	1	ROS	060612	1450	BO	63 35.8 N	011 15.0 W	GPS	305.4	5	9	CTD,LADCP,O2,SiO3,PO4,CO2

2683	1	ROS	060612	1502	EN	63 35.6 N	011 15.0 W	GPS	305.4	5	9	CTD,LADCP,O2,SiO3,PO4,CO2
2684	1	ROS	060612	1655	BE	63 28.9 N	010 49.1 W	GPS	444.67	7	13	CTD,LADCP,O2,SiO3,PO4,CO2
2684	1	ROS	060612	1706	BO	63 28.8 N	010 49.3 W	GPS	444.67	7	13	CTD,LADCP,O2,SiO3,PO4,CO2
2684	1	ROS	060612	1737	EN	63 28.3 N	010 50.5 W	GPS	444.67	7	13	CTD,LADCP,O2,SiO3,PO4,CO2
2685	1	ROS	060612	1925	BE	63 20.1 N	010 25.2 W	GPS	329.27	5	9	CTD,LADCP,O2,SiO3,PO4,CO2
2685	1	ROS	060612	1937	BO	63 20.0 N	010 25.0 W	GPS	329.27	5	9	CTD,LADCP,O2,SiO3,PO4,CO2
2685	1	ROS	060612	1949	EN	63 20.1 N	010 25.1 W	GPS	329.27	5	9	CTD,LADCP,O2,SiO3,PO4,CO2
2686	1	ROS	060612	2126	BE	63 14.0 N	009 58.3 W	GPS	488.55	8	13	CTD,LADCP,O2,SiO3,PO4,CO2
2686	1	ROS	060612	2142	BO	63 14.2 N	009 57.9 W	GPS	488.55	8	13	CTD,LADCP,O2,SiO3,PO4,CO2
2686	1	ROS	060612	2202	EN	63 14.6 N	009 57.5 W	GPS	488.55	8	13	CTD,LADCP,O2,SiO3,PO4,CO2
2687	1	ROS	060712	0038	BE	63 05.8 N	009 38.1 W	GPS	497.13	8	13	CTD,LADCP,O2,SiO3,PO4,CO2
2687	1	ROS	060712	0051	BO	63 06.0 N	009 38.4 W	GPS	497.13	8	13	CTD,LADCP,O2,SiO3,PO4,CO2
2687	1	ROS	060712	0109	EN	63 06.4 N	009 38.4 W	GPS	497.13	8	13	CTD,LADCP,O2,SiO3,PO4,CO2
2688	1	ROS	060712	0448	BE	62 58.0 N	009 09.1 W	GPS	449.88	4	12	CTD,LADCP,O2,SiO3,PO4,CO2
2688	1	ROS	060712	0504	BO	62 58.0 N	009 09.2 W	GPS	449.88	4	12	CTD,LADCP,O2,SiO3,PO4,CO2
2688	1	ROS	060712	0519	EN	62 57.9 N	009 09.6 W	GPS	449.88	4	12	CTD,LADCP,O2,SiO3,PO4,CO2
2689	1	ROS	060712	0724	BE	62 51.0 N	008 49.9 W	GPS	465.83	2	11	CTD,LADCP,O2,SiO3,PO4,CO2
2689	1	ROS	060712	0735	BO	62 51.1 N	008 49.7 W	GPS	465.83	2	11	CTD,LADCP,O2,SiO3,PO4,CO2
2689	1	ROS	060712	0750	EN	62 51.4 N	008 49.8 W	GPS	465.83	2	11	CTD,LADCP,O2,SiO3,PO4,CO2
2690	1	ROS	060712	0958	BE	62 44.0 N	008 27.0 W	GPS	482.18	7	12	CTD,LADCP,O2,SiO3,PO4,CO2
2690	1	ROS	060712	1009	BO	62 44.3 N	008 27.0 W	GPS	482.18	7	12	CTD,LADCP,O2,SiO3,PO4,CO2
2690	1	ROS	060712	1028	EN	62 44.9 N	008 26.6 W	GPS	482.18	7	12	CTD,LADCP,O2,SiO3,PO4,CO2
2691	1	ROS	060712	1238	BE	62 35.0 N	008 02.2 W	GPS	417.08	6	11	CTD,LADCP,O2,SiO3,PO4,CO2
2691	1	ROS	060712	1258	BO	62 35.0 N	008 02.4 W	GPS	417.08	6	11	CTD,LADCP,O2,SiO3,PO4,CO2
2691	1	ROS	060712	1313	EN	62 35.1 N	008 02.8 W	GPS	417.08	6	11	CTD,LADCP,O2,SiO3,PO4,CO2
2692	1	ROS	060712	1517	BE	62 26.0 N	007 39.0 W	GPS	105.49	5	6	CTD,LADCP,O2,SiO3,PO4,CO2
2692	1	ROS	060712	1528	BO	62 25.8 N	007 39.5 W	GPS	105.49	5	6	CTD,LADCP,O2,SiO3,PO4,CO2
2692	1	ROS	060712	1535	EN	62 25.6 N	007 39.9 W	GPS	105.49	5	6	CTD,LADCP,O2,SiO3,PO4,CO2
2693	1	ROS	060712	1727	BE	62 34.9 N	008 02.1 W	GPS	416.35	5	11	CTD,LADCP,O2,SiO3,PO4,CO2
2693	1	ROS	060712	1737	BO	62 35.0 N	008 02.3 W	GPS	416.35	5	11	CTD,LADCP,O2,SiO3,PO4,CO2
2693	1	ROS	060712	1752	EN	62 35.0 N	008 02.4 W	GPS	416.35	5	11	CTD,LADCP,O2,SiO3,PO4,CO2
2694	1	ROS	060712	1944	BE	62 43.9 N	008 26.9 W	GPS	486.37	6	13	CTD,LADCP,O2,SiO3,PO4,CO2
2694	1	ROS	060712	1957	BO	62 44.2 N	008 27.4 W	GPS	486.37	6	13	CTD,LADCP,O2,SiO3,PO4,CO2

2694	1	ROS	060712	2015	EN	62 44.3 N	008 27.7 W	GPS	486.37	6	13	CTD,LADCP,O2,SiO3,PO4,CO2
2695	1	ROS	060712	2153	BE	62 50.8 N	008 49.9 W	GPS	465.67	7	11	CTD,LADCP,O2,SiO3,PO4,CO2
2695	1	ROS	060712	2210	BO	62 51.2 N	008 49.6 W	GPS	465.67	7	11	CTD,LADCP,O2,SiO3,PO4,CO2
2695	1	ROS	060712	2224	EN	62 51.3 N	008 49.3 W	GPS	465.67	7	11	CTD,LADCP,O2,SiO3,PO4,CO2
2696	1	ROS	060812	0001	BE	62 57.8 N	009 09.0 W	GPS	451.15	6	11	CTD,LADCP,O2,SiO3,PO4,CO2
2696	1	ROS	060812	0019	BO	62 58.0 N	009 08.8 W	GPS	451.15	6	11	CTD,LADCP,O2,SiO3,PO4,CO2
2696	1	ROS	060812	0033	EN	62 58.2 N	009 08.7 W	GPS	451.15	6	11	CTD,LADCP,O2,SiO3,PO4,CO2
2697	1	ROS	060812	0246	BE	63 05.8 N	009 37.8 W	GPS	496.74	7	12	CTD,LADCP,O2,SiO3,PO4,CO2
2697	1	ROS	060812	0303	BO	63 05.9 N	009 38.1 W	GPS	496.74	7	12	CTD,LADCP,O2,SiO3,PO4,CO2
2697	1	ROS	060812	0320	EN	63 06.0 N	009 38.2 W	GPS	496.74	7	12	CTD,LADCP,O2,SiO3,PO4,CO2
2698	1	ROS	060812	0455	BE	63 13.8 N	009 57.7 W	GPS	486.74	7	12	CTD,LADCP,O2,SiO3,PO4,CO2
2698	1	ROS	060812	0510	BO	63 13.9 N	009 58.1 W	GPS	486.74	7	12	CTD,LADCP,O2,SiO3,PO4,CO2
2698	1	ROS	060812	0526	EN	63 13.8 N	009 58.7 W	GPS	486.74	7	12	CTD,LADCP,O2,SiO3,PO4,CO2
2699	1	ROS	060812	0658	BE	63 19.9 N	010 25.0 W	GPS	329.23	6	12	CTD,LADCP,O2,SiO3,PO4,CO2
2699	1	ROS	060812	0707	BO	63 19.9 N	010 25.6 W	GPS	329.23	6	12	CTD,LADCP,O2,SiO3,PO4,CO2
2699	1	ROS	060812	0722	EN	63 19.8 N	010 26.3 W	GPS	329.23	6	12	CTD,LADCP,O2,SiO3,PO4,CO2
2700	1	ROS	060812	0901	BE	63 28.7 N	010 49.0 W	GPS	444.66	4	13	CTD,LADCP,O2,SiO3,PO4,CO2
2700	1	ROS	060812	0916	BO	63 28.8 N	010 48.9 W	GPS	444.66	4	13	CTD,LADCP,O2,SiO3,PO4,CO2
2700	1	ROS	060812	0933	EN	63 29.0 N	010 48.8 W	GPS	444.66	4	13	CTD,LADCP,O2,SiO3,PO4,CO2
2701	1	ROS	060812	1114	BE	63 35.8 N	011 14.9 W	GPS	304.81	7	10	CTD,LADCP,O2,SiO3,PO4,CO2
2701	1	ROS	060812	1126	BO	63 36.1 N	011 14.9 W	GPS	304.81	7	10	CTD,LADCP,O2,SiO3,PO4,CO2
2701	1	ROS	060812	1139	EN	63 36.4 N	011 14.4 W	GPS	304.81	7	10	CTD,LADCP,O2,SiO3,PO4,CO2
2702	1	ROS	060812	1336	BE	63 43.9 N	011 40.1 W	GPS	350.13	5	13	CTD,LADCP,O2,SiO3,PO4,CO2
2702	1	ROS	060812	1357	BO	63 44.0 N	011 40.3 W	GPS	350.13	5	13	CTD,LADCP,O2,SiO3,PO4,CO2
2702	1	ROS	060812	1412	EN	63 44.1 N	011 40.2 W	GPS	350.13	5	13	CTD,LADCP,O2,SiO3,PO4,CO2
2703	1	ROS	060812	1543	BE	63 49.9 N	011 59.9 W	GPS	391.40	4	12	CTD,LADCP,O2,SiO3,PO4,CO2
2703	1	ROS	060812	1559	BO	63 49.8 N	012 00.3 W	GPS	391.40	4	12	CTD,LADCP,O2,SiO3,PO4,CO2
2703	1	ROS	060812	1614	EN	63 49.8 N	012 00.4 W	GPS	391.40	4	12	CTD,LADCP,O2,SiO3,PO4,CO2
2704	1	ROS	060812	1740	BE	63 56.9 N	012 19.9 W	GPS	460.05	5	13	CTD,LADCP,O2,SiO3,PO4,CO2
2704	1	ROS	060812	1751	BO	63 56.8 N	012 20.1 W	GPS	460.05	5	13	CTD,LADCP,O2,SiO3,PO4,CO2
2704	1	ROS	060812	1808	EN	63 56.6 N	012 20.9 W	GPS	460.05	5	13	CTD,LADCP,O2,SiO3,PO4,CO2
2705	1	ROS	060812	1911	BE	64 01.0 N	012 37.9 W	GPS	573.37	6	13	CTD,LADCP,O2,SiO3,PO4,CO2
2705	1	ROS	060812	1927	BO	64 01.0 N	012 38.3 W	GPS	573.37	6	13	CTD,LADCP,O2,SiO3,PO4,CO2

2705	1	ROS	060812	1945	EN	64 01.0 N	012 38.8 W	GPS	573.37	6	13	CTD,LADCP,O2,SiO3,PO4,CO2
2706	1	ROS	060812	2047	BE	64 05.0 N	012 52.1 W	GPS	579.74	7	14	CTD,LADCP,O2,SiO3,PO4,CO2
2706	1	ROS	060812	2059	BO	64 05.2 N	012 52.1 W	GPS	579.74	7	14	CTD,LADCP,O2,SiO3,PO4,CO2
2706	1	ROS	060812	2119	EN	64 05.4 N	012 52.4 W	GPS	579.74	7	14	CTD,LADCP,O2,SiO3,PO4,CO2
2707	1	ROS	060812	2210	BE	64 07.8 N	013 02.9 W	GPS	167.57	9	6	CTD,LADCP,O2,SiO3,PO4,CO2
2707	1	ROS	060812	2217	BO	64 07.9 N	013 03.1 W	GPS	167.57	9	6	CTD,LADCP,O2,SiO3,PO4,CO2
2707	1	ROS	060812	2225	EN	64 08.1 N	013 03.2 W	GPS	167.57	9	6	CTD,LADCP,O2,SiO3,PO4,CO2
2708	1	ROS	060812	2340	BE	64 13.9 N	013 20.9 W	GPS	173.84	5	6	CTD,LADCP,O2,SiO3,PO4,CO2
2708	1	ROS	060812	2348	BO	64 14.1 N	013 20.9 W	GPS	173.84	5	6	CTD,LADCP,O2,SiO3,PO4,CO2
2708	1	ROS	060812	2356	EN	64 14.2 N	013 21.0 W	GPS	173.84	5	6	CTD,LADCP,O2,SiO3,PO4,CO2
2709	1	ROS	060912	0100	BE	64 16.9 N	013 35.9 W	GPS	164.81	4	6	CTD,LADCP,O2,SiO3,PO4,CO2
2709	1	ROS	060912	0109	BO	64 17.0 N	013 36.1 W	GPS	164.81	4	6	CTD,LADCP,O2,SiO3,PO4,CO2
2709	1	ROS	060912	0116	EN	64 17.1 N	013 36.3 W	GPS	164.81	4	6	CTD,LADCP,O2,SiO3,PO4,CO2
2710	1	ROS	060912	0304	BE	64 24.5 N	014 02.8 W	GPS	107.11	7	5	CTD,LADCP,O2,SiO3,PO4,CO2
2710	1	ROS	060912	0311	BO	64 24.6 N	014 02.9 W	GPS	107.11	7	5	CTD,LADCP,O2,SiO3,PO4,CO2
2710	1	ROS	060912	0318	EN	64 24.7 N	014 02.9 W	GPS	107.11	7	5	CTD,LADCP,O2,SiO3,PO4,CO2
2711	1	ROS	060912	0504	BE	64 17.0 N	013 36.0 W	GPS	166.59	7	6	CTD,LADCP,O2,SiO3,PO4,CO2
2711	1	ROS	060912	0514	BO	64 16.9 N	013 35.9 W	GPS	166.59	7	6	CTD,LADCP,O2,SiO3,PO4,CO2
2711	1	ROS	060912	0520	EN	64 16.9 N	013 36.1 W	GPS	166.59	7	6	CTD,LADCP,O2,SiO3,PO4,CO2
2712	1	ROS	060912	0622	BE	64 14.0 N	013 21.1 W	GPS	176.47	4	8	CTD,LADCP,O2,SiO3,PO4,CO2
2712	1	ROS	060912	0631	BO	64 13.9 N	013 21.1 W	GPS	176.47	4	8	CTD,LADCP,O2,SiO3,PO4,CO2
2712	1	ROS	060912	0639	EN	64 13.9 N	013 21.4 W	GPS	176.47	4	8	CTD,LADCP,O2,SiO3,PO4,CO2
2713	1	ROS	060912	0758	BE	64 08.0 N	013 03.1 W	GPS	168.27	5	8	CTD,LADCP,O2,SiO3,PO4,CO2
2713	1	ROS	060912	0807	BO	64 07.9 N	013 03.1 W	GPS	168.27	5	8	CTD,LADCP,O2,SiO3,PO4,CO2
2713	1	ROS	060912	0815	EN	64 07.9 N	013 03.3 W	GPS	168.27	5	8	CTD,LADCP,O2,SiO3,PO4,CO2
2714	1	ROS	060912	0913	BE	64 05.0 N	012 52.0 W	GPS	580.30	6	15	CTD,LADCP,O2,SiO3,PO4,CO2
2714	1	ROS	060912	0926	BO	64 05.2 N	012 52.1 W	GPS	580.30	6	15	CTD,LADCP,O2,SiO3,PO4,CO2
2714	1	ROS	060912	0947	EN	64 05.4 N	012 52.0 W	GPS	580.30	6	15	CTD,LADCP,O2,SiO3,PO4,CO2
2715	1	ROS	060912	1055	BE	64 00.9 N	012 38.3 W	GPS	570.45	6	15	CTD,LADCP,O2,SiO3,PO4,CO2
2715	1	ROS	060912	1112	BO	64 01.2 N	012 37.8 W	GPS	570.45	6	15	CTD,LADCP,O2,SiO3,PO4,CO2
2715	1	ROS	060912	1133	EN	64 01.5 N	012 37.8 W	GPS	570.45	6	15	CTD,LADCP,O2,SiO3,PO4,CO2
2716	1	ROS	060912	1252	BE	63 56.9 N	012 20.0 W	GPS	461.15	6	15	CTD,LADCP,O2,SiO3,PO4,CO2
2716	1	ROS	060912	1306	BO	63 56.9 N	012 20.1 W	GPS	461.15	6	15	CTD,LADCP,O2,SiO3,PO4,CO2

2716	1	ROS	060912	1323	EN	63 56.9 N	012 20.2 W	GPS	461.15	6	15	CTD,LADCP,O2,SiO3,PO4,CO2
2717	1	ROS	060912	1454	BE	63 49.9 N	011 59.9 W	GPS	389.10	4	12	CTD,LADCP,O2,SiO3,PO4,CO2
2717	1	ROS	060912	1506	BO	63 49.8 N	012 00.0 W	GPS	389.10	4	12	CTD,LADCP,O2,SiO3,PO4,CO2
2717	1	ROS	060912	1521	EN	63 49.9 N	012 00.0 W	GPS	389.10	4	12	CTD,LADCP,O2,SiO3,PO4,CO2
2718	1	ROS	060912	1643	BE	63 43.9 N	011 39.9 W	GPS	349.08	3	12	CTD,LADCP,O2,SiO3,PO4,CO2
2718	1	ROS	060912	1654	BO	63 43.9 N	011 40.0 W	GPS	349.08	3	12	CTD,LADCP,O2,SiO3,PO4,CO2
2718	1	ROS	060912	1709	EN	63 43.7 N	011 40.1 W	GPS	349.08	3	12	CTD,LADCP,O2,SiO3,PO4,CO2
2719	1	ROS	060912	1851	BE	63 36.0 N	011 15.0 W	GPS	304.86	6	8	CTD,LADCP,O2,SiO3,PO4,CO2
2719	1	ROS	060912	1900	BO	63 35.9 N	011 15.1 W	GPS	304.86	6	8	CTD,LADCP,O2,SiO3,PO4,CO2
2719	1	ROS	060912	1911	EN	63 35.8 N	011 15.3 W	GPS	304.86	6	8	CTD,LADCP,O2,SiO3,PO4,CO2
2720	1	ROS	060912	2107	BE	63 28.9 N	010 49.1 W	GPS	445.16	9	12	CTD,LADCP,O2,SiO3,PO4,CO2
2720	1	ROS	060912	2118	BO	63 28.9 N	010 49.3 W	GPS	445.16	9	12	CTD,LADCP,O2,SiO3,PO4,CO2
2720	1	ROS	060912	2135	EN	63 28.9 N	010 49.5 W	GPS	445.16	9	12	CTD,LADCP,O2,SiO3,PO4,CO2
2721	1	ROS	060912	2330	BE	63 19.9 N	010 24.9 W	GPS	332.40	4	8	CTD,LADCP,O2,SiO3,PO4,CO2
2721	1	ROS	060912	2343	BO	63 20.0 N	010 24.8 W	GPS	332.40	4	8	CTD,LADCP,O2,SiO3,PO4,CO2
2721	1	ROS	060912	2355	EN	63 20.2 N	010 24.4 W	GPS	332.40	4	8	CTD,LADCP,O2,SiO3,PO4,CO2
2722	1	ROS	061012	0143	BE	63 13.9 N	009 57.9 W	GPS	489.18	7	12	CTD,LADCP,O2,SiO3,PO4,CO2
2722	1	ROS	061012	0155	BO	63 13.9 N	009 57.8 W	GPS	489.18	7	12	CTD,LADCP,O2,SiO3,PO4,CO2
2722	1	ROS	061012	0211	EN	63 14.1 N	009 57.5 W	GPS	489.18	7	12	CTD,LADCP,O2,SiO3,PO4,CO2
2723	1	ROS	061012	0348	BE	63 05.9 N	009 37.8 W	GPS	497.91	5	13	CTD,LADCP,O2,SiO3,PO4,CO2
2723	1	ROS	061012	0401	BO	63 05.9 N	009 38.0 W	GPS	497.91	5	13	CTD,LADCP,O2,SiO3,PO4,CO2
2723	1	ROS	061012	0418	EN	63 05.9 N	009 38.0 W	GPS	497.91	5	13	CTD,LADCP,O2,SiO3,PO4,CO2
2724	1	ROS	061012	0615	BE	62 57.9 N	009 09.0 W	GPS	448.23	6	14	CTD,LADCP,O2,SiO3,PO4,CO2
2724	1	ROS	061012	0629	BO	62 57.9 N	009 09.0 W	GPS	448.23	6	14	CTD,LADCP,O2,SiO3,PO4,CO2
2724	1	ROS	061012	0646	EN	62 57.9 N	009 09.1 W	GPS	448.23	6	14	CTD,LADCP,O2,SiO3,PO4,CO2
2725	1	ROS	061012	0810	BE	62 51.0 N	008 50.2 W	GPS	466.25	4	13	CTD,LADCP,O2,SiO3,PO4,CO2
2725	1	ROS	061012	0824	BO	62 50.9 N	008 50.2 W	GPS	466.25	4	13	CTD,LADCP,O2,SiO3,PO4,CO2
2725	1	ROS	061012	0840	EN	62 50.8 N	008 50.6 W	GPS	466.25	4	13	CTD,LADCP,O2,SiO3,PO4,CO2
2726	1	ROS	061012	1023	BE	62 44.0 N	008 27.2 W	GPS	483.83	2	14	CTD,LADCP,O2,SiO3,PO4,CO2
2726	1	ROS	061012	1039	BO	62 44.0 N	008 27.0 W	GPS	483.83	2	14	CTD,LADCP,O2,SiO3,PO4,CO2
2726	1	ROS	061012	1057	EN	62 44.2 N	008 26.7 W	GPS	483.83	2	14	CTD,LADCP,O2,SiO3,PO4,CO2
2727	1	ROS	061012	1256	BE	62 34.9 N	008 02.0 W	GPS	416.42	5	11	CTD,LADCP,O2,SiO3,PO4,CO2
2727	1	ROS	061012	1306	BO	62 35.0 N	008 02.4 W	GPS	416.42	5	11	CTD,LADCP,O2,SiO3,PO4,CO2

2727	1	ROS	061012	1320	EN	62 35.2 N	008 02.6 W	GPS	416.42	5	11	CTD,LADCP,O2,SiO3,PO4,CO2
2728	1	ROS	061012	1507	BE	62 26.0 N	007 39.0 W	GPS	103.23	6	5	CTD,LADCP,O2,SiO3,PO4,CO2
2728	1	ROS	061012	1517	BO	62 25.9 N	007 38.7 W	GPS	103.23	6	5	CTD,LADCP,O2,SiO3,PO4,CO2
2728	1	ROS	061012	1523	EN	62 26.0 N	007 38.5 W	GPS	103.23	6	5	CTD,LADCP,O2,SiO3,PO4,CO2
2729	1	ROS	061012	1655	BE	62 20.0 N	007 15.0 W	GPS	90.86	6	5	CTD,LADCP,O2,SiO3,PO4,CO2
2729	1	ROS	061012	1701	BO	62 20.1 N	007 14.9 W	GPS	90.86	6	5	CTD,LADCP,O2,SiO3,PO4,CO2
2729	1	ROS	061012	1706	EN	62 20.1 N	007 14.9 W	GPS	90.86	6	5	CTD,LADCP,O2,SiO3,PO4,CO2
2730	1	ROS	061112	0139	BE	61 49.9 N	006 21.9 W	GPS	80.03	4	5	CTD,LADCP,O2,SiO3,PO4,CO2
2730	1	ROS	061112	0147	BO	61 49.9 N	006 21.9 W	GPS	80.03	4	5	CTD,LADCP,O2,SiO3,PO4,CO2
2730	1	ROS	061112	0151	EN	61 49.9 N	006 21.9 W	GPS	80.03	4	5	CTD,LADCP,O2,SiO3,PO4,CO2
2731	1	ROS	061112	0341	BE	61 42.5 N	005 57.3 W	GPS	303.47	4	9	CTD,LADCP,O2,SiO3,PO4,CO2
2731	1	ROS	061112	0350	BO	61 42.6 N	005 57.5 W	GPS	303.47	4	9	CTD,LADCP,O2,SiO3,PO4,CO2
2731	1	ROS	061112	0401	EN	61 42.6 N	005 57.8 W	GPS	303.47	4	9	CTD,LADCP,O2,SiO3,PO4,CO2
2732	1	ROS	061112	0531	BE	61 36.9 N	005 35.8 W	GPS	318.35	5	9	CTD,LADCP,O2,SiO3,PO4,CO2
2732	1	ROS	061112	0542	BO	61 36.9 N	005 36.0 W	GPS	318.35	5	9	CTD,LADCP,O2,SiO3,PO4,CO2
2732	1	ROS	061112	0553	EN	61 36.9 N	005 36.1 W	GPS	318.35	5	9	CTD,LADCP,O2,SiO3,PO4,CO2
2733	1	ROS	061112	0710	BE	61 31.0 N	005 18.9 W	GPS	289.15	6	10	CTD,LADCP,O2,SiO3,PO4,CO2
2733	1	ROS	061112	0720	BO	61 31.0 N	005 18.9 W	GPS	289.15	6	10	CTD,LADCP,O2,SiO3,PO4,CO2
2733	1	ROS	061112	0731	EN	61 30.9 N	005 19.2 W	GPS	289.15	6	10	CTD,LADCP,O2,SiO3,PO4,CO2
2734	1	ROS	061112	0852	BE	61 24.9 N	005 00.9 W	GPS	225.96	4	8	CTD,LADCP,O2,SiO3,PO4,CO2
2734	1	ROS	061112	0902	BO	61 25.0 N	005 01.0 W	GPS	225.96	4	8	CTD,LADCP,O2,SiO3,PO4,CO2
2734	1	ROS	061112	0911	EN	61 25.0 N	005 01.2 W	GPS	225.96	4	8	CTD,LADCP,O2,SiO3,PO4,CO2
2735	1	ROS	061112	1034	BE	61 19.9 N	004 43.1 W	GPS	727.77	8	17	CTD,LADCP,O2,SiO3,PO4,CO2
2735	1	ROS	061112	1052	BO	61 19.8 N	004 43.6 W	GPS	727.77	8	17	CTD,LADCP,O2,SiO3,PO4,CO2
2735	1	ROS	061112	1115	EN	61 19.8 N	004 44.1 W	GPS	727.77	8	17	CTD,LADCP,O2,SiO3,PO4,CO2
2736	1	ROS	061112	1230	BE	61 16.0 N	004 28.0 W	GPS	1062.66	4	16	CTD,LADCP,O2,SiO3,PO4,CO2
2736	1	ROS	061112	1255	BO	61 16.4 N	004 28.0 W	GPS	1062.66	4	16	CTD,LADCP,O2,SiO3,PO4,CO2
2736	1	ROS	061112	1322	EN	61 16.5 N	004 28.0 W	GPS	1062.66	4	16	CTD,LADCP,O2,SiO3,PO4,CO2
2737	1	ROS	061112	1418	BE	61 12.0 N	004 18.1 W	GPS	1091.45	6	16	CTD,LADCP,O2,SiO3,PO4,CO2
2737	1	ROS	061112	1443	BO	61 12.1 N	004 17.8 W	GPS	1091.45	6	16	CTD,LADCP,O2,SiO3,PO4,CO2
2737	1	ROS	061112	1511	EN	61 12.3 N	004 17.8 W	GPS	1091.45	6	16	CTD,LADCP,O2,SiO3,PO4,CO2
2738	1	ROS	061112	1615	BE	61 08.0 N	004 03.9 W	GPS	1133.93	6	15	CTD,LADCP,O2,SiO3,PO4,CO2
2738	1	ROS	061112	1639	BO	61 08.1 N	004 03.8 W	GPS	1133.93	6	15	CTD,LADCP,O2,SiO3,PO4,CO2

2738	1	ROS	061112	1707	EN	61 08.2 N	004 03.8 W	GPS	1133.93	6	15	CTD,LADCP,O2,SiO3,PO4,CO2
2739	1	ROS	061112	1801	BE	61 03.9 N	003 51.9 W	GPS	1160.18	7	17	CTD,LADCP,O2,SiO3,PO4,CO2
2739	1	ROS	061112	1825	BO	61 03.9 N	003 51.6 W	GPS	1160.18	7	17	CTD,LADCP,O2,SiO3,PO4,CO2
2739	1	ROS	061112	1858	EN	61 03.8 N	003 51.3 W	GPS	1160.18	7	17	CTD,LADCP,O2,SiO3,PO4,CO2
2740	1	ROS	061112	1956	BE	60 59.0 N	003 38.0 W	GPS	1115.59	7	16	CTD,LADCP,O2,SiO3,PO4,CO2
2740	1	ROS	061112	2018	BO	60 58.9 N	003 37.8 W	GPS	1115.59	7	16	CTD,LADCP,O2,SiO3,PO4,CO2
2740	1	ROS	061112	2049	EN	60 58.8 N	003 37.5 W	GPS	1115.59	7	16	CTD,LADCP,O2,SiO3,PO4,CO2
2741	1	ROS	061112	2217	BE	60 52.0 N	003 18.0 W	GPS	684.91	7	15	CTD,LADCP,O2,SiO3,PO4,CO2
2741	1	ROS	061112	2232	BO	60 51.9 N	003 18.0 W	GPS	684.91	7	15	CTD,LADCP,O2,SiO3,PO4,CO2
2741	1	ROS	061112	2253	EN	60 51.8 N	003 18.1 W	GPS	684.91	7	15	CTD,LADCP,O2,SiO3,PO4,CO2
2742	1	ROS	061212	0038	BE	60 44.9 N	002 54.9 W	GPS	356.00	3	9	CTD,LADCP,O2,SiO3,PO4,CO2
2742	1	ROS	061212	0047	BO	60 44.8 N	002 55.1 W	GPS	356.00	3	9	CTD,LADCP,O2,SiO3,PO4,CO2
2742	1	ROS	061212	0059	EN	60 45.0 N	002 55.2 W	GPS	356.00	3	9	CTD,LADCP,O2,SiO3,PO4,CO2
2743	1	ROS	061212	0232	BE	60 37.9 N	002 36.0 W	GPS	131.45	6	5	CTD,LADCP,O2,SiO3,PO4,CO2
2743	1	ROS	061212	0243	BO	60 37.9 N	002 35.9 W	GPS	131.45	6	5	CTD,LADCP,O2,SiO3,PO4,CO2
2743	1	ROS	061212	0249	EN	60 37.9 N	002 36.1 W	GPS	131.45	6	5	CTD,LADCP,O2,SiO3,PO4,CO2
2744	1	ROS	061212	0421	BE	60 31.0 N	002 15.9 W	GPS	142.15	6	5	CTD,LADCP,O2,SiO3,PO4,CO2
2744	1	ROS	061212	0428	BO	60 30.9 N	002 15.9 W	GPS	142.15	6	5	CTD,LADCP,O2,SiO3,PO4,CO2
2744	1	ROS	061212	0434	EN	60 30.9 N	002 15.9 W	GPS	142.15	6	5	CTD,LADCP,O2,SiO3,PO4,CO2
2745	1	ROS	061212	0600	BE	60 25.0 N	001 55.1 W	GPS	112.52	7	5	CTD,LADCP,O2,SiO3,PO4,CO2
2745	1	ROS	061212	0608	BO	60 25.0 N	001 55.0 W	GPS	112.52	7	5	CTD,LADCP,O2,SiO3,PO4,CO2
2745	1	ROS	061212	0615	EN	60 25.0 N	001 55.0 W	GPS	112.52	7	5	CTD,LADCP,O2,SiO3,PO4,CO2
2746	1	ROS	061212	0749	BE	60 30.9 N	002 16.0 W	GPS	141.01	6	5	CTD,LADCP,O2,SiO3,PO4,CO2
2746	1	ROS	061212	0755	BO	60 30.9 N	002 16.1 W	GPS	141.01	6	5	CTD,LADCP,O2,SiO3,PO4,CO2
2746	1	ROS	061212	0803	EN	60 30.9 N	002 16.1 W	GPS	141.01	6	5	CTD,LADCP,O2,SiO3,PO4,CO2
2747	1	ROS	061212	0937	BE	60 37.9 N	002 35.9 W	GPS	133.45	6	6	CTD,LADCP,O2,SiO3,PO4,CO2
2747	1	ROS	061212	0946	BO	60 38.0 N	002 36.1 W	GPS	133.45	6	6	CTD,LADCP,O2,SiO3,PO4,CO2
2747	1	ROS	061212	0953	EN	60 38.0 N	002 36.3 W	GPS	133.45	6	6	CTD,LADCP,O2,SiO3,PO4,CO2
2748	1	ROS	061212	1120	BE	60 44.9 N	002 55.0 W	GPS	356.52	7	11	CTD,LADCP,O2,SiO3,PO4,CO2
2748	1	ROS	061212	1132	BO	60 45.0 N	002 55.1 W	GPS	356.52	7	11	CTD,LADCP,O2,SiO3,PO4,CO2
2748	1	ROS	061212	1144	EN	60 45.1 N	002 55.2 W	GPS	356.52	7	11	CTD,LADCP,O2,SiO3,PO4,CO2
2749	1	ROS	061212	1353	BE	60 51.9 N	003 18.0 W	GPS	686.98	5	16	CTD,LADCP,O2,SiO3,PO4,CO2
2749	1	ROS	061212	1408	BO	60 51.8 N	003 18.2 W	GPS	686.98	5	16	CTD,LADCP,O2,SiO3,PO4,CO2

2749	1	ROS	061212	1429	EN	60 51.7 N	003 18.5 W	GPS	686.98	5	16	CTD,LADCP,O2,SiO3,PO4,CO2
2750	1	ROS	061212	1609	BE	60 58.9 N	003 37.8 W	GPS	1115.15	6	17	CTD,LADCP,O2,SiO3,PO4,CO2
2750	1	ROS	061212	1634	BO	60 58.8 N	003 37.5 W	GPS	1115.15	6	17	CTD,LADCP,O2,SiO3,PO4,CO2
2750	1	ROS	061212	1704	EN	60 58.5 N	003 37.1 W	GPS	1115.15	6	17	CTD,LADCP,O2,SiO3,PO4,CO2
2751	1	ROS	061212	1824	BE	61 04.0 N	003 52.0 W	GPS	1160.89	7	18	CTD,LADCP,O2,SiO3,PO4,CO2
2751	1	ROS	061212	1847	BO	61 03.9 N	003 52.1 W	GPS	1160.89	7	18	CTD,LADCP,O2,SiO3,PO4,CO2
2751	1	ROS	061212	1919	EN	61 03.8 N	003 52.2 W	GPS	1160.89	7	18	CTD,LADCP,O2,SiO3,PO4,CO2
2752	1	ROS	061212	2019	BE	61 07.9 N	004 04.0 W	GPS	1132.28	8	18	CTD,LADCP,O2,SiO3,PO4,CO2
2752	1	ROS	061212	2041	BO	61 08.0 N	004 04.0 W	GPS	1132.28	8	18	CTD,LADCP,O2,SiO3,PO4,CO2
2752	1	ROS	061212	2111	EN	61 08.0 N	004 04.2 W	GPS	1132.28	8	18	CTD,LADCP,O2,SiO3,PO4,CO2
2753	1	ROS	061212	2220	BE	61 12.0 N	004 18.0 W	GPS	1090.93	6	17	CTD,LADCP,O2,SiO3,PO4,CO2
2753	1	ROS	061212	2241	BO	61 12.1 N	004 18.2 W	GPS	1090.93	6	17	CTD,LADCP,O2,SiO3,PO4,CO2
2753	1	ROS	061212	2312	EN	61 12.3 N	004 18.3 W	GPS	1090.93	6	17	CTD,LADCP,O2,SiO3,PO4,CO2
2754	1	ROS	061312	0009	BE	61 16.0 N	004 28.0 W	GPS	1063.99	8	17	CTD,LADCP,O2,SiO3,PO4,CO2
2754	1	ROS	061312	0033	BO	61 16.1 N	004 28.0 W	GPS	1063.99	8	17	CTD,LADCP,O2,SiO3,PO4,CO2
2754	1	ROS	061312	0102	EN	61 16.6 N	004 28.1 W	GPS	1063.99	8	17	CTD,LADCP,O2,SiO3,PO4,CO2
2755	1	ROS	061312	0213	BE	61 19.9 N	004 42.9 W	GPS	736.32	4	15	CTD,LADCP,O2,SiO3,PO4,CO2
2755	1	ROS	061312	0230	BO	61 19.8 N	004 43.3 W	GPS	736.32	4	15	CTD,LADCP,O2,SiO3,PO4,CO2
2755	1	ROS	061312	0252	EN	61 19.6 N	004 44.1 W	GPS	736.32	4	15	CTD,LADCP,O2,SiO3,PO4,CO2
2756	1	ROS	061312	0412	BE	61 25.0 N	005 01.0 W	GPS	224.13	5	7	CTD,LADCP,O2,SiO3,PO4,CO2
2756	1	ROS	061312	0421	BO	61 25.0 N	005 01.2 W	GPS	224.13	5	7	CTD,LADCP,O2,SiO3,PO4,CO2
2756	1	ROS	061312	0430	EN	61 25.0 N	005 01.3 W	GPS	224.13	5	7	CTD,LADCP,O2,SiO3,PO4,CO2
2757	1	ROS	061312	0547	BE	61 30.9 N	005 18.8 W	GPS	289.03	4	12	CTD,LADCP,O2,SiO3,PO4,CO2
2757	1	ROS	061312	0559	BO	61 30.9 N	005 18.9 W	GPS	289.03	4	12	CTD,LADCP,O2,SiO3,PO4,CO2
2757	1	ROS	061312	0613	EN	61 30.8 N	005 19.1 W	GPS	289.03	4	12	CTD,LADCP,O2,SiO3,PO4,CO2
2758	1	ROS	061312	0730	BE	61 36.9 N	005 36.0 W	GPS	319.64	6	9	CTD,LADCP,O2,SiO3,PO4,CO2
2758	1	ROS	061312	0740	BO	61 36.9 N	005 36.1 W	GPS	319.64	6	9	CTD,LADCP,O2,SiO3,PO4,CO2
2758	1	ROS	061312	0751	EN	61 36.9 N	005 36.2 W	GPS	319.64	6	9	CTD,LADCP,O2,SiO3,PO4,CO2
2759	1	ROS	061312	0917	BE	61 42.5 N	005 57.5 W	GPS	296.23	6	10	CTD,LADCP,O2,SiO3,PO4,CO2
2759	1	ROS	061312	0929	BO	61 42.5 N	005 57.6 W	GPS	296.23	6	10	CTD,LADCP,O2,SiO3,PO4,CO2
2759	1	ROS	061312	0940	EN	61 42.4 N	005 57.8 W	GPS	296.23	6	10	CTD,LADCP,O2,SiO3,PO4,CO2
2760	1	ROS	061412	0101	BE	59 30.0 N	004 35.9 W	GPS	089.18	7	5	CTD,LADCP,O2,SiO3,PO4,CO2
2760	1	ROS	061412	0108	BO	59 30.0 N	004 35.9 W	GPS	089.18	7	5	CTD,LADCP,O2,SiO3,PO4,CO2

2760	1	ROS	061412	0114	EN	59 30.0 N	004 36.0 W	GPS	089.18	7	5	CTD,LADCP,O2,SiO3,PO4,CO2
2761	1	ROS	061412	0351	BE	59 29.9 N	005 17.9 W	GPS	108.62	8	5	CTD,LADCP,O2,SiO3,PO4,CO2
2761	1	ROS	061412	0400	BO	59 29.9 N	005 18.0 W	GPS	108.62	8	5	CTD,LADCP,O2,SiO3,PO4,CO2
2761	1	ROS	061412	0405	EN	59 29.9 N	005 18.0 W	GPS	108.62	8	5	CTD,LADCP,O2,SiO3,PO4,CO2
2762	1	ROS	061412	0629	BE	59 29.9 N	005 59.8 W	GPS	136.89	7	6	CTD,LADCP,O2,SiO3,PO4,CO2
2762	1	ROS	061412	0638	BO	59 30.0 N	006 00.1 W	GPS	136.89	7	6	CTD,LADCP,O2,SiO3,PO4,CO2
2762	1	ROS	061412	0646	EN	59 30.0 N	006 00.2 W	GPS	136.89	7	6	CTD,LADCP,O2,SiO3,PO4,CO2
2763	1	ROS	061412	0901	BE	59 29.9 N	006 40.0 W	GPS	590.74	7	16	CTD,LADCP,O2,SiO3,PO4,CO2
2763	1	ROS	061412	0917	BO	59 30.0 N	006 40.3 W	GPS	590.74	7	16	CTD,LADCP,O2,SiO3,PO4,CO2
2763	1	ROS	061412	0937	EN	59 30.1 N	006 40.4 W	GPS	590.74	7	16	CTD,LADCP,O2,SiO3,PO4,CO2
2764	1	ROS	061412	1148	BE	59 29.9 N	007 19.9 W	GPS	1061.87	5	16	CTD,LADCP,O2,SiO3,PO4,CO2
2764	1	ROS	061412	1212	BO	59 30.0 N	007 20.0 W	GPS	1061.87	5	16	CTD,LADCP,O2,SiO3,PO4,CO2
2764	1	ROS	061412	1240	EN	59 30.0 N	007 20.1 W	GPS	1061.87	5	16	CTD,LADCP,O2,SiO3,PO4,CO2
2765	1	ROS	061412	1458	BE	59 29.9 N	007 59.9 W	GPS	1137.52	7	17	CTD,LADCP,O2,SiO3,PO4,CO2
2765	1	ROS	061412	1533	BO	59 30.1 N	007 59.9 W	GPS	1137.52	7	17	CTD,LADCP,O2,SiO3,PO4,CO2
2765	1	ROS	061412	1603	EN	59 30.2 N	007 59.9 W	GPS	1137.52	7	17	CTD,LADCP,O2,SiO3,PO4,CO2
2766	1	ROS	061412	1821	BE	59 29.9 N	008 40.0 W	GPS	1379.51	7	21	CTD,LADCP,O2,SiO3,PO4,CO2
2766	1	ROS	061412	1849	BO	59 30.1 N	008 40.1 W	GPS	1379.51	7	21	CTD,LADCP,O2,SiO3,PO4,CO2
2766	1	ROS	061412	1924	EN	59 30.1 N	008 40.2 W	GPS	1379.51	7	21	CTD,LADCP,O2,SiO3,PO4,CO2
2767	1	ROS	061412	2143	BE	59 29.9 N	009 20.1 W	GPS	1484.19	8	20	CTD,LADCP,O2,SiO3,PO4,CO2
2767	1	ROS	061412	2209	BO	59 30.2 N	009 20.5 W	GPS	1484.19	8	20	CTD,LADCP,O2,SiO3,PO4,CO2
2767	1	ROS	061412	2248	EN	59 30.6 N	009 20.9 W	GPS	1484.19	8	20	CTD,LADCP,O2,SiO3,PO4,CO2
2768	1	ROS	061512	0137	BE	59 29.9 N	009 59.9 W	GPS	1061.82	8	17	CTD,LADCP,O2,SiO3,PO4,CO2
2768	1	ROS	061512	0208	BO	59 30.1 N	010 00.1 W	GPS	1061.82	8	17	CTD,LADCP,O2,SiO3,PO4,CO2
2768	1	ROS	061512	0236	EN	59 30.3 N	010 00.1 W	GPS	1061.82	8	17	CTD,LADCP,O2,SiO3,PO4,CO2
2769	1	ROS	061512	0509	BE	59 30.0 N	010 40.0 W	GPS	1545.64	6	21	CTD,LADCP,O2,SiO3,PO4,CO2
2769	1	ROS	061512	0538	BO	59 30.1 N	010 40.4 W	GPS	1545.64	6	21	CTD,LADCP,O2,SiO3,PO4,CO2
2769	1	ROS	061512	0619	EN	59 30.2 N	010 40.6 W	GPS	1545.64	6	21	CTD,LADCP,O2,SiO3,PO4,CO2
2770	1	ROS	061512	0836	BE	59 29.9 N	011 19.8 W	GPS	1631.47	1	21	CTD,LADCP,O2,SiO3,PO4,CO2
2770	1	ROS	061512	0912	BO	59 29.9 N	011 20.8 W	GPS	1631.47	1	21	CTD,LADCP,O2,SiO3,PO4,CO2
2770	1	ROS	061512	0954	EN	59 29.6 N	011 20.9 W	GPS	1631.47	1	21	CTD,LADCP,O2,SiO3,PO4,CO2
2771	1	ROS	061512	1213	BE	59 30.0 N	011 59.9 W	GPS	1507.05	9	21	CTD,LADCP,O2,SiO3,PO4,CO2
2771	1	ROS	061512	1245	BO	59 30.2 N	012 00.7 W	GPS	1507.05	9	21	CTD,LADCP,O2,SiO3,PO4,CO2

2771	1	ROS	061512	1325	EN	59 30.3 N	012 01.3 W	GPS	1507.05	9	21	CTD,LADCP,O2,SiO3,PO4,CO2
2772	1	ROS	061512	1546	BE	59 30.0 N	012 39.7 W	GPS	1356.10	10	19	CTD,LADCP,O2,SiO3,PO4,CO2
2772	1	ROS	061512	1621	BO	59 30.2 N	012 40.3 W	GPS	1356.10	10	19	CTD,LADCP,O2,SiO3,PO4,CO2
2772	1	ROS	061512	1657	EN	59 30.1 N	012 40.4 W	GPS	1356.10	10	19	CTD,LADCP,O2,SiO3,PO4,CO2
2773	1	ROS	061512	1920	BE	59 30.0 N	013 19.9 W	GPS	1305.42	5	19	CTD,LADCP,O2,SiO3,PO4,CO2
2773	1	ROS	061512	1947	BO	59 30.1 N	013 20.0 W	GPS	1305.42	5	19	CTD,LADCP,O2,SiO3,PO4,CO2
2773	1	ROS	061512	2023	EN	59 30.2 N	013 20.1 W	GPS	1305.42	5	19	CTD,LADCP,O2,SiO3,PO4,CO2
2774	1	ROS	061512	2249	BE	59 30.0 N	013 59.9 W	GPS	1007.37	6	16	CTD,LADCP,O2,SiO3,PO4,CO2
2774	1	ROS	061512	2307	BO	59 30.1 N	014 00.1 W	GPS	1007.37	6	16	CTD,LADCP,O2,SiO3,PO4,CO2
2774	1	ROS	061512	2335	EN	59 30.2 N	014 00.4 W	GPS	1007.37	6	16	CTD,LADCP,O2,SiO3,PO4,CO2
2775	1	ROS	061612	0159	BE	59 29.9 N	014 39.9 W	GPS	1016.23	7	16	CTD,LADCP,O2,SiO3,PO4,CO2
2775	1	ROS	061612	0218	BO	59 30.1 N	014 40.1 W	GPS	1016.23	7	16	CTD,LADCP,O2,SiO3,PO4,CO2
2775	1	ROS	061612	0247	EN	59 30.2 N	014 40.4 W	GPS	1016.23	7	16	CTD,LADCP,O2,SiO3,PO4,CO2
2776	1	ROS	061612	0510	BE	59 30.0 N	015 19.8 W	GPS	1532.40	7	20	CTD,LADCP,O2,SiO3,PO4,CO2
2776	1	ROS	061612	0536	BO	59 30.0 N	015 19.8 W	GPS	1532.40	7	20	CTD,LADCP,O2,SiO3,PO4,CO2
2776	1	ROS	061612	0617	EN	59 30.0 N	015 19.9 W	GPS	1532.40	7	20	CTD,LADCP,O2,SiO3,PO4,CO2
2777	1	ROS	061612	0840	BE	59 30.0 N	016 00.0 W	GPS	1566.11	7	21	CTD,LADCP,O2,SiO3,PO4,CO2
2777	1	ROS	061612	0911	BO	59 30.3 N	016 00.1 W	GPS	1566.11	7	21	CTD,LADCP,O2,SiO3,PO4,CO2
2777	1	ROS	061612	0952	EN	59 30.3 N	016 00.4 W	GPS	1566.11	7	21	CTD,LADCP,O2,SiO3,PO4,CO2
2778	1	ROS	061612	1215	BE	59 29.9 N	016 39.9 W	GPS	1094.35	5	21	CTD,LADCP,O2,SiO3,PO4,CO2
2778	1	ROS	061612	1239	BO	59 29.9 N	016 39.9 W	GPS	1094.35	5	21	CTD,LADCP,O2,SiO3,PO4,CO2
2778	1	ROS	061612	1311	EN	59 30.0 N	016 39.8 W	GPS	1094.35	5	21	CTD,LADCP,O2,SiO3,PO4,CO2
2779	1	ROS	061612	1538	BE	59 29.9 N	017 19.8 W	GPS	1805.79	7	21	CTD,LADCP,O2,SiO3,PO4,CO2
2779	1	ROS	061612	1615	BO	59 30.2 N	017 20.1 W	GPS	1805.79	7	21	CTD,LADCP,O2,SiO3,PO4,CO2
2779	1	ROS	061612	1659	EN	59 30.4 N	017 20.3 W	GPS	1805.79	7	21	CTD,LADCP,O2,SiO3,PO4,CO2
2780	1	ROS	061612	1919	BE	59 30.0 N	017 59.9 W	GPS	2224.89	7	21	CTD,LADCP,O2,SiO3,PO4,CO2
2780	1	ROS	061612	1954	BO	59 30.1 N	018 00.1 W	GPS	2224.89	7	21	CTD,LADCP,O2,SiO3,PO4,CO2
2780	1	ROS	061612	2047	EN	59 30.3 N	018 00.1 W	GPS	2224.89	7	21	CTD,LADCP,O2,SiO3,PO4,CO2
2781	1	ROS	061612	2303	BE	59 29.9 N	018 40.0 W	GPS	2772.45	8	21	CTD,LADCP,O2,SiO3,PO4,CO2
2781	1	ROS	061612	2348	BO	59 30.1 N	018 41.6 W	GPS	2772.45	8	21	CTD,LADCP,O2,SiO3,PO4,CO2
2781	1	ROS	061712	0050	EN	59 30.7 N	018 42.9 W	GPS	2772.45	8	21	CTD,LADCP,O2,SiO3,PO4,CO2
2782	1	ROS	061712	0257	BE	59 30.0 N	019 20.0 W	GPS	2740.67	7	21	CTD,LADCP,O2,SiO3,PO4,CO2
2782	1	ROS	061712	0343	BO	59 30.5 N	019 21.1 W	GPS	2740.67	7	21	CTD,LADCP,O2,SiO3,PO4,CO2

2782	1	ROS	061712	0448	EN	59 30.9 N	019 21.3 W	GPS	2740.67	7	21	CTD,LADCP,O2,SiO3,PO4,CO2
2783	1	ROS	061712	0657	BE	59 29.9 N	019 59.9 W	GPS	2806.03	7	21	CTD,LADCP,O2,SiO3,PO4,CO2
2783	1	ROS	061712	0753	BO	59 29.9 N	019 59.9 W	GPS	2806.03	7	21	CTD,LADCP,O2,SiO3,PO4,CO2
2783	1	ROS	061712	0858	EN	59 29.9 N	020 00.0 W	GPS	2806.03	7	21	CTD,LADCP,O2,SiO3,PO4,CO2
2784	1	ROS	061712	1114	BE	59 29.9 N	020 39.9 W	GPS	2867.33	7	21	CTD,LADCP,O2,SiO3,PO4,CO2
2784	1	ROS	061712	1210	BO	59 30.0 N	020 40.3 W	GPS	2867.33	7	21	CTD,LADCP,O2,SiO3,PO4,CO2
2784	1	ROS	061712	1300	EN	59 30.1 N	020 39.9 W	GPS	2867.33	7	21	CTD,LADCP,O2,SiO3,PO4,CO2
2784	2	ROS	061712	1329	BE	59 30.1 N	020 39.5 W	GPS	2867.81	4	21	CTD,LADCP,O2,SiO3,PO4,CO2
2784	2	ROS	061712	1424	BO	59 30.1 N	020 39.3 W	GPS	2867.81	4	21	CTD,LADCP,O2,SiO3,PO4,CO2
2784	2	ROS	061712	1531	EN	59 30.1 N	020 39.2 W	GPS	2867.81	4	21	CTD,LADCP,O2,SiO3,PO4,CO2
2785	1	ROS	061712	1757	BE	59 29.9 N	021 19.7 W	GPS	2898.81	7	21	CTD,LADCP,O2,SiO3,PO4,CO2
2785	1	ROS	061712	1845	BO	59 30.3 N	021 18.7 W	GPS	2898.81	7	21	CTD,LADCP,O2,SiO3,PO4,CO2
2785	1	ROS	061712	1949	EN	59 30.8 N	021 17.3 W	GPS	2898.81	7	21	CTD,LADCP,O2,SiO3,PO4,CO2
2786	1	ROS	061712	2230	BE	59 29.9 N	021 59.9 W	GPS	2787.01	6	21	CTD,LADCP,O2,SiO3,PO4,CO2
2786	1	ROS	061712	2319	BO	59 30.3 N	021 59.5 W	GPS	2787.01	6	21	CTD,LADCP,O2,SiO3,PO4,CO2
2786	1	ROS	061812	0022	EN	59 30.9 N	021 58.8 W	GPS	2787.01	6	21	CTD,LADCP,O2,SiO3,PO4,CO2
2787	1	ROS	061812	0254	BE	59 29.9 N	022 39.9 W	GPS	2491.40	7	21	CTD,LADCP,O2,SiO3,PO4,CO2
2787	1	ROS	061812	0336	BO	59 30.2 N	022 39.5 W	GPS	2491.40	7	21	CTD,LADCP,O2,SiO3,PO4,CO2
2787	1	ROS	061812	0431	EN	59 30.6 N	022 39.2 W	GPS	2491.40	7	21	CTD,LADCP,O2,SiO3,PO4,CO2
2788	1	ROS	061812	0655	BE	59 29.9 N	023 19.8 W	GPS	2427.33	7	21	CTD,LADCP,O2,SiO3,PO4,CO2
2788	1	ROS	061812	0741	BO	59 29.9 N	023 19.3 W	GPS	2427.33	7	21	CTD,LADCP,O2,SiO3,PO4,CO2
2788	1	ROS	061812	0836	EN	59 29.8 N	023 18.5 W	GPS	2427.33	7	21	CTD,LADCP,O2,SiO3,PO4,CO2
2789	1	ROS	061812	1109	BE	59 30.0 N	023 59.9 W	GPS	2561.05	5	21	CTD,LADCP,O2,SiO3,PO4,CO2
2789	1	ROS	061812	1157	BO	59 30.1 N	023 59.3 W	GPS	2561.05	5	21	CTD,LADCP,O2,SiO3,PO4,CO2
2789	1	ROS	061812	1256	EN	59 30.4 N	023 58.7 W	GPS	2561.05	5	21	CTD,LADCP,O2,SiO3,PO4,CO2
2790	1	ROS	061812	1528	BE	59 30.0 N	024 39.7 W	GPS	2559.45	5	21	CTD,LADCP,O2,SiO3,PO4,CO2
2790	1	ROS	061812	1621	BO	59 30.0 N	024 39.7 W	GPS	2559.45	5	21	CTD,LADCP,O2,SiO3,PO4,CO2
2790	1	ROS	061812	1721	EN	59 30.0 N	024 39.6 W	GPS	2559.45	5	21	CTD,LADCP,O2,SiO3,PO4,CO2
2791	1	ROS	061812	1936	BE	59 29.9 N	025 20.0 W	GPS	2484.51	5	21	CTD,LADCP,O2,SiO3,PO4,CO2
2791	1	ROS	061812	2016	BO	59 30.0 N	025 19.9 W	GPS	2484.51	5	21	CTD,LADCP,O2,SiO3,PO4,CO2
2791	1	ROS	061812	2111	EN	59 30.1 N	025 20.0 W	GPS	2484.51	5	21	CTD,LADCP,O2,SiO3,PO4,CO2
2792	1	ROS	061812	2333	BE	59 30.0 N	025 59.9 W	GPS	2401.30	7	21	CTD,LADCP,O2,SiO3,PO4,CO2
2792	1	ROS	061912	0016	BO	59 30.1 N	025 59.7 W	GPS	2401.30	7	21	CTD,LADCP,O2,SiO3,PO4,CO2

2792	1	ROS	061912	0108	EN	59 30.5 N	025 59.4 W	GPS	2401.30	7	21	CTD,LADCP,O2,SiO3,PO4,CO2
2793	1	ROS	061912	0333	BE	59 29.9 N	026 40.0 W	GPS	2260.20	5	21	CTD,LADCP,O2,SiO3,PO4,CO2
2793	1	ROS	061912	0414	BO	59 30.1 N	026 40.5 W	GPS	2260.20	5	21	CTD,LADCP,O2,SiO3,PO4,CO2
2793	1	ROS	061912	0507	EN	59 30.4 N	026 40.7 W	GPS	2260.20	5	21	CTD,LADCP,O2,SiO3,PO4,CO2
2794	1	ROS	061912	0720	BE	59 30.0 N	027 20.0 W	GPS	1904.46	7	21	CTD,LADCP,O2,SiO3,PO4,CO2
2794	1	ROS	061912	0757	BO	59 30.2 N	027 20.2 W	GPS	1904.46	7	21	CTD,LADCP,O2,SiO3,PO4,CO2
2794	1	ROS	061912	0844	EN	59 30.3 N	027 20.3 W	GPS	1904.46	7	21	CTD,LADCP,O2,SiO3,PO4,CO2
2795	1	ROS	061912	1059	BE	59 29.9 N	027 59.9 W	GPS	2011.57	6	21	CTD,LADCP,O2,SiO3,PO4,CO2
2795	1	ROS	061912	1138	BO	59 29.7 N	028 00.1 W	GPS	2011.57	6	21	CTD,LADCP,O2,SiO3,PO4,CO2
2795	1	ROS	061912	1227	EN	59 29.3 N	028 00.3 W	GPS	2011.57	6	21	CTD,LADCP,O2,SiO3,PO4,CO2
2796	1	ROS	061912	1459	BE	59 30.0 N	028 40.0 W	GPS	1685.89	8	21	CTD,LADCP,O2,SiO3,PO4,CO2
2796	1	ROS	061912	1530	BO	59 30.3 N	028 40.2 W	GPS	1685.89	8	21	CTD,LADCP,O2,SiO3,PO4,CO2
2796	1	ROS	061912	1613	EN	59 30.7 N	028 40.1 W	GPS	1685.89	8	21	CTD,LADCP,O2,SiO3,PO4,CO2
2797	1	ROS	061912	1833	BE	59 30.0 N	029 19.9 W	GPS	1408.36	4	20	CTD,LADCP,O2,SiO3,PO4,CO2
2797	1	ROS	061912	1901	BO	59 30.1 N	029 19.9 W	GPS	1408.36	4	20	CTD,LADCP,O2,SiO3,PO4,CO2
2797	1	ROS	061912	1939	EN	59 30.1 N	029 19.9 W	GPS	1408.36	4	20	CTD,LADCP,O2,SiO3,PO4,CO2
2798	1	ROS	061912	2156	BE	59 29.9 N	030 00.0 W	GPS	1424.62	no data	19	CTD,LADCP,O2,SiO3,PO4,CO2
2798	1	ROS	061912	2223	BO	59 29.8 N	030 00.0 W	GPS	1424.62	no data	19	CTD,LADCP,O2,SiO3,PO4,CO2
2798	1	ROS	061912	2300	EN	59 29.7 N	030 00.0 W	GPS	1424.62	no data	19	CTD,LADCP,O2,SiO3,PO4,CO2
2799	1	ROS	062012	0122	BE	59 30.0 N	030 39.9 W	GPS	1537.94	9	20	CTD,LADCP,O2,SiO3,PO4,CO2
2799	1	ROS	062012	0152	BO	59 30.0 N	030 40.1 W	GPS	1537.94	9	20	CTD,LADCP,O2,SiO3,PO4,CO2
2799	1	ROS	062012	0229	EN	59 29.8 N	030 40.3 W	GPS	1537.94	9	20	CTD,LADCP,O2,SiO3,PO4,CO2
2800	1	ROS	062012	0502	BE	59 29.9 N	031 19.8 W	GPS	1790.67	8	21	CTD,LADCP,O2,SiO3,PO4,CO2
2800	1	ROS	062012	0535	BO	59 29.7 N	031 19.5 W	GPS	1790.67	8	21	CTD,LADCP,O2,SiO3,PO4,CO2
2800	1	ROS	062012	0622	EN	59 29.6 N	031 19.4 W	GPS	1790.67	8	21	CTD,LADCP,O2,SiO3,PO4,CO2
2801	1	ROS	062012	0843	BE	59 30.0 N	031 59.7 W	GPS	1761.00	4	20	CTD,LADCP,O2,SiO3,PO4,CO2
2801	1	ROS	062012	0919	BO	59 30.2 N	031 59.4 W	GPS	1761.00	4	20	CTD,LADCP,O2,SiO3,PO4,CO2
2801	1	ROS	062012	1003	EN	59 30.4 N	031 59.3 W	GPS	1761.00	4	20	CTD,LADCP,O2,SiO3,PO4,CO2
2802	1	ROS	062012	1230	BE	59 30.0 N	032 39.9 W	GPS	2069.18	5	21	CTD,LADCP,O2,SiO3,PO4,CO2
2802	1	ROS	062012	1310	BO	59 29.6 N	032 39.6 W	GPS	2069.18	5	21	CTD,LADCP,O2,SiO3,PO4,CO2
2802	1	ROS	062012	1401	EN	59 29.0 N	032 39.0 W	GPS	2069.18	5	21	CTD,LADCP,O2,SiO3,PO4,CO2
2803	1	ROS	062012	1642	BE	59 29.9 N	033 19.8 W	GPS	2177.32	5	21	CTD,LADCP,O2,SiO3,PO4,CO2
2803	1	ROS	062012	1724	BO	59 29.5 N	033 20.0 W	GPS	2177.32	5	21	CTD,LADCP,O2,SiO3,PO4,CO2

2803	1	ROS	062012	1818	EN	59 29.2 N	033 20.0 W	GPS	2177.32	5	21	CTD,LADCP,O2,SiO3,PO4,CO2
2804	1	ROS	062012	2038	BE	59 30.0 N	033 59.8 W	GPS	2649.13	7	21	CTD,LADCP,O2,SiO3,PO4,CO2
2804	1	ROS	062012	2130	BO	59 30.5 N	034 00.0 W	GPS	2649.13	7	21	CTD,LADCP,O2,SiO3,PO4,CO2
2804	1	ROS	062012	2230	EN	59 31.0 N	034 00.0 W	GPS	2649.13	7	21	CTD,LADCP,O2,SiO3,PO4,CO2
2805	1	ROS	062112	0054	BE	59 29.9 N	034 39.9 W	GPS	2831.30	6	13	CTD,LADCP,O2,SiO3,PO4,CO2
2805	1	ROS	062112	0145	BO	59 30.0 N	034 39.8 W	GPS	2831.30	6	13	CTD,LADCP,O2,SiO3,PO4,CO2
2805	1	ROS	062112	0229	EN	59 29.8 N	034 39.9 W	GPS	2831.30	6	13	CTD,LADCP,O2,SiO3,PO4,CO2
2805	2	ROS	062112	0234	BE	59 29.8 N	034 39.9 W	GPS	2831.06	6	21	CTD,LADCP,O2,SiO3,PO4,CO2
2805	2	ROS	062112	0234	BO	59 29.8 N	034 39.9 W	GPS	2831.06	6	21	CTD,LADCP,O2,SiO3,PO4,CO2
2805	2	ROS	062112	0253	EN	59 29.8 N	034 40.2 W	GPS	2831.06	6	21	CTD,LADCP,O2,SiO3,PO4,CO2
2806	1	ROS	062112	0519	BE	59 30.0 N	035 20.0 W	GPS	1972.28	7	20	CTD,LADCP,O2,SiO3,PO4,CO2
2806	1	ROS	062112	0558	BO	59 30.0 N	035 20.0 W	GPS	1972.28	7	20	CTD,LADCP,O2,SiO3,PO4,CO2
2806	1	ROS	062112	0644	EN	59 30.0 N	035 20.1 W	GPS	1972.28	7	20	CTD,LADCP,O2,SiO3,PO4,CO2
2807	1	ROS	062112	0856	BE	59 29.9 N	035 59.8 W	GPS	3136.40	6	21	CTD,LADCP,O2,SiO3,PO4,CO2
2807	1	ROS	062112	0954	BO	59 30.1 N	036 00.2 W	GPS	3136.40	6	21	CTD,LADCP,O2,SiO3,PO4,CO2
2807	1	ROS	062112	1106	EN	59 30.3 N	036 00.4 W	GPS	3136.40	6	21	CTD,LADCP,O2,SiO3,PO4,CO2
2808	1	ROS	062112	1322	BE	59 29.9 N	036 39.8 W	GPS	3144.01	6	21	CTD,LADCP,O2,SiO3,PO4,CO2
2808	1	ROS	062112	1423	BO	59 30.1 N	036 39.4 W	GPS	3144.01	6	21	CTD,LADCP,O2,SiO3,PO4,CO2
2808	1	ROS	062112	1534	EN	59 30.2 N	036 38.8 W	GPS	3144.01	6	21	CTD,LADCP,O2,SiO3,PO4,CO2
2809	1	ROS	062112	1755	BE	59 29.9 N	037 19.9 W	GPS	3198.08	7	21	CTD,LADCP,O2,SiO3,PO4,CO2
2809	1	ROS	062112	1854	BO	59 30.0 N	037 20.0 W	GPS	3198.08	7	21	CTD,LADCP,O2,SiO3,PO4,CO2
2809	1	ROS	062112	2004	EN	59 30.0 N	037 20.1 W	GPS	3198.08	7	21	CTD,LADCP,O2,SiO3,PO4,CO2
2810	1	ROS	062112	2224	BE	59 29.9 N	037 59.9 W	GPS	3157.16	8	21	CTD,LADCP,O2,SiO3,PO4,CO2
2810	1	ROS	062112	2320	BO	59 30.0 N	038 00.2 W	GPS	3157.16	8	21	CTD,LADCP,O2,SiO3,PO4,CO2
2810	1	ROS	062212	0026	EN	59 30.2 N	038 00.4 W	GPS	3157.16	8	21	CTD,LADCP,O2,SiO3,PO4,CO2
2811	1	ROS	062212	0242	BE	59 29.9 N	038 40.0 W	GPS	3039.34	8	21	CTD,LADCP,O2,SiO3,PO4,CO2
2811	1	ROS	062212	0333	BO	59 29.9 N	038 39.7 W	GPS	3039.34	8	21	CTD,LADCP,O2,SiO3,PO4,CO2
2811	1	ROS	062212	0438	EN	59 29.9 N	038 39.7 W	GPS	3039.34	8	21	CTD,LADCP,O2,SiO3,PO4,CO2
2812	1	ROS	062212	0658	BE	59 30.0 N	039 19.9 W	GPS	2965.57	6	21	CTD,LADCP,O2,SiO3,PO4,CO2
2812	1	ROS	062212	0753	BO	59 30.1 N	039 19.8 W	GPS	2965.57	6	21	CTD,LADCP,O2,SiO3,PO4,CO2
2812	1	ROS	062212	0858	EN	59 30.1 N	039 19.6 W	GPS	2965.57	6	21	CTD,LADCP,O2,SiO3,PO4,CO2
2813	1	ROS	062212	1119	BE	59 30.0 N	040 00.1 W	GPS	2948.25	8	21	CTD,LADCP,O2,SiO3,PO4,CO2
2813	1	ROS	062212	1214	BO	59 30.2 N	039 59.8 W	GPS	2948.25	8	21	CTD,LADCP,O2,SiO3,PO4,CO2

2813	1	ROS	062212	1319	EN	59 30.5 N	039 59.4 W	GPS	2948.25	8	21	CTD,LADCP,O2,SiO3,PO4,CO2
2814	1	ROS	062212	1545	BE	59 30.0 N	040 39.7 W	GPS	2614.52	6	21	CTD,LADCP,O2,SiO3,PO4,CO2
2814	1	ROS	062212	1638	BO	59 30.1 N	040 40.0 W	GPS	2614.52	6	21	CTD,LADCP,O2,SiO3,PO4,CO2
2814	1	ROS	062212	1738	EN	59 30.1 N	040 39.6 W	GPS	2614.52	6	21	CTD,LADCP,O2,SiO3,PO4,CO2
2815	1	ROS	062212	1858	BE	59 34.0 N	040 59.8 W	GPS	2428.33	7	21	CTD,LADCP,O2,SiO3,PO4,CO2
2815	1	ROS	062212	1942	BO	59 33.8 N	041 00.2 W	GPS	2428.33	7	21	CTD,LADCP,O2,SiO3,PO4,CO2
2815	1	ROS	062212	2038	EN	59 33.5 N	041 00.2 W	GPS	2428.33	7	21	CTD,LADCP,O2,SiO3,PO4,CO2
2816	1	ROS	062212	2153	BE	59 38.6 N	041 15.9 W	GPS	2201.27	9	21	CTD,LADCP,O2,SiO3,PO4,CO2
2816	1	ROS	062212	2232	BO	59 38.2 N	041 15.2 W	GPS	2201.27	9	21	CTD,LADCP,O2,SiO3,PO4,CO2
2816	1	ROS	062212	2325	EN	59 37.8 N	041 15.1 W	GPS	2201.27	9	21	CTD,LADCP,O2,SiO3,PO4,CO2
2817	1	ROS	062312	0045	BE	59 42.6 N	041 31.9 W	GPS	2021.57	8	21	CTD,LADCP,O2,SiO3,PO4,CO2
2817	1	ROS	062312	0120	BO	59 42.3 N	041 31.6 W	GPS	2021.57	8	21	CTD,LADCP,O2,SiO3,PO4,CO2
2817	1	ROS	062312	0208	EN	59 41.9 N	041 31.1 W	GPS	2021.57	8	21	CTD,LADCP,O2,SiO3,PO4,CO2
2818	1	ROS	062312	0334	BE	59 46.5 N	041 46.9 W	GPS	1852.84	7	21	CTD,LADCP,O2,SiO3,PO4,CO2
2818	1	ROS	062312	0411	BO	59 46.1 N	041 45.4 W	GPS	1852.84	7	21	CTD,LADCP,O2,SiO3,PO4,CO2
2818	1	ROS	062312	0501	EN	59 45.5 N	041 43.7 W	GPS	1852.84	7	21	CTD,LADCP,O2,SiO3,PO4,CO2
2818	2	ROS	062312	0541	BE	59 46.6 N	041 47.0 W	GPS	1850.62	8	21	CTD,LADCP,O2,SiO3,PO4,CO2
2818	2	ROS	062312	0616	BO	59 46.2 N	041 46.5 W	GPS	1850.62	8	21	CTD,LADCP,O2,SiO3,PO4,CO2
2818	2	ROS	062312	0644	EN	59 45.9 N	041 46.2 W	GPS	1850.62	8	21	CTD,LADCP,O2,SiO3,PO4,CO2
2819	1	ROS	062312	0802	BE	59 50.8 N	042 03.1 W	GPS	1645.62	6	20	CTD,LADCP,O2,SiO3,PO4,CO2
2819	1	ROS	062312	0835	BO	59 50.7 N	042 03.2 W	GPS	1645.62	6	20	CTD,LADCP,O2,SiO3,PO4,CO2
2819	1	ROS	062312	0918	EN	59 50.6 N	042 02.9 W	GPS	1645.62	6	20	CTD,LADCP,O2,SiO3,PO4,CO2
2820	1	ROS	062312	0952	BE	59 51.4 N	042 06.3 W	GPS	1584.93	5	20	CTD,LADCP,O2,SiO3,PO4,CO2
2820	1	ROS	062312	1023	BO	59 51.3 N	042 06.4 W	GPS	1584.93	5	20	CTD,LADCP,O2,SiO3,PO4,CO2
2820	1	ROS	062312	1105	EN	59 51.1 N	042 06.5 W	GPS	1584.93	5	20	CTD,LADCP,O2,SiO3,PO4,CO2
2821	1	ROS	062312	1138	BE	59 52.3 N	042 09.2 W	GPS	1450.88	5	19	CTD,LADCP,O2,SiO3,PO4,CO2
2821	1	ROS	062312	1205	BO	59 52.3 N	042 09.0 W	GPS	1450.88	5	19	CTD,LADCP,O2,SiO3,PO4,CO2
2821	1	ROS	062312	1243	EN	59 52.3 N	042 08.9 W	GPS	1450.88	5	19	CTD,LADCP,O2,SiO3,PO4,CO2
2822	1	ROS	062312	1317	BE	59 52.9 N	042 11.9 W	GPS	0974.35	6	13	CTD,LADCP,O2,SiO3,PO4,CO2
2822	1	ROS	062312	1336	BO	59 53.0 N	042 11.7 W	GPS	0974.35	6	13	CTD,LADCP,O2,SiO3,PO4,CO2
2822	1	ROS	062312	1401	EN	59 53.1 N	042 11.6 W	GPS	0974.35	6	13	CTD,LADCP,O2,SiO3,PO4,CO2
2823	1	ROS	062312	1428	BE	59 53.5 N	042 15.6 W	GPS	0378.74	5	10	CTD,LADCP,O2,SiO3,PO4,CO2
2823	1	ROS	062312	1442	BO	59 53.4 N	042 15.5 W	GPS	0378.74	5	10	CTD,LADCP,O2,SiO3,PO4,CO2

2823	1	ROS	062312	1455	EN	59 53.4 N	042 15.4 W	GPS	0378.74	5	10	CTD,LADCP,O2,SiO3,PO4,CO2
2824	1	ROS	062312	1528	BE	59 54.0 N	042 19.1 W	GPS	0321.23	5	8	CTD,LADCP,O2,SiO3,PO4,CO2
2824	1	ROS	062312	1539	BO	59 54.0 N	042 19.3 W	GPS	0321.23	5	8	CTD,LADCP,O2,SiO3,PO4,CO2
2824	1	ROS	062312	1550	EN	59 53.9 N	042 19.4 W	GPS	0321.23	5	8	CTD,LADCP,O2,SiO3,PO4,CO2
2825	1	ROS	062312	1623	BE	59 53.8 N	042 21.9 W	GPS	0234.45	6	7	CTD,LADCP,O2,SiO3,PO4,CO2
2825	1	ROS	062312	1629	BO	59 53.8 N	042 21.9 W	GPS	0234.45	6	7	CTD,LADCP,O2,SiO3,PO4,CO2
2825	1	ROS	062312	1639	EN	59 53.7 N	042 22.0 W	GPS	0234.45	6	7	CTD,LADCP,O2,SiO3,PO4,CO2

Table 2

	O2, ml/l	Silicate, µMol kg^{-1}	Phosphate, µMol kg^{-1}
Total amount of analyzed samples	1589	1602	1599
Number of duplicates	202	224	224
Mean difference of duplicates	0,006	0,186	0,010
Min difference of duplicates	0,000	0,001	0,000
Max difference of duplicates	0,034	1,123	0,149
Median difference of duplicates	0,005	0,110	0,008
Standard deviation of difference	0,006	0,205	0,013
Accuracy	0,084%	4,012%	1,679%

Table 3

	O2, ml/l	Silicate, µMol kg^{-1}	Phosphate, µMol kg^{-1}
Total amount of analyzed samples	1286	1295	1315
Number of duplicates	118	127	127
Mean difference of duplicates	0,006	0,31	0,008
Min difference of duplicates	0,000	0,001	0,000
Max difference of duplicates	0,018	1,261	0,038
Median difference of duplicates	0,004	0,250	0,006
Standard deviation of difference	0,005	0,261	0,007
Accuracy	0,074%	3,095%	0,715%

Table 4

Number of stations	**139**
Total Niskin	1497
Total sampled	**1393**
T NisK / T Sampled	10.77
AT Total measured	**1384** 99.35% Total sampled
pH Total measured	**1391** 99.86% Total sampled
CT Total measured	**1226** 88.5% Total sampled
CRM used	10 (Batch #94 and #108)

Table 5

Number of Stations	**67**
Total Niskin	1253
Total sampled	**1253**
T NisK / T Sampled	18.70
AT Total Measured	**1219** 97.28% Total sampled
pH potenciometic Total Sampled	**1253** 100 % Total sampled
pH-UV Total sampled	**983** 76.05 % Total sampled
CT Total Sampled	**953** 76.05 % Total sampled
CRM used	10 (Batch #108)

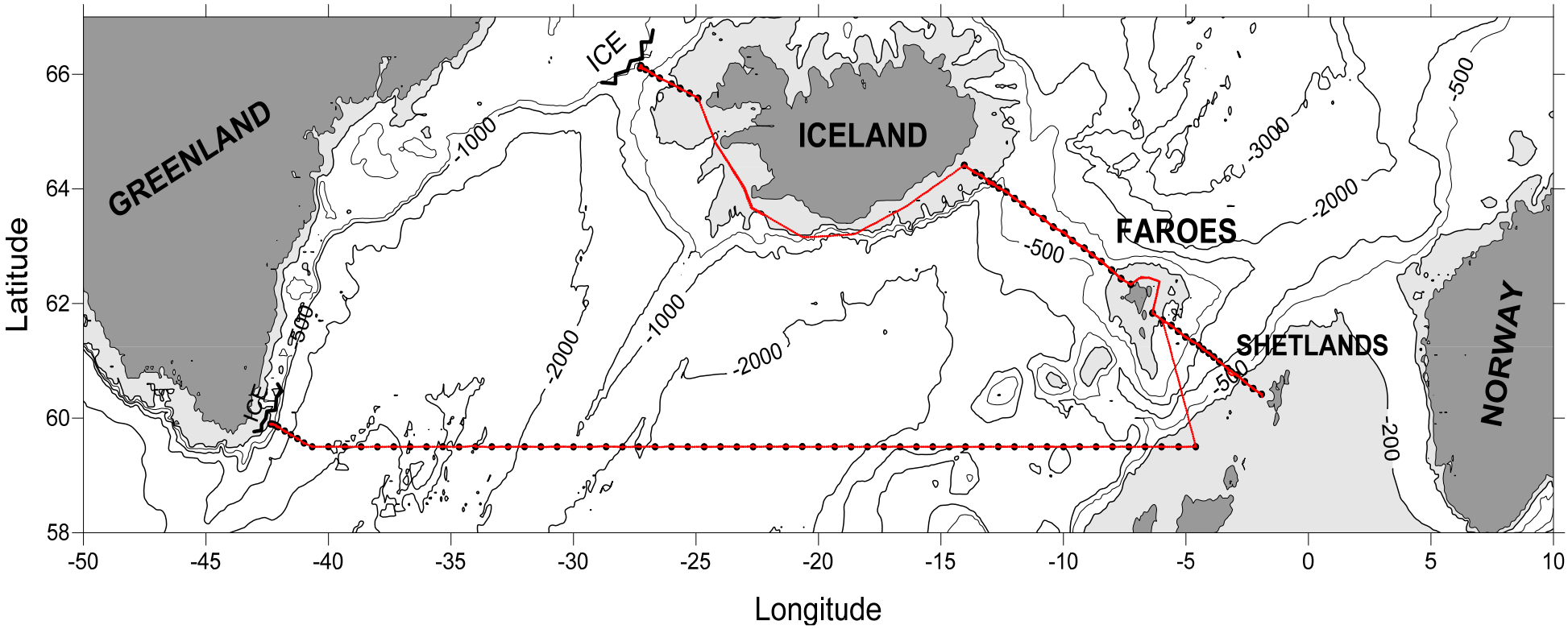

Fig. 1 Station locations (black circles) and ship track (in red). The shelf area with depth less than 200 m is shaded.

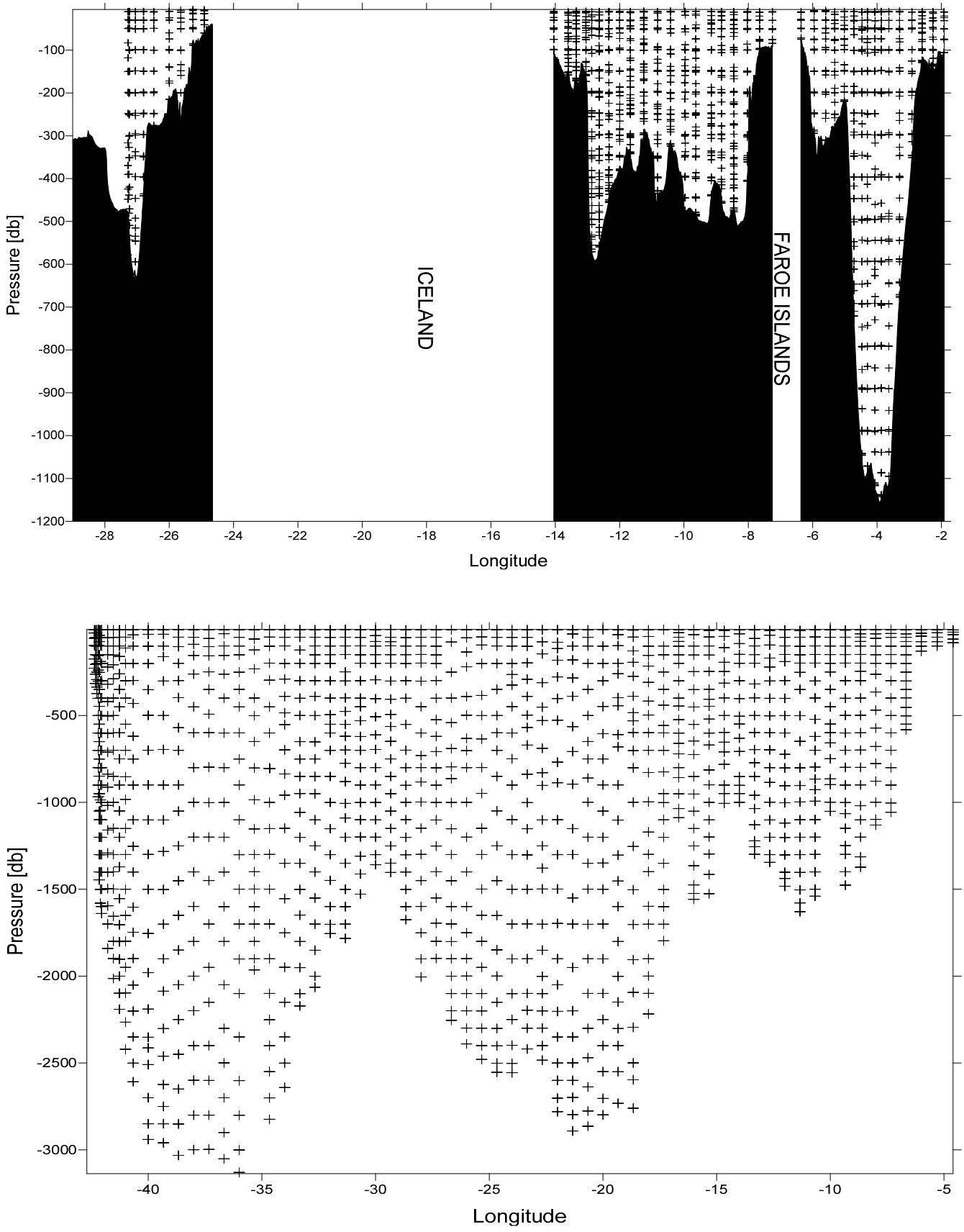

Figure 2. Vertical distribution of samples (a) along the sill sections, (b) along the 59.5 section.

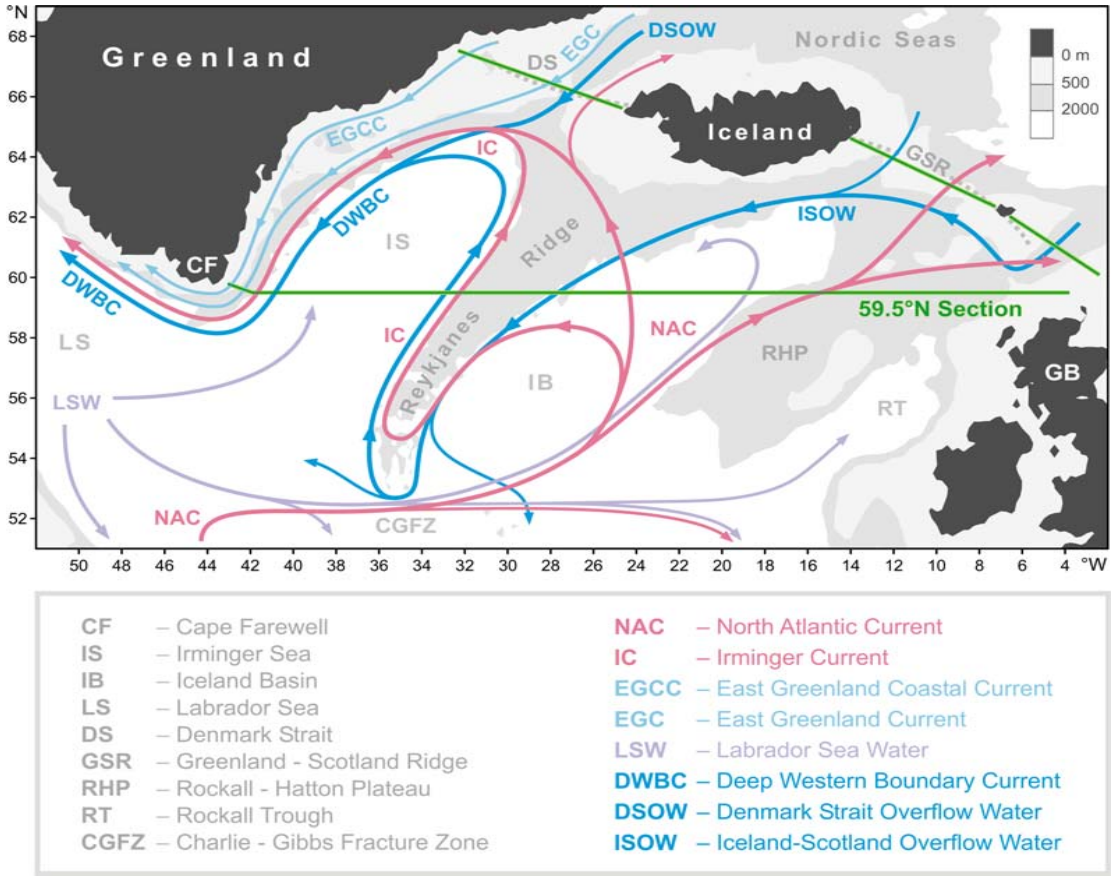

Figure 3. Schematic diagram of the large-scale circulation in the northern North Atlantic compiled from [Schmitz and McCartney, 1993; Schott and Brandt, 2007; Sutherland and Pickart, 2008; Lherminier et al., 2010]. Abbreviations for the main topographic features, currents and water masses are explained in the legend. The nominal locations of the 59.5°N hydrographic section (1997 – present) and sections across the straits between Greenland, Iceland, Faeroe and Shetland Islands (2011 – present) are shown with the solid green lines.

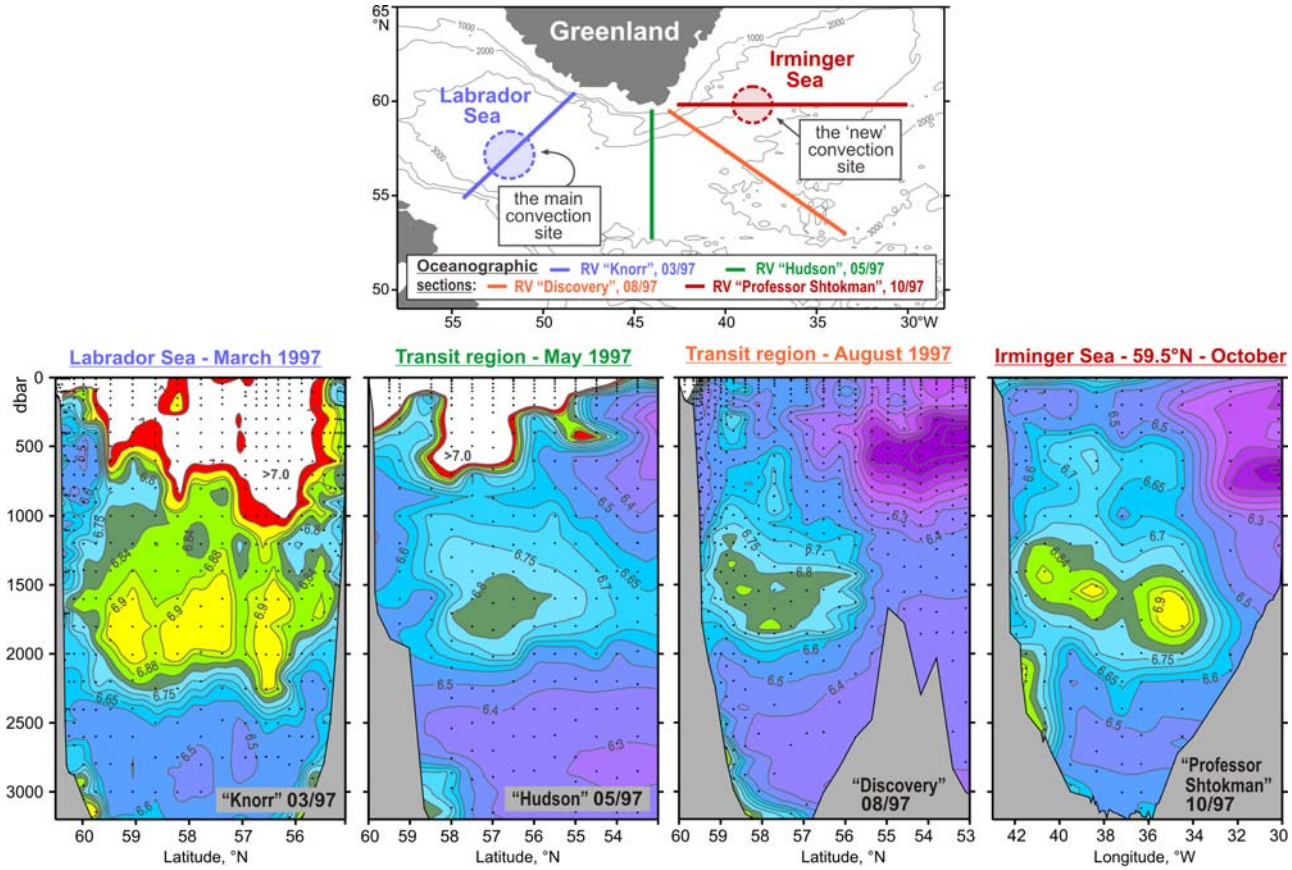

Figure 4. Oxygen concentrations (ml/l) in the water column (lower panel) as observed in March–October 1997 in four hydrographic sections (upper panel) ending nearby the southern tip of Greenland. A separate oxygen maximum in the LSW layer (1000–2000 m) in the Irminger Sea at 59.5°N strongly implies local convective renewal of LSW before 1997. Adapted from [Falina et al., 2007].

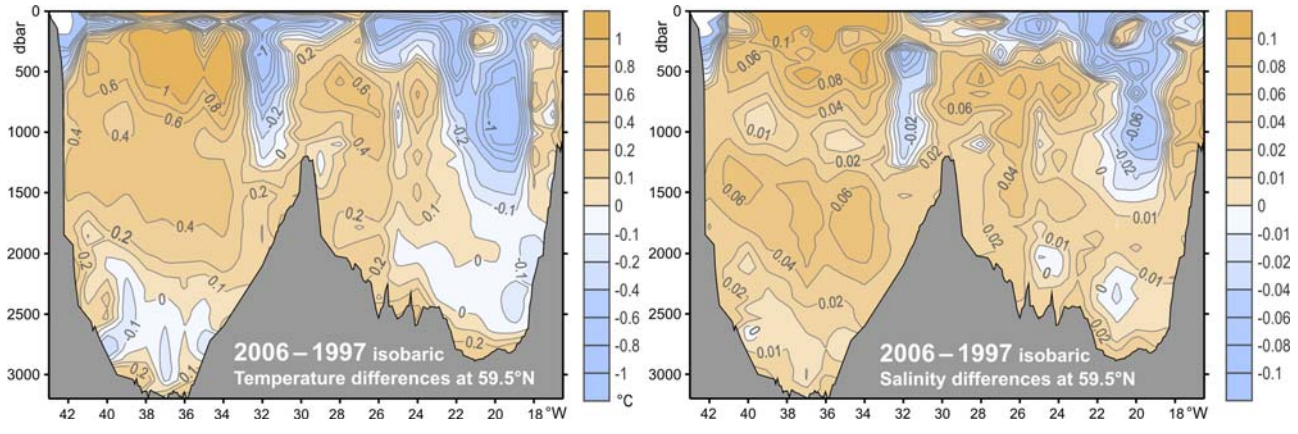

Figure 5. Warming and salinification in the northern North Atlantic between the mid-1990s and mid-2000s, as observed at 59.5°N. The figure shows the 2006–1997 temperature (°C, left) and salinity (right) differences on isobaric surfaces in the Irminger Sea and Iceland Basin. Adapted from [Sarafanov et al., 2007].

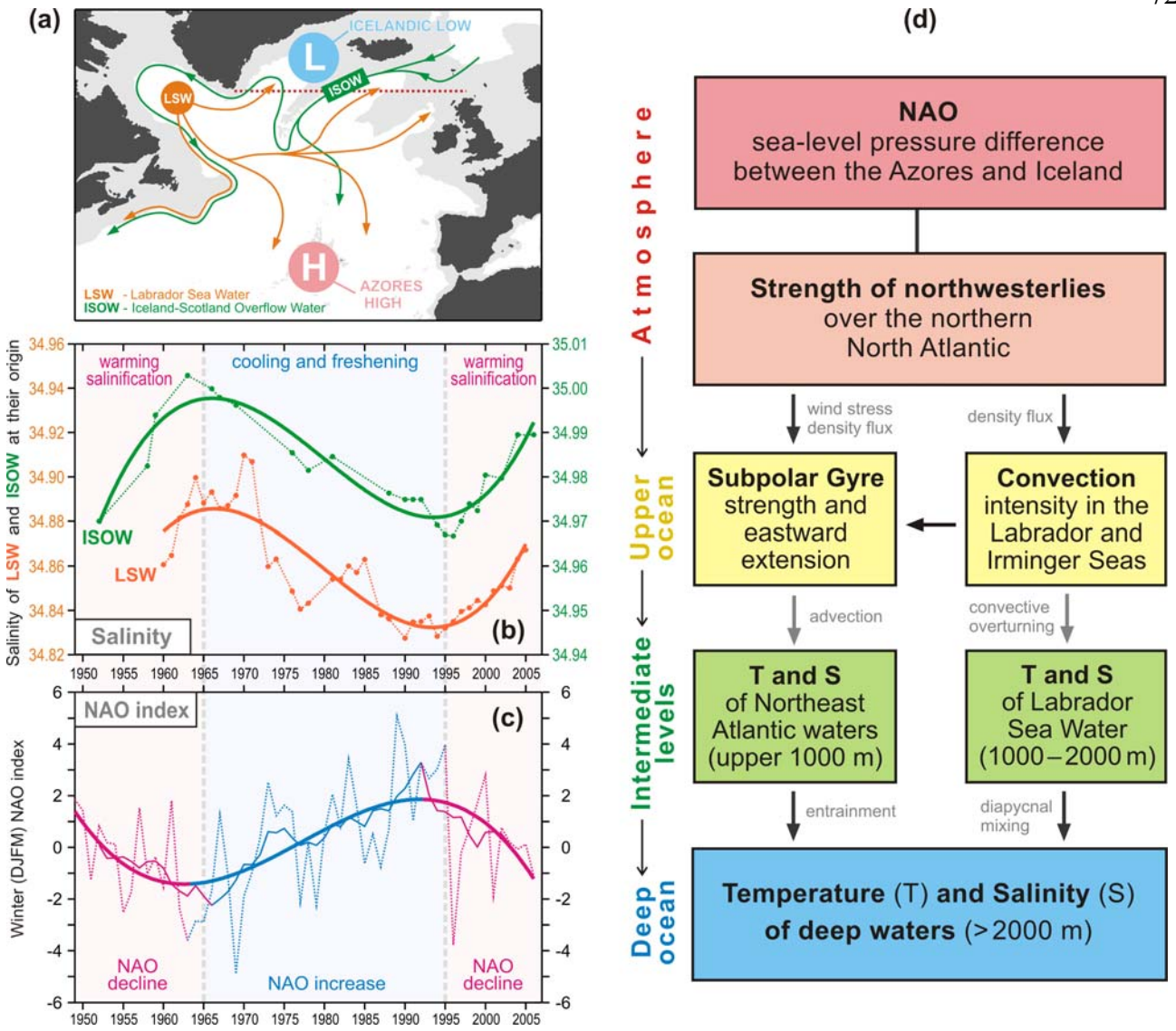

Figure 6. Coherence of the decadal salinity changes (1950s – 2000s) of the intermediate (LSW) and deep (ISOW) waters in the northern North Atlantic and their link to the North Atlantic Oscillation (NAO) index. **(a)** Schematic representation of the LSW and ISOW pathways and locations of the Icelandic Low (L) and Azores High (H) centers constituting the NAO dipole pattern. The red dotted line indicates the 59.5°N transatlantic section. **(b)** Salinity time series for LSW in the Labrador Sea [Yashayaev, 2007] and ISOW in the Iceland basin [Boessenkool et al., 2007; Sarafanov et al., 2007] overlaid by the third order polynomial fits. **(c)** Time series of the winter NAO index, after [Hurrell, 1995], overlaid by 7-year running mean and third order polynomial fit. **(d)** Mechanism of the NAO effect on the decadal changes in temperature (T) and salinity (S) of the northern North Atlantic intermediate and deep waters. Positive / negative links shown with the dark / light grey arrows mean that changes in 'causative' and 'consequential' characteristics have the same / opposite sign(s). The overall effect of the NAO on T and S of the in the water column is negative: persistent NAO decline leads to warming and salinification of the water masses and vice versa, as shown in (b) and (c). Adapted from [Sarafanov, 2009].

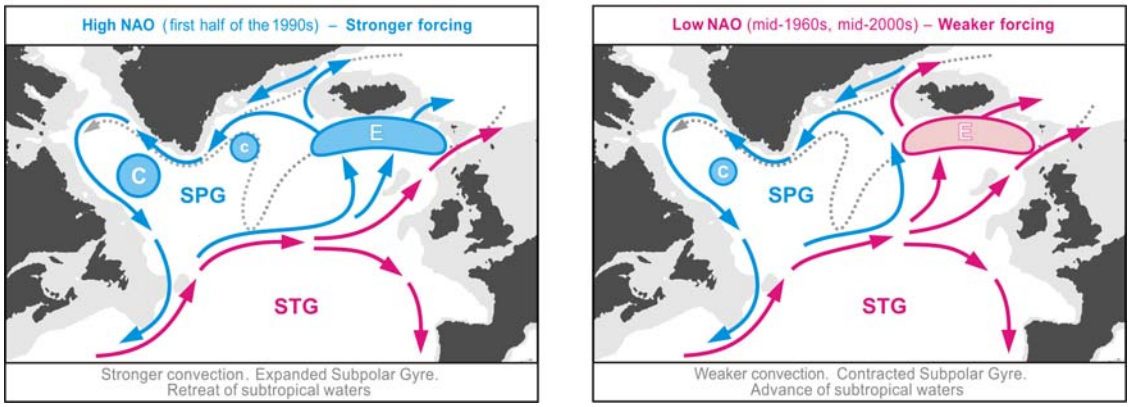

Figure 7. Schematic representation of the upper-ocean circulation and convection intensity in the northern North Atlantic under high (left) and low (right) NAO conditions. Blue (magenta) solid arrows indicate the upper-ocean flows with higher fraction of colder fresher subpolar (warmer saltier subtropical) waters. The main pathways of the Nordic overflow-derived deep waters are shown with the dotted curves. "C" and "E" symbols are used to denote, respectively, the deep convection sites and the domain, where the Atlantic waters are entrained into ISOW. Larger (smaller) circles indicate stronger (weaker) convection. SPG and STG – the subpolar and subtropical gyres, respectively. Adapted from [Sarafanov, 2009].

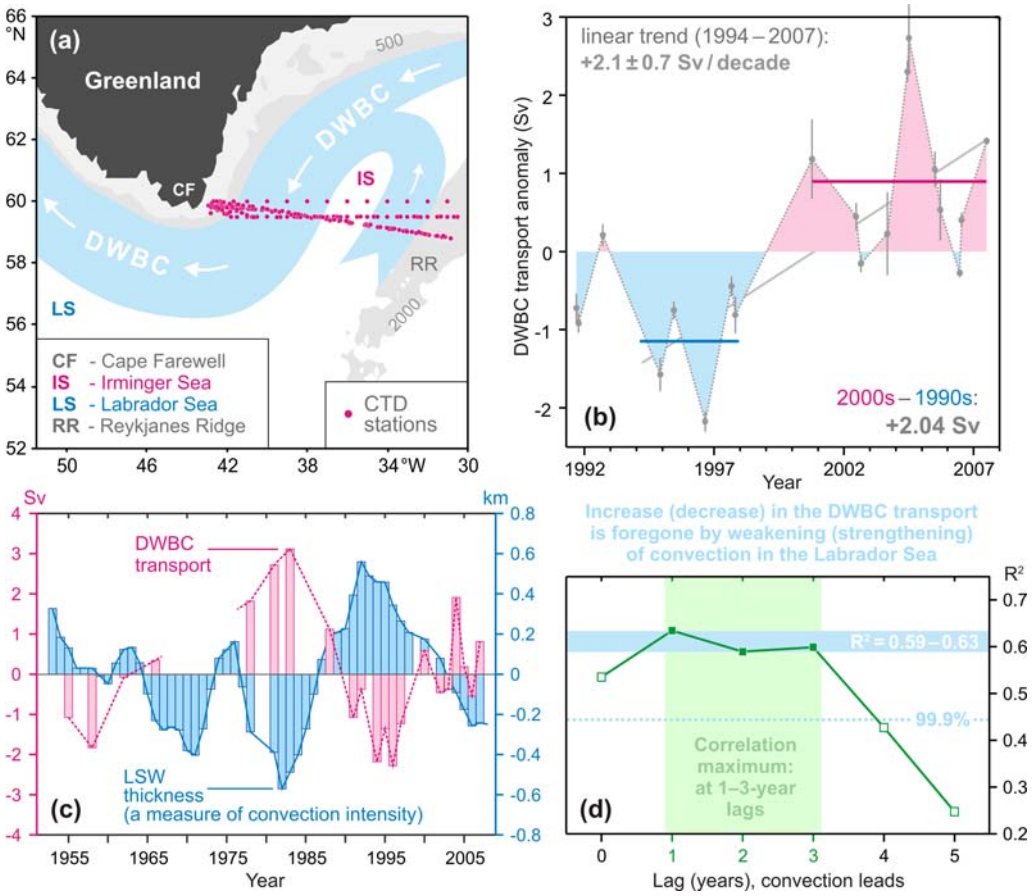

Figure 8. The Deep Western Boundary Current (DWBC) transport variability and its link to the convection intensity in the Labrador Sea. **(a)** Locations of the hydrographic sections (1991–2007) and schematic of the deep water circulation in the Irminger Sea. **(b)** The DWBC transport anomalies at Cape Farewell in 1991–2007, 1 Sv = 10^6 m^3 s^{-1}. The 1994–1997 and 2000–2007 mean anomalies and the 1994–2007 linear trend are shown. **(c)** Anomalies of the DWBC transport at Cape Farewell and the Labrador Sea Water (LSW) thickness in the Labrador Sea in the 1950s–2000s. **(d)** Correlation coefficient (R^2) for the two times series shown in **(c)** at the 0–5-year lag, the LSW thickness leads. The correlation maximum is achieved at the 1–3-year lag. The DWBC transport anomalies in the southern Irminger Sea are foregone by the convection intensity anomalies in the Labrador Sea. Adapted from [Sarafanov et al., 2009].

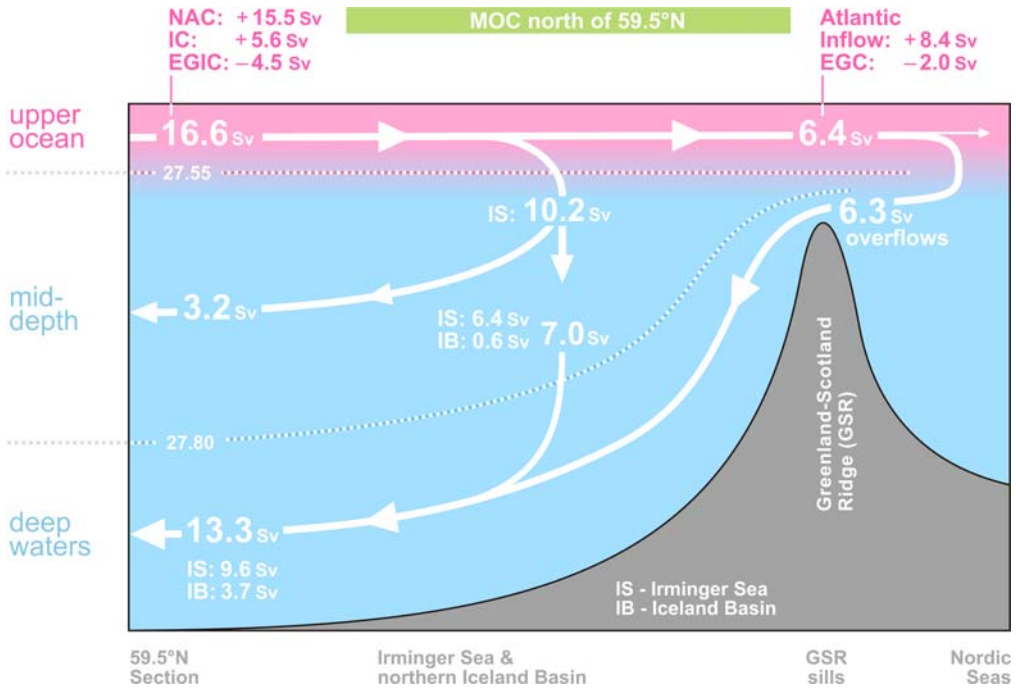

Figure 9. Schematic diagram of the Meridional Overturning Circulation (MOC) at the northern periphery of the Atlantic Ocean, northeast of Cape Farewell. The dotted lines refer to the σ_0 isopycnals 27.55 and 27.80. The arrows denote the integral meridional and diapycnal volume fluxes. Where the signs are specified, the positive (negative) transports are northward (southward). The NAC and EGIC transports in the upper layer ($\sigma_0 < 27.55$) at 59.5°N are the throughputs accounting for the recirculations. EGIC – the East Greenland / Irminger Current – refers to the upper part of the Western Boundary Current. Other abbreviations are explained in the legend to **Figure 3**. Adapted from [Sarafanov et al., 2012].

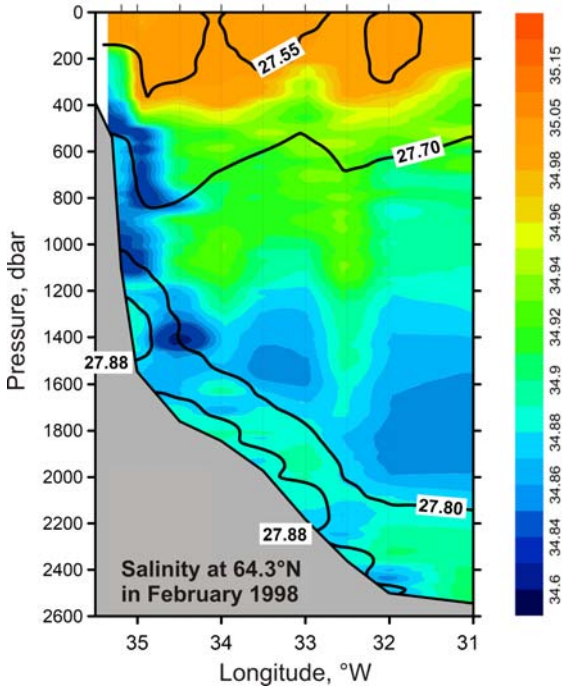

Figure 10. Salinity observed in the northwestern Irminger Sea at 64.3°N in February 1998. The σ_0 isopycnals 27.55, 27.70, 27.80 and 27.88 are plotted as the thick black lines; the station locations are marked with the ticks on the top axis. The plot shows fresh dense waters descending (cascading) down the continental slope of Greenland down to the LSW layer ($27.70 < \sigma_0 < 27.80$) and the layer of the Nordic Seas overflow-derived deep waters ($\sigma_0 > 27.80$). Adapted from [Falina et al., 2012].

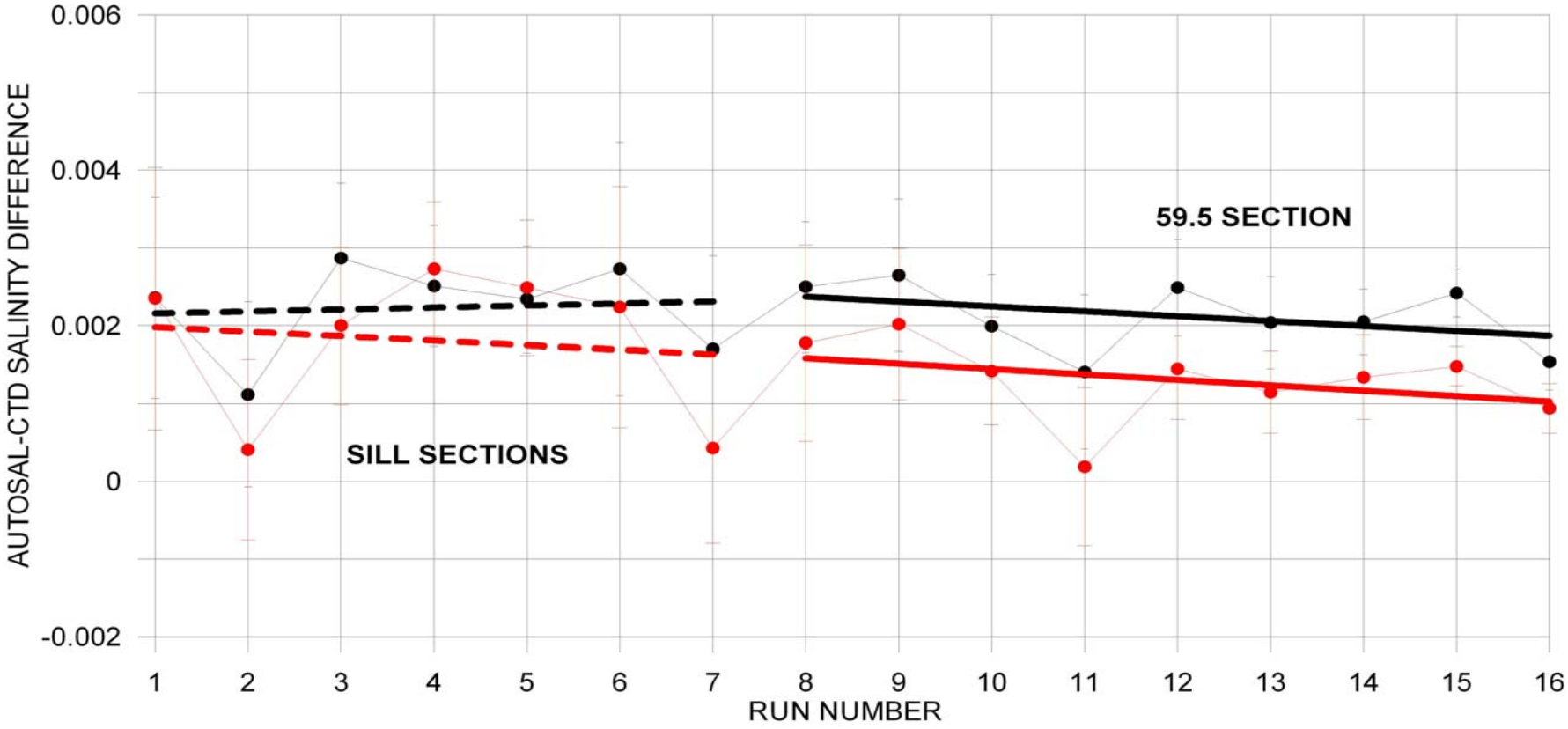

Figure 11 Autosal 8400B CTD salinity difference for primary (in black) and secondary (in red) conductivity sensors based on 860 salinity samples measurements (16 runs) during 38 cruise of R/V *Akademik Ioffe*. Vertical bars show standard deviation of each run.

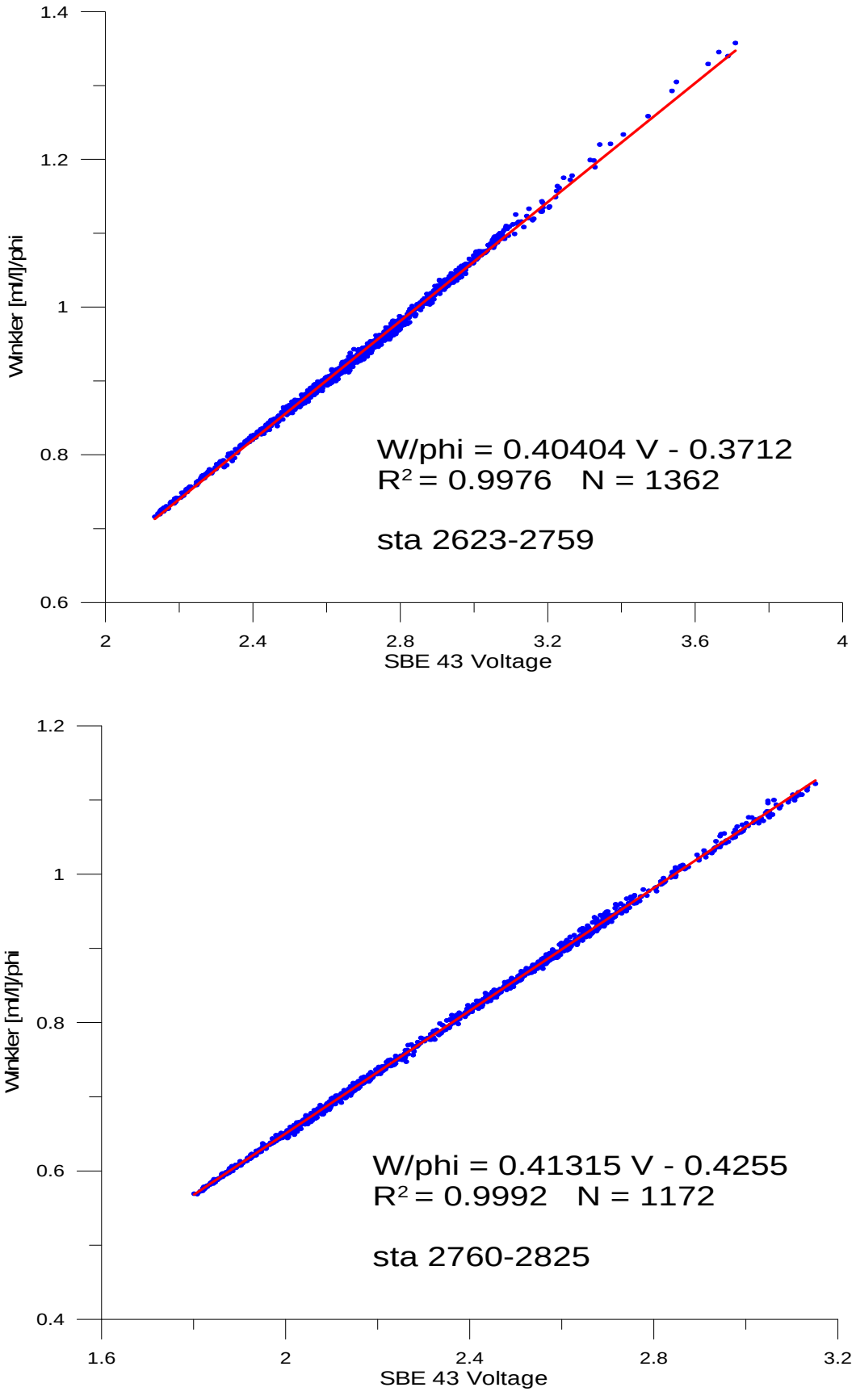

Figure 12 Regression line for Winkler oxygen divided by φ versus SBE 43 output voltage (a) the sill sections, (b) the 59.5 section.

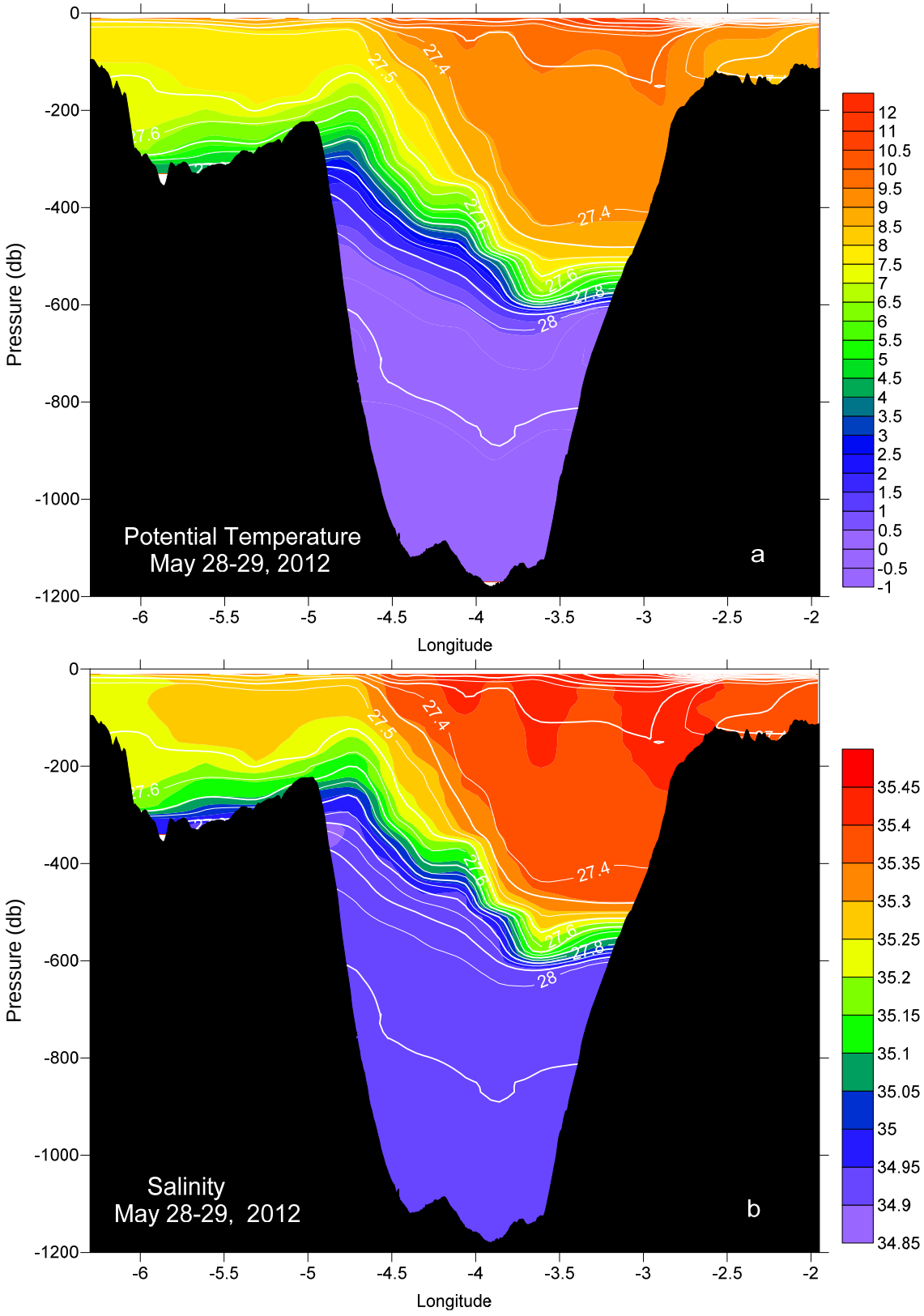

Figure 13 The vertical distribution of (a) potential temperature and (b) salinity between Shetlands and Faroe Islands in May 2012. Density is shown in white.

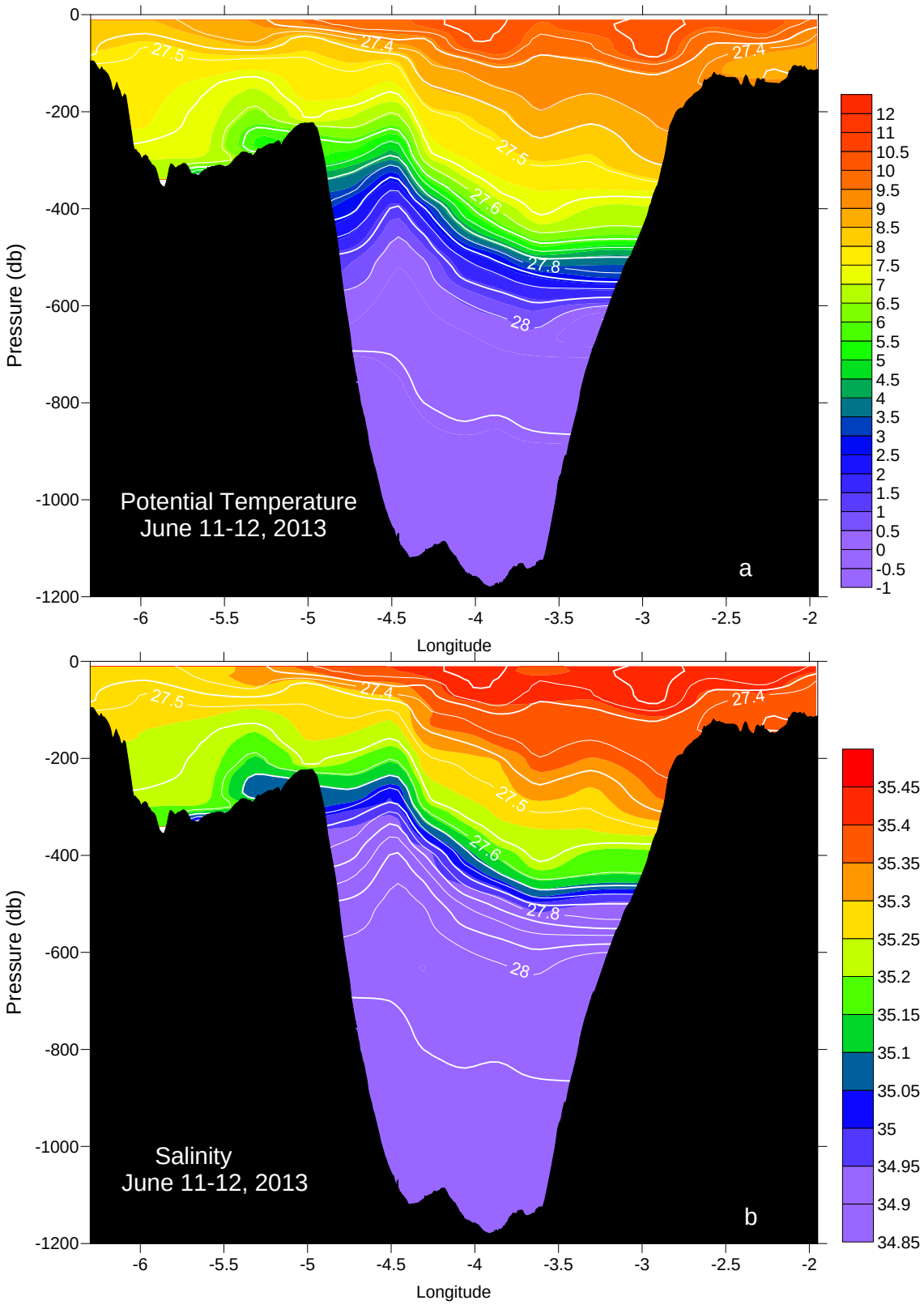

Figure 14 The vertical distribution of (a) potential temperature and (b) salinity between Shetlands and Faroe Islands in June 2012. Density is shown in white.

.

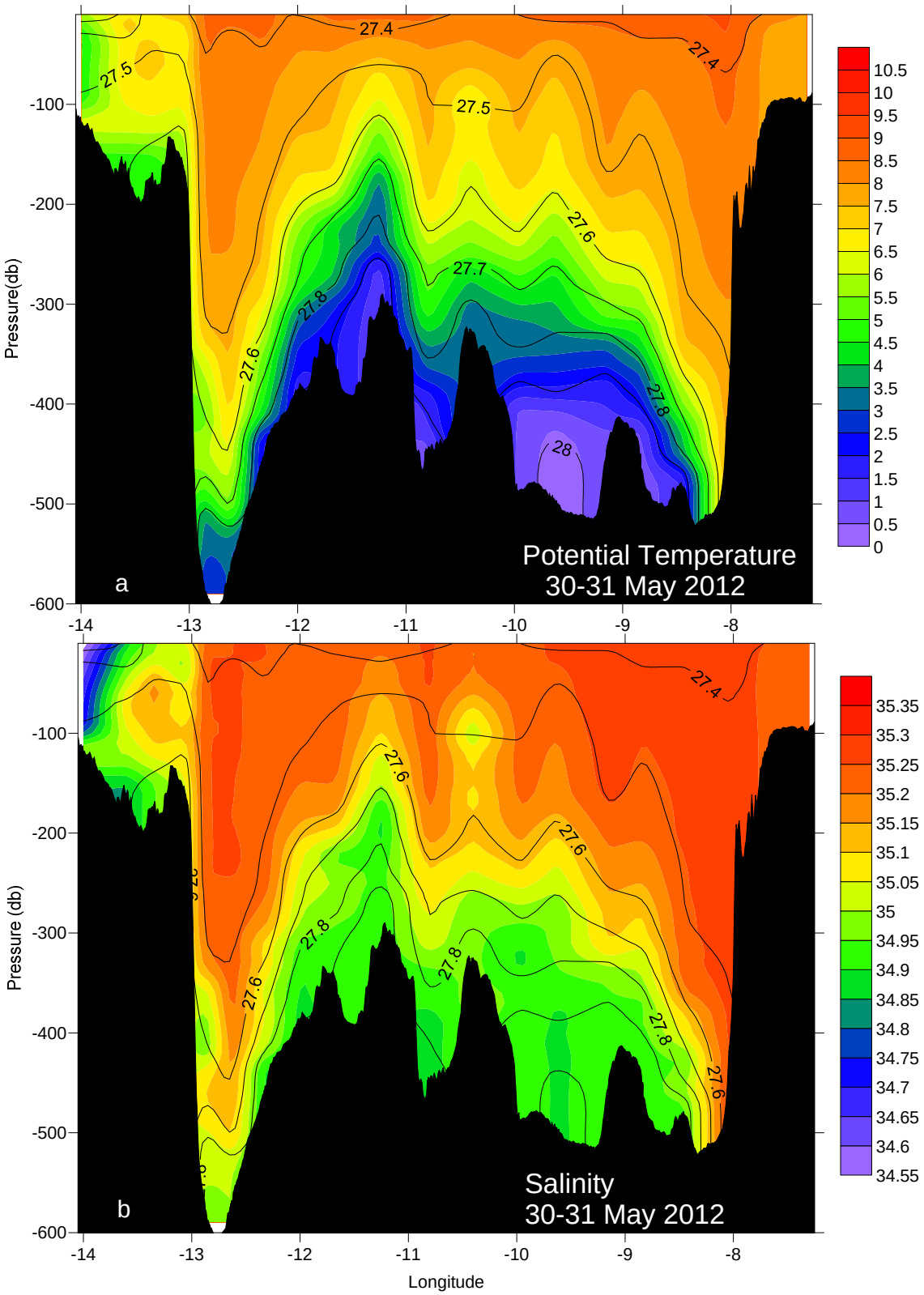

Figure 15 The vertical distribution of (a) potential temperature and (b) salinity between Iceland and Faroe Islands in May 2012. Density is shown in black.

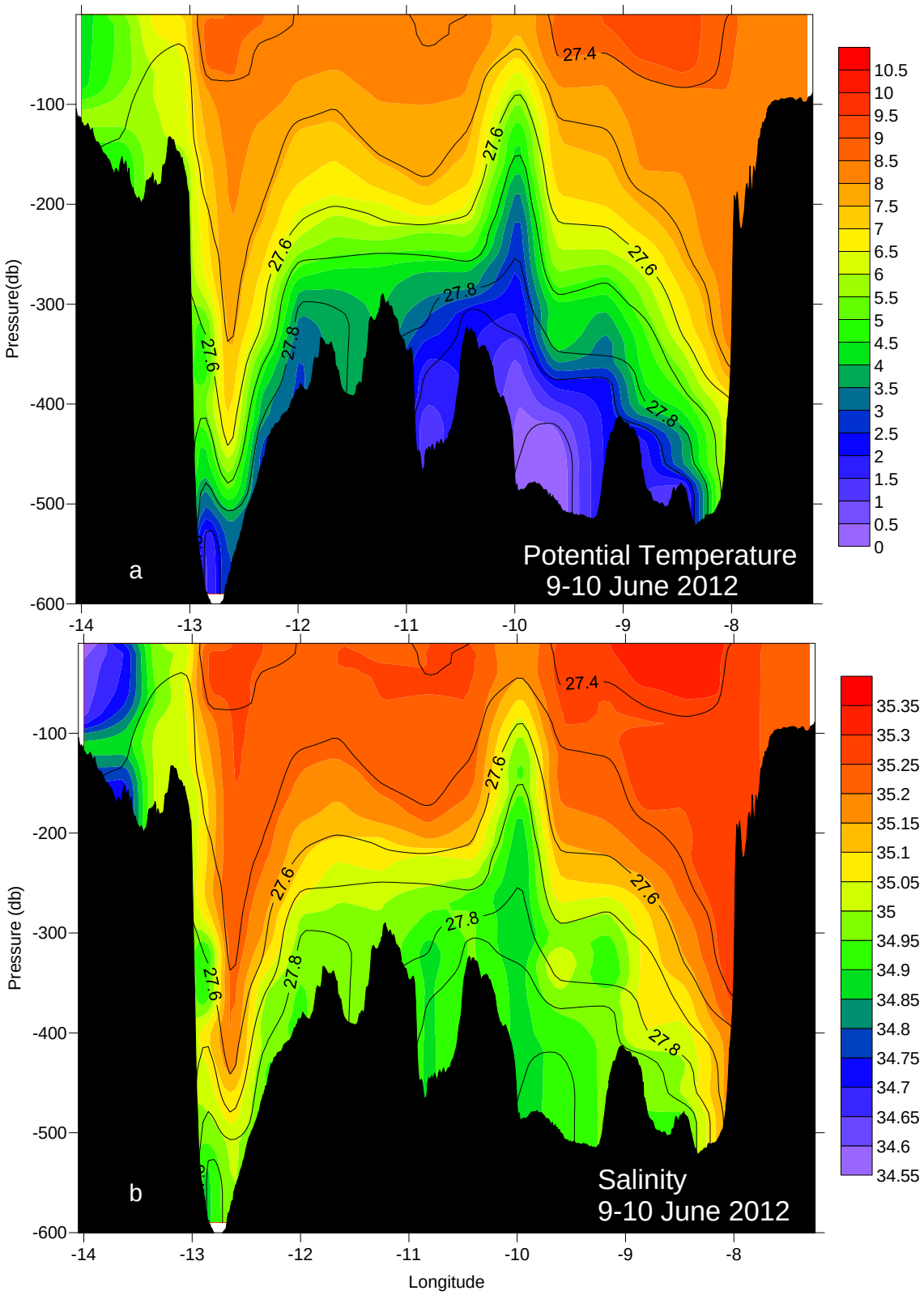

Figure 16 The vertical distribution of (a) potential temperature and (b) salinity between Iceland and ice edge near Greenland in June 2012. Density is shown in black.

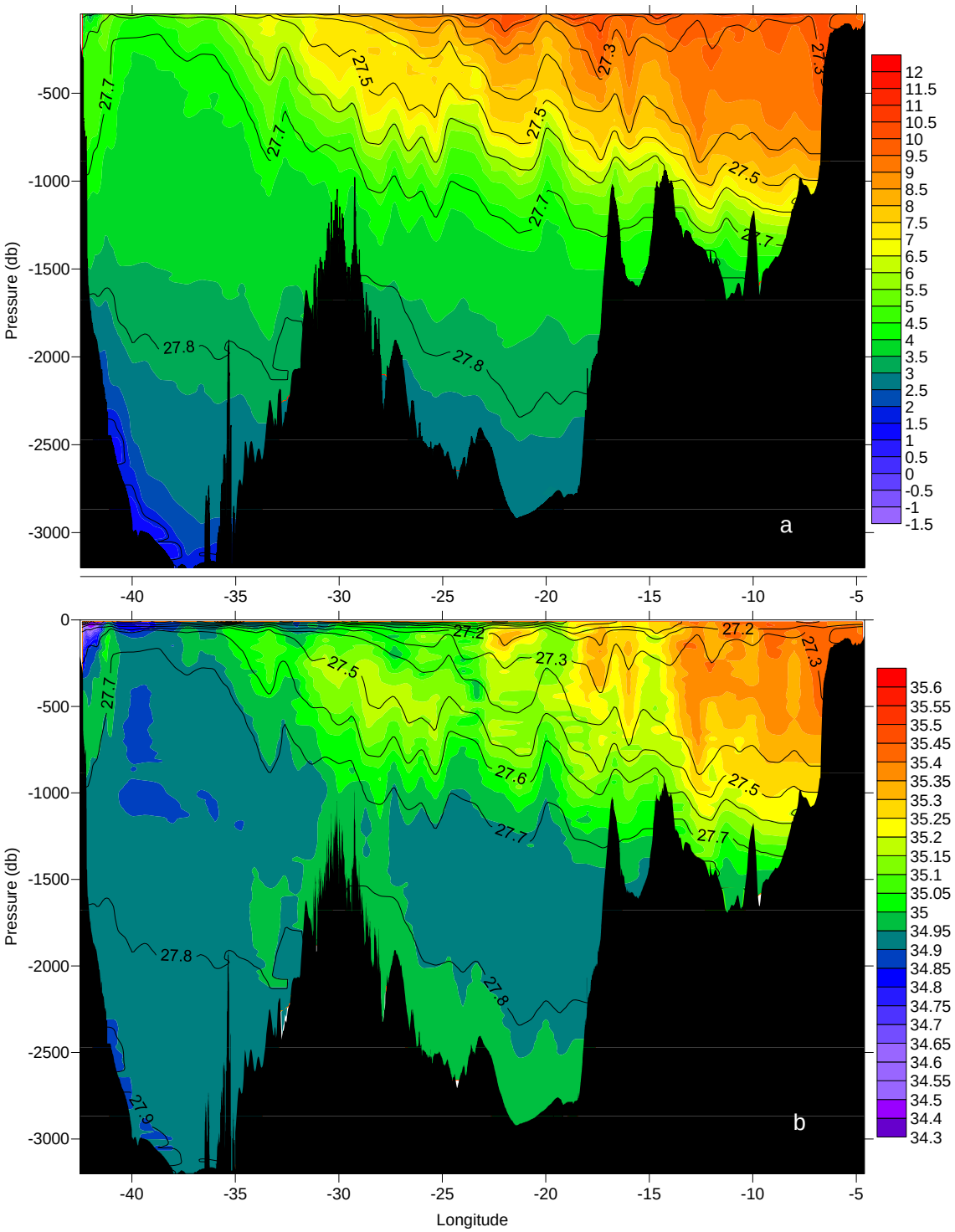

Figure 17 The vertical distribution of (a) potential temperature and (b) salinity along 59.5 N in June 2012. Density is shown in black.

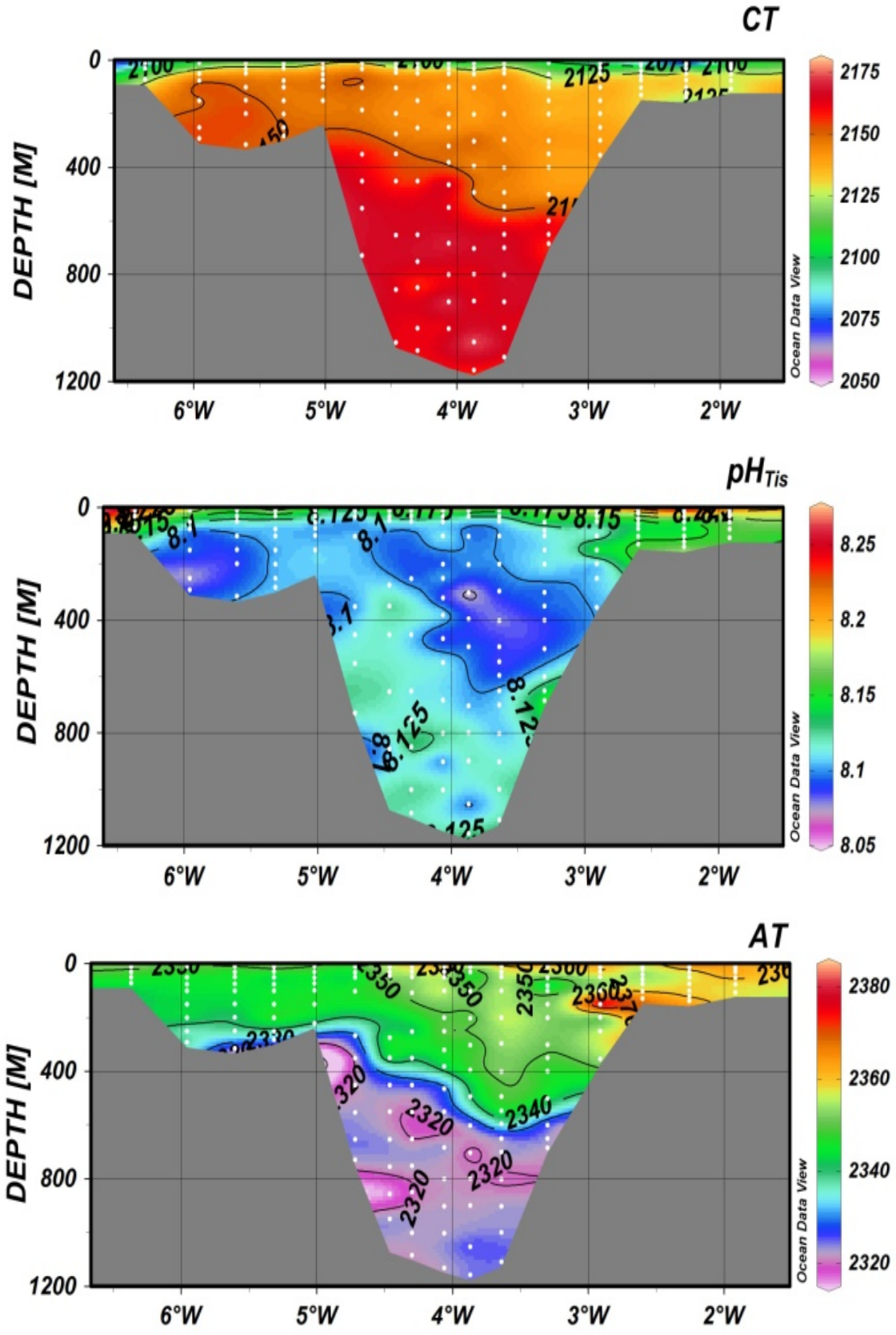

Figure 18 The vertical distribution of (a) dissolved inorganic carbon (CT) (b) in situ PH and (c) total alkalinity (AT) between Shetlands and Faroe Islands in May 2012.

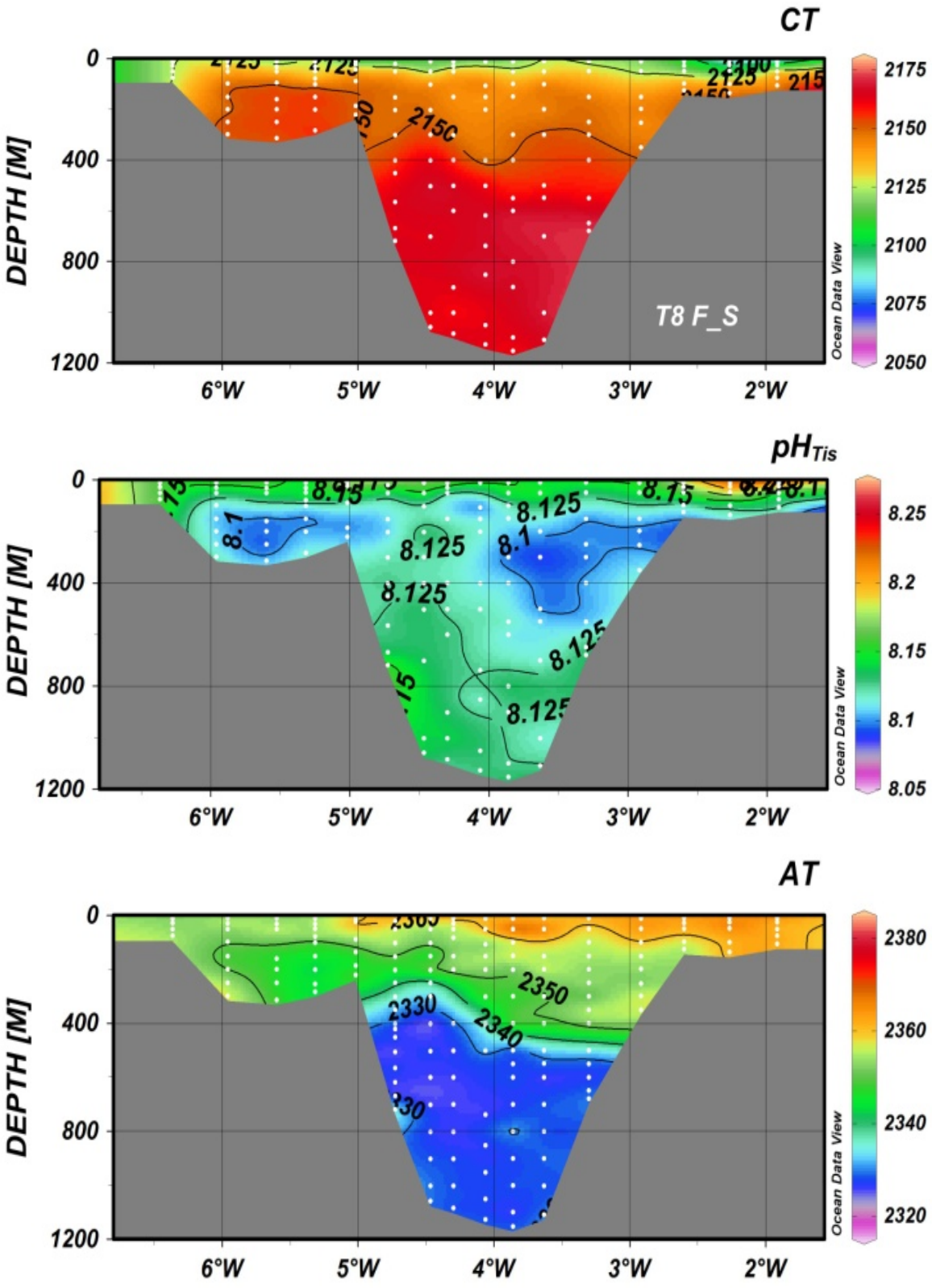

Figure 19 The vertical distribution of (a) dissolved inorganic carbon (CT) (b) in situ PH and (c) total alkalinity (AT) between Shetlands and Faroe Islands in June 2012.

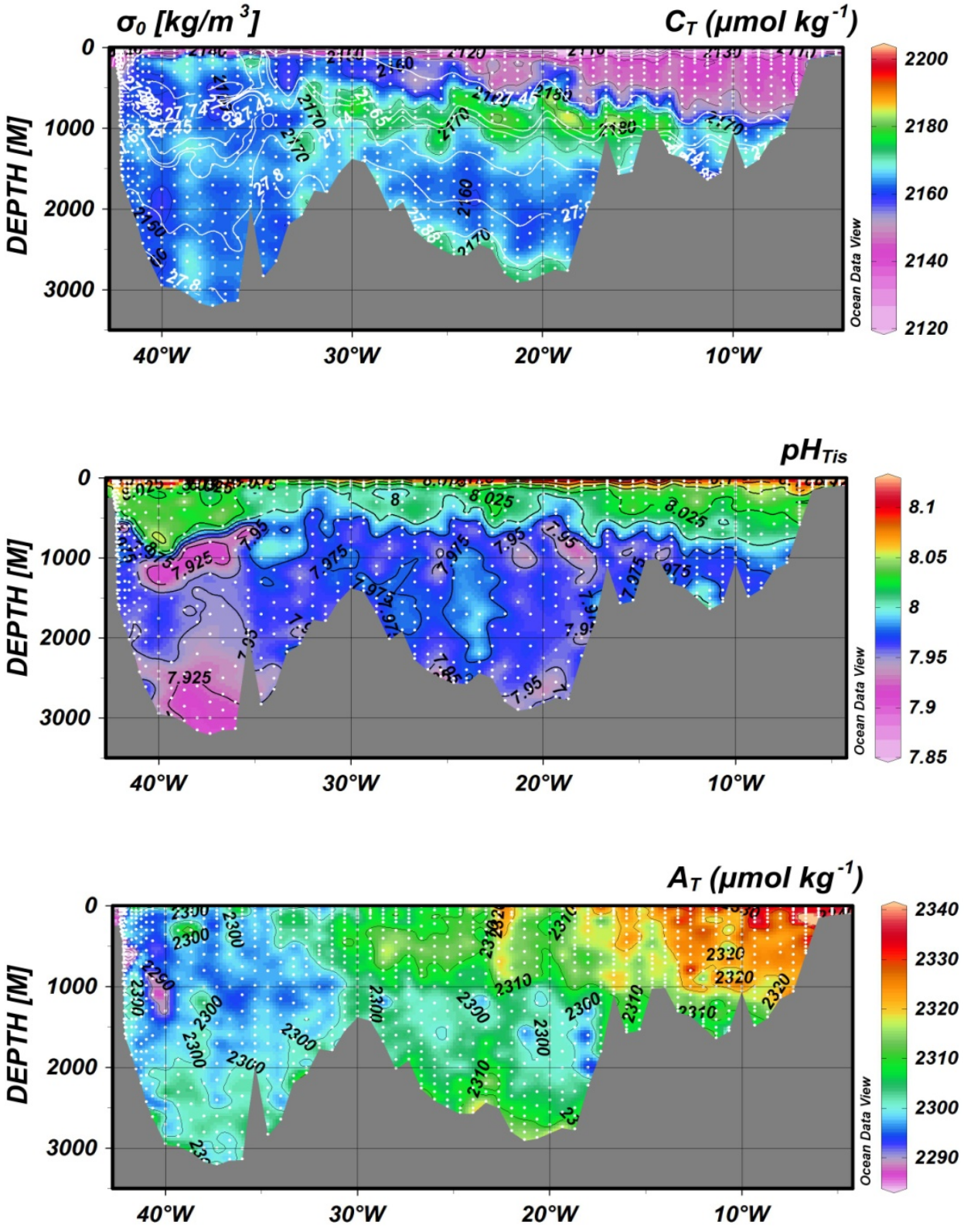

Figure 20 The vertical distribution of (a) dissolved inorganic carbon (CT) (b) in situ PH and (c) total alkalinity (AT) between Iceland and Faroe Islands in June 2012.